

ISMRM Best Practices for Safety Testing of Experimental RF Hardware

Authors

Nicola De Zanche, Cornelis (Nico) van den Berg, David Brunner, Joseph Murphy-Boesch, Joseph Rispoli, Gregor Adriany, Nikolai Avdievich, Nicolas Boulant, Wyger Brink, Ryan Brown, Thomas Fiedler, Kyle Gilbert, Laleh Golestani Rad, Bernhard Gruber, Boris Keil, Oliver Kraff, Arthur Magill, Azma Mareyam, Lucia Navarro de Lara, Sukhoon Oh, Mahdwesha Rao, Tales Santini, Bart Steensma, Lukas Winter, Sossena Wood, Filiz Yetişir

Revision History

2019-09-19 First draft for circulation
2021-07-26 Version circulated to ISMRM leadership
2022-03-07 Finalized preamble

Preamble

This document was written by a working group of twenty-six experts who are members of the Safety and Engineering Study Groups of the International Society for Magnetic Resonance in Medicine (ISMRM). While the authors are based in several countries and continents, no assurance is given that these recommendations comply with the law in any particular jurisdiction. The reader is responsible for assuring, before implementing any of the recommendations below, that the reader is complying with the laws and regulations of the jurisdiction in which the reader is located.

By accessing or downloading this document, you, the reader, agree to the following:

Disclaimer of Warranty

This document is based on information believed to be accurate and current as of the date it was written, as indicated on the first page of this document. Reasonable efforts were made to confirm the accuracy of the information contained in this document, but no assurance can be given that it is error-free. Some information contained in this document is based on on-going research and not on published standards or consensus of the authors. Adherence to the recommendations in this document may not ensure safety in every situation. The ISMRM is under no obligation to update these recommendations in the event of changes in technology, professional or ethical standards, or the law.

ACCORDINGLY, THIS DOCUMENT AND THE INFORMATION, RECOMMENDATIONS, CONCLUSIONS AND DATA CONTAINED HEREIN ARE PROVIDED ON AN "AS IS" BASIS, WITHOUT WARRANTY, EXPRESS OR IMPLIED, INCLUDING WARRANTIES BASED ON FITNESS FOR A PARTICULAR PURPOSE. WITHOUT LIMITING THE GENERALITY OF THE FOREGOING, THE ISMRM EXPRESSLY DISCLAIMS ANY REPRESENTATION OR WARRANTY THAT THE INFORMATION AND RECOMMENDATIONS CONTAINED IN THIS DOCUMENT ARE ACCURATE OR COMPLETE OR THAT THE RECOMMENDATIONS COMPLY WITH THE LAWS OR REGULATIONS OF ANY JURISDICTION.

Exclusion of Liability

This document is for information purposes only and is not a substitute for the advice of an expert. While the ISMRM facilitated the development of this document, it did not write this document or independently verify the accuracy or completeness of the information or the recommendations set forth below. Under no circumstances shall the information contained in this document be construed as medical advice.

Reliance on the information or recommendations in this document is at your own risk. IN NO EVENT SHALL THE AUTHORS OF THIS DOCUMENT OR THE ISMRM OR ANY OF ITS DIRECTORS, OFFICERS, EMPLOYEES OR AGENTS BE LIABLE FOR ANY DIRECT, INDIRECT, GENERAL, SPECIAL OR PUNITIVE DAMAGES, OR ANY OTHER DAMAGES OF ANY KIND, WHETHER BASED ON CLAIMS OF PERSONAL INJURY, WRONGFUL DEATH, LOSS OF USE, LOST PROFITS, INTERRUPTION OF SERVICE OR LOSS OF DATA, WHETHER IN ANY ACTION OR CLAIM BASED, WITHOUT LIMITATION, ON NEGLIGENCE OR ANY OTHER TORT, BREACH OF CONTRACT OR ON ANY OTHER LEGAL THEORY.

No Endorsement

Nothing in this document should be construed as an endorsement of any product or service provided by any manufacturer or supplier.

Copyright



This work is licensed under the Creative Commons Attribution-NonCommercial International ([CC-BY-NC 4.0](https://creativecommons.org/licenses/by-nc/4.0/)) license. The license does not apply to content for which the authors or [ISMRM](#) are not the copyright owners.

Scope and Aims

The guidelines and recommendations contained in this document are intended to assist experts in MRI scanner hardware with obtaining local research ethics approvals for radio frequency (RF) devices built at the research site. Such devices are typically used on research subjects and not on the general patient population, in which case additional requirements likely apply. Typical users of this document are RF engineers and others with experience with electronics design, simulation and construction. Judgement and familiarity with general aspects of MRI safety are required (see [Background](#)).

The processes included in these recommendations apply mostly to RF coils, which are the most common RF devices that a site will build in-house and, because of the inherent proximity to the human body, require a careful assessment of safety. Indeed, according to an analysis of adverse events reported to the FDA [1], RF coils were found to be responsible for the majority (54%) of thermal events (e.g., burns) caused by contact with an object.

With appropriate adjustments, the same processes can be used on other RF devices used in transmitting and receiving chains (because they can influence the RF fields in and around the coils), as well as coil inserts and additions such as high-permittivity pads and metamaterial structures. Other relevant items and inserts that are not strictly RF devices include physiology transducers such as electroencephalography (EEG) electrode caps, as well as devices designed to deliver energy such as transcranial magnetic stimulation (TMS) coils and high-intensity focused ultrasound (HIFU) transducers.

These recommendations form the basis for a risk management process to safeguard against hazards and should be an integral part of an ongoing comprehensive safety program. They constitute good practices, but they are not to be interpreted as mandatory, neither technically nor legally. Because ethics approvals typically apply only to a single, or a limited number of sites, these recommendations are not intended for devices built commercially, or for devices distributed in quantities beyond the individual research site.

These recommendations were written by a geographically diverse team whose members span several countries and continents. However, all possible jurisdictions and institutions could not be covered, and laws in your specific jurisdiction may dictate different requirements.

This document is only a guide and does not claim to be exhaustive. All foreseeable devices and situations may not be covered, and thus the user's experience and judgement are required throughout. It is the individual site's responsibility to select which requirements and procedures are applicable in a given situation. In other words, the applicability of these recommendations depends on the circumstances.

The information in this document is believed to be accurate at the time of writing. Many recommendations are based on existing standards (c.f. [Standards](#)) to which we defer for more details. Where possible, standards and other publications are provided as [References](#). There may be applicable documents beyond those listed, as well as updates to the standards from time to time.

The aims of this document are:

- to assist the with obtaining local research ethics approvals for RF devices built at the research site;
- to standardize between sites the processes and documentation needed for ethics approvals; and
- to stimulate further research on methods to ensure the safety of site-built RF devices.

Background

Magnetic resonance imaging (MRI) and spectroscopy (MRS) are non-invasive techniques used, respectively, for imaging the human anatomy and measuring the chemical composition of tissues. Since their introduction to clinical practice in the 1980's, these powerful tools have transformed medicine. One of the advantages of MR over techniques such as computed tomography and nuclear medicine is that it does not use ionizing radiation, which increases the likelihood of developing cancer. Instead, MR uses static and low-frequency magnetic fields, as well as radio frequency (RF) fields, none of which is associated with ionizing radiation dose, but nevertheless are associated with other risks.

The present document addresses the safety hazards of the devices that research labs sometimes need to build to create, detect (receive) or modify the RF fields, and the hazards due to the RF fields themselves. The document expands on an earlier effort by Hoffmann et al.[2] to summarize the safety procedures for RF devices. For safety recommendations regarding static and low-frequency (gradient) magnetic fields we defer to other documents such as those published by the ACR (American College of Radiology), AAPM (American Association of Physicists in Medicine), ASTM International (formerly American Society for Testing and Materials), ISMRM, NEMA (National Electrical Manufacturers Association), FDA (Food and Drug Administration, USA), and other institutions, as well as national and international safety codes and standards.

In MR, the RF fields are responsible for excitation and detection of the nuclear magnetization, from which information about the anatomy and chemical composition can be obtained. The RF fields are created by antenna-like devices known in the industry as “coils”, which are connected to high-power transmitters and/or high-sensitivity receivers. The repetitive, high-power pulses transmitted by the coils can lead to heating in the body's tissues. This heating is an intrinsic safety hazard that must be mitigated to avoid tissue burns or elevation of core body temperature. Commercial MR systems typically employ some combination of design features, hardware devices and software to enforce limits on heating and temperatures.

Coils perform best when they are tailored to the specific anatomical region being investigated, but they may not be available for all regions or sizes of subjects. In some cases, coils are simply not available commercially because some research MR systems are developed in-house by the research site. In other situations, research labs have devised unconventional and unique RF systems to test out new MR scanning paradigms. In all such situations, labs must build their own coils or other hardware that can influence the RF fields to which the human body is exposed during scanning. The responsibility for ensuring RF safety thus falls on the lab. The objective of these recommendations is to assist labs in ensuring the safety of lab-developed RF devices, as well as other hardware that can modify the RF behaviour of an RF device (e.g., coil).

How to Use this Document

This document is organized as follows. Page numbers are prefixed with the part and chapter numbers to facilitate navigation. Each chapter has its own detailed table of contents, and the PDF file is optimized for electronic viewing using hyperlinks and bookmarks, which can be used to jump quickly to a desired section from anywhere in the document. References to specific sections in this document, or sections in cited documents, are indicated by the section sign (§) or by hyperlinks whose names correspond to the section titles.

Front matter consists of these introductory pages up to the List of Abbreviations on the next page.

Part I: Analysis of Failures and Safety Risks describes the risk management process and how to perform and report a risk analysis. These are the core tasks and processes that form the foundation of this document and provide a framework for analysing and mitigating safety risks.

Part II: Technical Considerations and Risk Mitigation provides the most commonly used risk mitigation techniques including best practices for safe mechanical and electronic design as well as best practices for RF simulations and validation. Consequently, Part II is further subdivided into the corresponding chapters:

- A. Housing and Mechanical Safety
- B. Safety of Electronics
- C. RF Safety

These technical guidelines must not be interpreted as an exhaustive, rigid set of rules. Many uncommon situations do exist, and the methods of Part I should instead be relied upon to identify, analyse and mitigate all potential safety risks in each situation.

Part III includes References and the Appendices, including lists of the most relevant Standards and other publications.

List of Abbreviations

The following abbreviations are used in this document. Additional abbreviations are found in the list of relevant [Standards](#) and in Appendix [D](#).

ABC	Absorbing boundary condition
AC	alternating current
AIMD	Active implantable medical device
CAD	Computer-aided design
DC	direct current
DUT	Device under test
EM	Electromagnetic
EMI	Electromagnetic interference
ECG	electrocardiogram
EEG	Electroencephalography
ESD	Electrostatic discharge
FDTD	Finite difference time domain
FEM	Finite element method
FIT	Finite integration technique
FLIR	Forward-looking infrared
FMEA	Failure Modes and Effects Analysis
FOV	Field of View
FR-4	flame retardant 4 (according to NEMA LI 1-1998)
FTA	Fault Tree Analysis
GRE	gradient-recalled echo
HDT	heat deflection temperature
HF	high frequency (3 – 30 MHz)
HIFU	High-intensity focused ultrasound
IC	integrated circuit
LED	light-emitting diode
MCM	multi-chip module
MDR	Medical Device Regulation (European Union)
MEMS	Microelectromechanical systems

MOOP	method of operator protection
MOPP	method of patient protection
MRI	magnetic resonance imaging
MRS	magnetic resonance spectroscopy
PCB	printed circuit board
PIN	positive-intrinsic-negative (diode)
PMMA	Poly(methyl methacrylate)
POM	Polyoxymethylene
PRF	Proton resonance frequency
PTFE	Polytetrafluoroethylene
pTx	Parallel transmit
PVC	Polyvinyl chloride
PVP	Polyvinylpyrrolidone
QA	Quality assurance
RF	Radio frequency
Rx	receive
SAR	Specific absorption rate
SFC	Single fault condition
SPR	Safety and Performance Requirements
sTx	Single channel transmit
TE	echo time
TEM	Transverse electromagnetic
TMS	Transcranial magnetic stimulation
TPU	Thermoplastic polyurethane
TR	repetition time
TSL	tissue-simulating liquids (and gels)
UHF	ultra-high frequency (300 MHz – 1 GHz)
VNA	Vector network analyzer
VOP	Virtual observation point

Part I:

Analysis of Failures and Safety Risks

Page I.*

1	Definitions.....	2
2	Risk Management Process.....	2
2.1	Risk Analysis.....	3
2.1.1	Single Fault Safety.....	3
2.1.2	Typical Risks associated with RF hardware.....	3
2.1.2.1	Mechanical Hazards	4
2.1.2.2	Electrical Hazards	4
2.1.2.3	Tissue Heating (SAR)	4
2.1.2.4	Other Hazards.....	4
2.1.3	Failure Modes and Effects Analysis (FMEA).....	4
2.1.3.1	General Organization.....	5
2.1.3.2	Tracking and Reporting FMEA's	5
2.1.4	Fault Tree Analysis (FTA)	6
2.1.4.1	General organization.....	6
2.1.4.2	Reporting and tracking hazards and faults	7
2.1.4.3	Example	7
2.2	Risk Estimation	8
2.2.1	Qualitative Risk Estimation	8
2.2.2	Risk Matrix	9
2.3	Risk Evaluation and Control.....	10
2.4	Residual Risk Estimation	10
2.5	Risk Management Documentation	11

Designing, constructing and operating site-built RF hardware requires identifying and controlling potential conditions (e.g., failures) that pose risks to the safety of human subjects. Managing risks requires an analysis of the possible failures and the corresponding severity of the risk. This section describes the methods used to analyse risks associated with the technical considerations (and mitigations) described in the second part of these recommendations. The risk analysis can assist in identifying the efforts required to mitigate risk (note that it is unrealistic, if not impossible, to eliminate risk completely). Risk management begins at the design stage and continues through manufacturing and operation of RF hardware. Risk management is central to the IEC 60601-1 standard (§4.2 therein) and is discussed in detail in other standards such as ISO 14971, which is specific to medical devices, and the ISO 31000 series, which are more general.

1 Definitions

- **harm:** physical injury or damage to the health of people, or damage to property or the environment (ISO 14971)
- **failure:**
 1. inability of an item, product or service to perform required functions on demand due to one or more defects (ASQ Quality Glossary)
 2. loss of ability to perform as required (IEC 60050-192-03-01)
- **fault:** inability to perform as required, due to an internal state (IEC 60050-192-04-01)
- **hazard(ous state):**
 1. condition, event, or circumstance that could lead to or contribute to an unplanned or undesired event [3]
 2. potential source of harm (ISO 14971)
 3. state that has the potential to cause harm to persons, significant material damage or other unacceptable consequences (IEC 60050-192-02-26)
- **probability:** statistical likelihood of an event or occurrence
- **severity:** measure of the possible consequences of a hazard (ISO 14971)
- **risk:** combination of the probability of occurrence of harm and the severity of that harm (ISO 14971)
- **safety:** freedom from unacceptable risk (ISO 14971)

The risks associated with site-built RF hardware can vary depending on various factors such as:

- the operating frequency (Larmor frequency given by nucleus and field strength)
- the specific role of the device (e.g., coil vs. RF chain component)
- strategy adopted by the MRI scanner for detecting failures in real time

The processes in this chapter allow a systematic, documented analysis, which should be followed to inform how to address the risks when building a device to be used in an MR scanner.

2 Risk Management Process

Risk management is the process of identifying risks and developing strategies to mitigate them. The following is a simplified risk management process along the lines of that described in ISO 14971. This standard is widely used in industry, is specific to medical devices, and is summarized in more detail in other publications such as Ref. [4].

2.1 Risk Analysis

Several techniques for risk analysis have been developed (see Annex G of [ISO 14971](#)). In these recommendations two of these processes will be briefly described (see referenced standards for details): (i) [Failure Modes and Effects Analysis \(FMEA\)](#) and (ii) [Fault Tree Analysis](#). An example FMEA report is provided to illustrate how to perform the analysis following either of these two procedures.

A risk analysis may yield a hazard that develops when a device fails in one or more ways. These modes of failure are addressed one at a time, and the evaluation of failure modes is governed by the IEC rules for single fault safety (§4.7 of [IEC 60601-1](#)). The basic rules are that failures are treated one at a time, and that should a particular fault occur the device should remain safe, i.e., “single fault safe”. Treatment of a failure mode is related to its risk, and where more than one failure can occur, additional rules apply, as summarized in the following section.

2.1.1 Single Fault Safety

On a procedural basis, risk analysis involves the sequential identification of specific modes of failure, the components associated with a failure, and any undue effect it is likely to have on a patient or subject. A medical device is considered to be “single fault safe” if the risk presented to the patient by that fault has been adequately mitigated through design and fault detection.

The [IEC 60601-1](#) standard identifies two broad categories for mitigation of risk resulting from a single fault. The first means for mitigation (§4.7(a)) is to include design features that render the likelihood of failure to be negligible. As an example, normal operation of a device might require that a high voltage be passed to some internal components of the device, presenting a shock hazard to the patient. Mitigation of this hazard could be to electrically isolate these components and any metal parts using mechanically strong and highly insulating materials for the device former.

A second type of failure (§4.7(b)) is one that has a finite probability of occurring and cannot be rendered improbable (“for the life of the instrument”). In this situation, two paths for mitigation are identified. The first is that the device can sustain the failure without causing risk to the patient, and the failure can be detected before a second means of reducing risk fails. In the receive-only coil example provided in [§1.2.1.3.2](#), the second means of reducing risk might be a blocking circuit or a fuse in series with the coil element. The detection could be active monitoring of the primary coil blocking circuits by the MRI system, which can stop the imaging sequence. The second path for mitigation can be that the second means of failure is also highly unlikely, in the manner of §4.7(a) of [IEC 60601-1](#).

In the event of a cascade of failures, where a primary failure is likely to cause other components within the device to fail, the cascade is considered to be a single fault for which single-fault safety must be assessed.

Specific conditions that must be single-fault safe are listed in §13.2 of [IEC 60601-1](#).

2.1.2 Typical Risks associated with RF hardware

In these recommendations we have chosen to describe in detail typical hazards that fall into three broad categories for RF hardware. Additional hazards encountered in MRI (see e.g., [IEC 60601-2-33](#), [FDA Guidance 340](#), [FDA Guidance 19011](#), [ACR MR Safety Manual](#)) are beyond the scope of this document. Because there is some overlap between the three categories, this classification is not mandatory but

can be of assistance when organizing the risk analysis documentation. The categories and typical hazards are briefly described below.

2.1.2.1 Mechanical Hazards

Mechanical hazards (addressed specifically in §9 of IEC IEC 60601-1) are those related to the enclosure and supporting structure of the device, including the shapes as well as physical and chemical properties of the materials used. The typical hazards of this type are associated with surfaces for subject support, sharp edges and pinch points, and electrical insulation used to protect from contact with conductors.

2.1.2.2 Electrical Hazards

Electrical hazards (addressed in §8 and others of IEC 60601-1) are those related to the electrical components of the device, including all conductors. The typical fault conditions of this type include the RF stresses from high-power external fields from transmit (body) coils or local transmit elements. These stresses generally produce shorts or opens in the components or their connections. Other hazards would include excessive coil (surface) temperature in case diodes of active or passive detuning circuits fail. The effects of failures should be considered in the manner in which they affect subject safety as opposed to how they affect the quality of the hardware and data (e.g., images).

2.1.2.3 Tissue Heating (SAR)

Heating due to RF (ohmic) losses in tissue can lead to increases in core body temperature as well as more severe effects like burns or other tissue damage (see §II.C). It is therefore essential to characterize the ability of the RF device (e.g., coil) to produce or modify the electromagnetic fields that lead to tissue heating both locally as well as over larger portions of the anatomy. Heating due to RF fields is addressed in IEC 60601-2-33 as well as other standards.

2.1.2.4 Other Hazards

Other hazards need not be associated with hardware design or failures, but should nevertheless be considered in the analysis. These include operator errors associated with how the RF coil is handled, used and connected to the MRI system. They can also include disconnects and malfunctions with the MRI system itself. The latter can include software issues related to coil files and default states programmed into the controlling software. These general hazards are addressed in both IEC 60601-1 (e.g., §12) and IEC 60601-2-33.

Occasionally, coils are used in tandem with other sensors and hardware (EEG, TMS, HIFU, etc.) and issues related to such combinations should be analysed in addition to the hazards associated with the individual systems.

2.1.3 Failure Modes and Effects Analysis (FMEA)

The purpose of a failure modes and effects analysis (FMEA, IEC 60812) is to identify potential failures of a device and to determine the effects of these failures upon safety and reliability. FMEA is used extensively in industry for product development, to monitor safety, improve reliability, and reduce costs in the manufacturing process. The analysis can be very detailed, in that it evaluates the design and function of the individual parts of a device and evaluates the effect of a failure, or possibly several failures, from each part. The analysis is generally performed with a spreadsheet so individual parts can be identified and logged, and the failures and their effects can be logged in succeeding columns. The focus here is safety, but because separate pieces of the coil are evaluated, the FMEA can expand into

the realm of reliability, which can quickly dominate the report. For custom RF hardware, reliability needs to be considered, but mainly as it affects safety and the design life of the coil for the project at hand. FMEA typically works by looking at single-fault conditions, e.g., analysing components one at a time. This approach is appropriate for relatively simple systems such as RF coils where multiple independent failures are highly unlikely.

2.1.3.1 General Organization

There is no required organization to the FMEA. However, it is generally convenient to begin by separating issues into those that are mechanical and electrical in nature. Human factors, such as for initial setup and/or monitoring, might then be considered, and if a situation exists where MRI is combined with other sensors or stimulation (e.g., EEG or TMS), issues related to them can be captured separately. In product development, FMEA is generally employed to improve the reliability of a device. To the extent that reliability affects safety, it should be included in the FMEA. In a research setting, a coil or associated device should be designed to last for the duration of the study.

2.1.3.2 Tracking and Reporting FMEA's

A Failure Mode and Effect Analysis analyses the cause and effect relationships between parts that might fail or create a hazard, and the effects first upon the coil itself and then upon a human subject. This step-by-step analysis is generally captured in the form of a spreadsheet so that individual potential failures (e.g., those due to failures of single parts) can be identified and logged. An example of this format and a few entries that might be found in an FMEA are shown in [Table 1](#). The first column of the FMEA identifies an item or part of the coil, and the second column describes a possible failure associated with the part. The next column captures the effect of the failure upon the coil and the nature of the hazard, followed by the hazard created for a human subject. For a coil to remain safe, some form of mitigation of each hazard needs to be provided, and this is captured in the last column of the FMEA. Some common failure modes for RF receive coils are listed in [Appendix A](#).

The Active or Tracking FMEA

An FMEA analysis often uncovers a situation in which the mitigation of a failure is not resolved, and in this case, it becomes a tool for tracking changes to the design of the coil. The FMEA tool becomes a “live” document, with additional columns added to identify solutions and track progress in design and testing. In industry, the document serves as an important record in “design control,” to verify safety testing and verify reporting of any design changes to a company’s “master record”. The FMEA remains active until all methods of mitigation have been resolved and verified. An FMEA final report can be prepared by removing all of the actionable items captured in the supplementary columns of the active FMEA.

The Reporting FMEA

Once all significant failure modes have been identified and the risks associated with them mitigated, the FMEA can be attached to a safety report. An overview for the FMEA is recommended to introduce it and to highlight any special risks that were taken into account. Extensive footnoting to the line items is recommended to expand on table entries and clarify methods used for mitigation.

Table 1: An example of the format of an FMEA and some common entries.

Failure Modes and Effects Analysis				
Item/Function	Potential Failure Mode	Local Effect	Potential Patient Effect	Mitigation
Reference Drawing(s): Schematic SK-001				
System Cable	Looping of the Cable near the body coil	High shield current induced on the cable	Patient contact with cable may cause RF burn	Length of cable shortened to prevent looping
Detuning circuit in Rx-only Element	Component failure, element remains tuned	High induced RF current	High SAR beneath element, tissue heating	Fuses added in series with Rx coil loops
Reference Drawing(s): Mechanical Drawing DR-001				
Coil Housing	Cracked Housing	Pinch point created on patient surface	Patient discomfort, injury	Operator warning: do not use coil if damaged

2.1.4 Fault Tree Analysis (FTA)

Fault tree analysis (FTA, [IEC 61025](#)) is an alternative to FMEA for populating the risk table [5]. In FTA the analysis begins by identifying undesired states of the system, rather than starting from the individual failures that can lead to that state. It is a top-down process that begins by naming hazardous conditions (e.g., excessive SAR) and finding all possible ways that the hazard can occur. FTA can sometimes identify failures or combinations of failures that are not immediately obvious in FMEA. Therefore, it is not uncommon to perform both FTA and FMEA to populate the risk table. FTA also works well early in the design stage when all the components of the system have not been designed in detail. Unlike FMEA, FTA is designed to identify hazards due to multiple independent failures, and thus it is valuable to analyse complex systems. For commercial devices, some jurisdictions prefer or require FTA over FMEA.

2.1.4.1 General organization

In the FTA, the construction of the fault tree is the main action of the process. The possible hazards define the top of the tree, and subsequent levels represent stages of increasing amount of detail:

- Top level: combines subsystems
- Medium level: subsystem involved on a failure, failure states
- Bottom Level: basic events, component failures

To construct an FT, the following steps are followed:

1. Define a fault condition, writing down the top level failure
2. Identify all possible causes of the fault condition (events). These are level two elements; they fall just below the top level.

3. Structure the tree with logic gates (“AND”, “OR”) that introduce relationships between the single events.
4. Break down each element of the second level to lower levels with additional logic gates.

Methodology of the FT construction can be: (i) iterative, (ii) structured or (iii) methodical. For more information about the risk management process, see references such as [4], [6], [7] and [IEC 61025](#).

2.1.4.2 Reporting and tracking hazards and faults

Once the FT is totally characterized, results and conclusions can be obtained. Based on probability and Boolean algebra, probability of event occurrence can be obtained. A cut set is defined as a set of events that together can cause the top failure or hazard event to occur. The cut sets allow probability calculations to assist with finding the weak and critical links in the design.

After these calculations are performed in all branches of the tree, the FT can be used to evaluate risks and guide decision making, to determine if the developed hardware is safe, to identify root causes and identify critical components and failure modes.

Evaluation of risks can be done in FTA either qualitatively or quantitatively like in FMEA (see §1.2.2 below).

2.1.4.3 Example

[Figure 1](#) shows the fault tree for the analysis of an actively-detuned receive-only surface coil, including some common faults and how they can lead to hazards for the subject. Based on the actual electrical circuit, events like “faulty detuning circuit” can be further broken down into failures of the individual components.

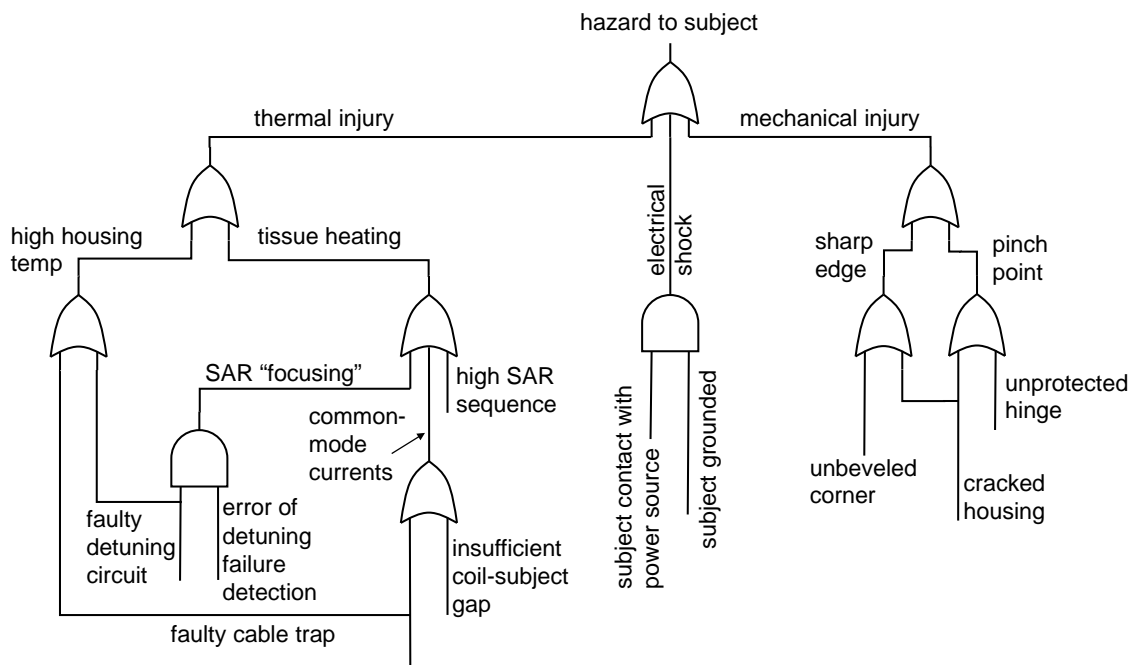


Figure 1: example of FTA for a receive-only surface coil.

2.2 Risk Estimation

Once the hazards have been identified each one is assigned a risk which is obtained by multiplying the severity of the occurrence with its probability. High-risk hazards must be addressed, e.g., by modifying the design, until all potential hazards are associated with an acceptable level of risk. If the probability of a hazard cannot be estimated, the severity is used as the risk (i.e., high probability is assumed). Risk estimates are recorded in the risk table for each hazard.

2.2.1 Qualitative Risk Estimation

The purpose of risk estimation is to assist with decisions made to control risks. Each hazardous situation is assigned a level of severity ([Table 2](#)) and probability ([Table 3](#)). The number of possible levels of severity and probability (not necessarily equal) is a choice made by the person or organization performing the risk analysis.

Table 2: Example of qualitative severity levels (ISO 14971)

Terms	Description
Catastrophic	Results in death
Critical	Results in permanent impairment or life-threatening injury
Serious	Results in injury or impairment requiring professional medical intervention
Minor	Results in temporary injury or impairment not requiring professional medical intervention
Negligible	Inconvenience or temporary discomfort

Table 3: Example of qualitative probability levels

Terms	Description
Frequent, Certain	Almost always happens
Probable, Likely	Likely to happen
Occasional, Possible	Can happen, but not frequently
Remote, Unlikely	Unlikely to happen
Improbable, Rare	Almost never happens

2.2.2 Risk Matrix

The risk of each hazardous situation is obtained by combining probability and severity in a risk matrix or table ([Table 4](#)).

Table 4: Example of a risk matrix

Severity → Probability ↓	Negligible	Minor	Serious	Critical	Catastrophic
Frequent					
Probable					unacceptable
Occasional					risk
Remote	acceptable	risk			
Improbable					

The matrix thus allows risks to be classified as acceptable (green cells) or unacceptable (dark red) based on their location. The partition of the risk matrix into acceptable or unacceptable regions is a choice made by the person or organization performing the risk analysis. This choice is based not only on technical knowledge but is also based on the perceptions, values and expectations of the institutions and the public. The risk matrix is typically included in the [Risk Management Documentation](#), and the numbers referencing each risk in the FMEA or FTA are often indicated in the corresponding cells.

A more stratified classification of risks is also possible ([Table 5](#)).

Table 5: Example of risk matrix with 3 levels of risk.

Severity → Probability ↓	Negligible	Minor	Serious	Critical	Catastrophic
Frequent					High risk
Probable					
Occasional			Medium risk		
Remote					
Improbable	Low risk				

Sometimes, numerical values are assigned to the severity and probability to arrive at a final risk value equal to the product of each value ([Table 6](#))

Table 6: Example of risk matrix with calculated numerical risk assignments.

	Severity →	Negligible	Minor	Serious	Critical	Catastrophic
Probability ↓		1	2	3	4	5
Frequent	5	5	10	15	20	25
Probable	4	4	8	12	16	20
Occasional	3	3	6	9	12	15
Remote	2	2	4	6	8	10
Improbable	1	1	2	3	4	5

However, it must be emphasized that because the **numerical assignments are not quantitative** (e.g., an event of critical severity is not necessarily two times worse than one of minor severity), care must be taken to avoid assigning a quantitative value to the risk product ($R=S \times P$). For example, a serious, frequent event ($R = 15$) does not necessarily carry the same risk as one that is occasional and catastrophic. Note also that the partitions of [Table 4](#) cannot be achieved simply by applying thresholds to the risk product (e.g., neither $R \leq 3$ nor $R \leq 4$ will select the 6 cells closest to the bottom left corner of the matrix).

2.3 Risk Evaluation and Control

After the risks have been estimated it must be decided which risks require mitigation (control measures). Mitigation is implemented using design choices or adjustments (see [Part II](#) of these recommendations). If there are no practical means to mitigate a risk by design, clear warnings and/or instructions must be provided in the device’s manual on how to avoid that hazard. Risk mitigation is incomplete unless those instructions are followed. For each hazard the corresponding control measures can also be recorded in the FMEA or FTA table (see Tracking and Reporting FMEA’s).

2.4 Residual Risk Estimation

For risks that were mitigated in [§I.2.3](#), the probability, severity, and risk are updated to account for the control measures taken. These updated estimates are recorded in the FMEA or FTA documentation (table). It is common and sufficient to provide only the final residual risk, rather than both before and after mitigation. However, the control measures should be listed to record the mitigation strategies that were adopted, including risk mitigation by warnings and other information that is included in the user manual.

2.5 Risk Management Documentation

It is good practice to keep accurate records (e.g., lab notebooks) throughout the design and construction phases of RF devices. Documentation required for local ethics board approval will largely depend on the jurisdiction (applicable laws), policies of the individual institution, and complexity of the device. We therefore cannot broadly recommend minimum documentation, but it is typical to include some or all of the following:

- User Instructions or Manual
- design documentation (schematics, CAD drawings/layouts, bill of materials, etc.)
- data sheets of materials and components
- testing procedures and conditions
- test results (data or pass/fail)
- summary risk management chart or table
- risk matrix
- list of references

The lists in §4.2.4 and 4.2.5 of [FDA Guidance 340](#) are also relevant.

Part II:

Technical Considerations and Risk Mitigation

A. Housing and Mechanical Safety

Page II.A.*

1	Outer Enclosure (Housing)	2
1.1	Electrical Insulation	2
1.2	Ingress Protection	3
1.3	Biocompatibility and Toxicity	3
1.3.1	Out-gassing.....	3
1.4	Cleaning and Infection Control.....	4
2	Mechanical Construction	4
2.1	Strength and Stability.....	4
2.2	Mechanical Injury	4
2.3	Safety Systems and Emergency Procedures.....	5
2.4	Subject Comfort	5
2.5	Connectors and Cable Management	5
3	Temperature Limits.....	6
3.1	MR-compatible Temperature Probes	6
3.2	Surface Temperature Limits.....	6
3.3	Internal Temperature Limits	6
4	Material Properties	7
4.1	Mechanical.....	7
4.2	Ignition Temperature and Flammability.....	7
4.3	NMR Signal	8
4.4	Magnetism.....	8
4.4.1	Testing for Magnetic Materials	9
4.5	RF Permittivity and Losses	10
5	Labelling and Instructions.....	10

The recommendations in this chapter cover generic safety considerations common to a variety of components, modules and devices including coil housings, other mechanical supports, cables, cable traps, RF materials, etc. General requirements for medical devices are legislated in documents such as the European Union's EU Medical Device Regulation 2017/745(MDR), specifically Annex I: General Safety and Performance Requirements (SPR). More detailed and specific guidance is provided by widely-adopted international standards such as IEC 60601-1 and IEC 60601-2-33.

1 Outer Enclosure (Housing)

We use the term “housing” generally to describe an enclosure containing electrical circuits and/or components. Housings for RF coils are typically in contact with, or close proximity to the human body and therefore require close attention to the safety considerations in this chapter. Because of the likelihood of direct contact, it is especially prudent to expect that housings will be subjected to foreseeable human errors or misuse in addition to normal use (see Other Hazards).

1.1 Electrical Insulation

IEC 60601-1 (especially §8) requires an enclosure to protect the human body against electric shock (see also Protection from Electrical Shock Hazards). This requirement is especially important if voltages greater than approximately 50V are present.

For frequencies below 1 MHz the relevant sections are §8 and 13 of IEC 60601-1, and exceptions in §201.8 of IEC 60601-2-33, which describe requirements for both normal operation and Single Fault Safety operation. Specifically:

- electric fields and voltages according to §8.8. The minimum required thickness of insulation depends on the highest expected voltages (e.g., across capacitors in a coil) and the dielectric strength of the material [2]. If the dielectric strength of the material is not known, an appropriate test (e.g., ASTM D149, IEC 60243 series) is performed to measure it.
- touch and leakage currents according to §8.7. Maximum currents are defined for both DC and AC fields (in the range of 0.1 Hz to 1 MHz). It is because of the current limits in this section that the subject must never be able to touch a grounded conductor.

If needed, high voltage measurements on electrical insulation are described in detail in the IEC 60060 series.

For RF devices used in MR scanners (coils, cables, cable traps, connectors, etc.) the requirements of IEC 60601-1 are supplemented by §201.12.4.103.2 of IEC 60601-2-33 to address the ability of RF fields to induce substantial local heating simply by proximity to conductors (even if isolated from powered circuits). Therefore, it is almost universal to prevent direct contact between the subject and any conductive materials (e.g., exposed metallic fasteners, connector shields), even if they are electrically isolated (floating) from conductors carrying RF currents. (It may be possible to demonstrate that an isolated, exposed metal part does not acquire a significant voltage or potential and present a significant risk. However, the process of doing so is generally difficult and expensive, and it is preferred if metal screws and conductors are simply not allowed to be exposed.)

An additional consideration for devices that come into close proximity with the body, like surface coils, is the stray capacitance between conductive parts and body surfaces. This capacitance can support displacement currents (see Figure 8 in Part II.B or Fig. 1 in [8]) and the corresponding conduction

currents in the body lead to local SAR hot spots. In addition to using common-mode current traps (§II.B.5.3), these currents can be limited by reducing the capacitance using an appropriate thickness of insulation (e.g., foam). The minimum thickness will depend on various factors such as permittivity of the material, conductor dimensions, frequency of operation, and expected voltage between the conductors and the human body. The current standards do not comment on this aspect of insulation of RF devices and it is left to the designer to ensure such stray capacitances do not lead to a hazard.

1.2 Ingress Protection

The housing also protects against the ingress of foreign materials that can compromise the electrical insulation or the electronics inside (§11.6 of [IEC 60601-1](#)). This includes protection from liquids spilled accidentally (e.g., phantom materials or biological fluids), liquids used for cleaning, as well as particulate matter or larger objects. More details on degrees of ingress protection (IP) ratings and testing are found in [IEC 60529](#).

Bear in mind that connectors may have different IP ratings (meaning the degree of protection against ingress into the housing) depending on whether they are mated or unmated. When unmated, connectors may need protective covers to prevent foreign materials from compromising the contacts or creating hazardous conditions.

1.3 Biocompatibility and Toxicity

According to §11.7 of [IEC 60601-1](#), materials that come or may come into contact with the subjects or operators (typically through the skin) must be assessed for toxicity and allergenic properties. Materials known to be carcinogenic, hormone-mimicking, phthalates and other toxins should not come into contact with or be released into operators or subjects. Similarly, common allergens such as latex should be avoided, especially on contact surfaces. These requirements typically apply to housings, padding materials, bulk materials (in case of spillage) and their containers, paints, surface treatments, etc.

It is also prudent to investigate the toxicity of materials inside enclosures (e.g., electrical components) because those materials can be released under failures or other conditions (see [Out-gassing](#)). Ideally, no compounds known to be toxic should be employed in the device, and if non-standard, toxic substances are employed, the associated risks must be assessed and mitigated.

Relevant information can be found in [ISO 10993-1](#) and [ISO 10993-10](#), as well as the [EU Medical Device Regulation 2017/745](#), Restriction of Hazardous Substances (RoHS) Directive and the Substances of Very High Concern (SVHC) list of the European Chemical Agency (ECHA).

1.3.1 Out-gassing

Materials and components should not off-gas (or out-gas) toxic substances or noxious odours under all expected operating conditions and temperatures (see [Biocompatibility and Toxicity](#)). While materials can be chosen to minimize the release of toxic fumes in case of combustion (e.g., by avoiding halogenated compounds), this often comes at the expense of increased flammability (see [Ignition Temperature and Flammability](#)).

Adhesives are especially prone to out-gassing, and some are compliant with the stringent requirements of [ASTM E595](#). This and other suitable standards originate from aerospace and military applications, where use in high vacuum or recirculated air environments impose stringent limits on out-gassing. Materials compliant with such standards are also used in medical applications.

1.4 Cleaning and Infection Control

Enclosures that are in proximity or come into contact with the human body must be cleanable with standard medical disinfectants to prevent the transmission of diseases (§11.6.6 of [IEC 60601-1](#)). Similarly, the enclosure's materials should be resistant to other substances that it may foreseeably come into contact with (biological fluids, phantom solutions, etc.), as well as increasingly common ultraviolet disinfection lights.

Gaps or rough surfaces that can trap pathogens (e.g., seams between sections of the housing) should be avoided or minimized because they can create inaccessible regions that prevent thorough cleaning.

2 Mechanical Construction

Good practices in mechanical design and construction can prevent many hazards and ensure safe, reliable operation.

2.1 Strength and Stability

To prevent injury and electrical failures the housing must be robust and mechanically stable (§9.4 of [IEC 60601-1](#)) at room temperature as well as under worst-case heating conditions (see [Temperature Limits](#)). Any movable parts, hinges, mechanical connections, etc. must operate reliably. Furthermore, large housings may require a stable and reproducible connection to the patient support (couch).

The housing should be (§15.3 of [IEC 60601-1](#))

- a. strong enough to support the expected weight of the corresponding anatomy;
- b. strong enough to survive frequent rough handling by non-experts; and
- c. impact resistant in case it is accidentally dropped.

Additionally, mechanical design should take into account the possibility of substantial vibrations during scanning. For [Subject Comfort](#), the housing should not amplify acoustical noise.

If drop or rough handling tests are required, the procedures are described, respectively, in §15.3.4 and §15.3.5 of [IEC 60601-1](#).

If the device has substantial size and/or weight (> 20kg) the housing should have handles or equivalent gripping points for easy, reliable moving and carrying (§9.4.4 of [IEC 60601-1](#)). Weight should be limited to allow safe handling by a single operator. Where this is impractical, labels should clearly inform operators that multiple handlers are required (see also [Labelling and Instructions](#)).

Any electrical parts inside the housing must be attached and supported (§8.10 of [IEC 60601-1](#)) mechanically to the housing to prevent electrical failures.

See also [Material Properties](#) for related topics.

2.2 Mechanical Injury

Careful mechanical design and fabrication can minimize the risk of mechanical hazards such as pointed or sharp edges (§9.3 of [IEC 60601-1](#) and [EU Medical Device Regulation 2017/745 SPR 20](#)). Whenever possible, surfaces expected to come into contact with subjects or operators should also be smooth to

avoid friction-related injuries. Similarly, it is recommended to use flush or recessed fasteners wherever possible and appropriate.

Moving parts (e.g., hinges) should not introduce additional hazards such as pinching or shearing points in which the extremities, skin, hair, etc. may get pinched or trapped ([EU Medical Device Regulation 2017/745](#) SPR 11). In addition to mechanical injury, these hazards introduce a risk of transmission of infections if multiple people are successively injured by the same device. Protective covers may therefore be required.

In case of mechanical failure or accidental impact, housings and other mechanical parts must not shatter or crack producing sharp edges (See [Material Properties](#)).

2.3 Safety Systems and Emergency Procedures

Mechanical design (indeed also electrical design) should not interfere with, bypass, or impede existing safety systems and emergency procedures, including emergency field run-down (quench button), safety in the event of magnet quench, subject monitoring and communications, emergency evacuation of a subject, etc. If these changes cannot be avoided, instructions must be provided (see [Labelling and Instructions](#)) to describe alternate procedures ([IEC 60601-2-33](#) §201.7.9.2.101).

2.4 Subject Comfort

Housing design should allow for comfortable and ergonomic subject positioning, especially if prolonged stationary subject placement is expected during scans. Similarly, because ear plugs may not be adequate hearing protection for many MRI scanners, head coil housings should allow for the use of adequate headphone-type hearing protection (see [IEC 60601-2-33](#) §201.9.6.2.1 and §201.7.9.2.101, as well as [Sound pressure emitting devices](#)).

2.5 Connectors and Cable Management

Connectors and cables are as much of a challenge to address mechanically as they are electrically.

Similarly to the housing, cables must be electrically insulated from the subject and ensure [Single Fault Safety](#) (§8 and 13 of [IEC 60601-1](#), and §201.8 of [IEC 60601-2-33](#)). Extra thick or double insulation layers may be needed.

Cables exiting a housing must be fastened securely to the housing (e.g., using cable glands) to prevent electrical failures caused by the cable rotating or pulling out. Use strain reliefs whenever possible to maintain a minimum bending radius. Inside the housing, wires and cables must also be fastened appropriately to prevent failures due to vibration or displacement (§8.10 of [IEC 60601-1](#)).

If connectors are used instead of cable penetrations to bring conductors out of a housing, the connectors must be attached directly to the housing (e.g., using an appropriate bulkhead-style connector), not only to the PCB or to the electronics inside. This is the strongest possible mechanical connection and prevents failures due to flexing, twisting or snapping off the connector. When the two parts of the connection are mated there should be no exposed metal that can come in contact with the body (see [Electrical Insulation](#) and [Protection from Electrical Shock Hazards](#)).

Connectors should provide a retention or latching mechanism to prevent accidental unmating and unreliable connections. Connectors should be readily handled with gloved hands, and unmated without

the use of tools (§8.10.3 of [IEC 60601-1](#)). Unmated connectors must not compromise other safety features (e.g., by exposing high-voltage contacts).

Cables and connectors must also allow a safe and fast removal of a subject (§9.2.5 of [IEC 60601-1](#)) from the scanner in case of emergency (e.g., quench, cardiac arrest, etc.). This may require the use of connectors without locking mechanisms (e.g., snap-on connectors instead of screw-type) in cases where the cable routing prevents extraction of the patient table when cables are connected.

Standard methods exist for testing cable ([ASTM D4565](#)) and connector performance ([EIA-364 series](#)), including reliability (EIA-364 TP-09), aging and other factors that degrade performance over time.

3 Temperature Limits

Under all operating conditions, safe temperatures must be ensured by careful design of the electronics (e.g., [Voltage, Current and Power Rating Verification](#)) and enclosure. If active cooling is needed, it must be provided by ventilation or other means, bearing in mind considerations such as [Electrical Insulation](#), [Ingress Protection](#), [Grounding](#), etc.

3.1 MR-compatible Temperature Probes

Safety testing may require temperature measurements performed during scanning or in the harsh scanner environment, thus requiring temperature sensors that are immune to, and do not disturb, the static, gradient and RF fields. Wired sensors (e.g., thermistors, thermocouples) therefore have limited application and must be used with care. Fibre optic (e.g., Fluoroptic®) temperature probes are nonmagnetic and nonconductive, and are suitable for local temperature measurements in a limited number of points. The measurement electronics of fibre optic probes can be placed at a considerable, safe distance from the scanner. Infrared thermometers also allow single-point measurements at a distance, but, for accuracy, may need to be positioned close to the DUT and the surface emissivity of the material must be known. Similarly, infrared cameras (i.e., forward-looking infrared or FLIR) can capture temperature maps but compatibility with the B_0 field must be carefully considered to prevent projectile hazards and damage to the camera.

3.2 Surface Temperature Limits

Under idle and worst-case scanning scenarios the temperature of the surfaces that are likely to come into contact with the body must not exceed the maxima listed in §11.1 of [IEC 60601-1](#) (under most conditions 43°C). Surface temperatures can be measured readily during scanning using fibre optic temperature probes attached to a finite number of representative locations or suspected hot spots.

Specific surface temperature limits for MRI coils are described in [IEC 60601-2-33](#), Annex AA.1, subclause “Concerning 201.12.4.103.1 Limits of temperature”. This section specifies a maximum 4°C temperature rise following 20 minutes of scanning at the “highest clinical whole-body SAR” allowed by the scanner. A similar testing procedure in Ref. [2] uses 30 minutes of scanning at the 6-min SAR limit (see §II.C) for the respective body part.

3.3 Internal Temperature Limits

Temperatures within an enclosure must be kept within the safe range of materials and components to prevent failure, off-gassing, and potentially ignition. Fibre optic temperature probes (see §II.A.3.1) are

particularly convenient to determine internal temperature in this situation because they are non-conductive. In addition to allowing safe placement near high voltages they create minimal perturbations in RF fields even in close proximity to conductors. On signal-emitting phantoms [MR Thermometry](#) can also be used.

4 Material Properties

The following considerations apply generally to all materials and assemblies such as electrical components, connectors, cables, etc. While the first two properties below are available for a wide variety of materials, the remaining, MR-specific properties are more challenging to find. An ongoing effort to compile this information can be found in the [Opensourceimaging Wiki](#).

4.1 Mechanical

To prevent mechanical failure, the properties (e.g., stiffness, toughness, tensile strength, etc.) of the materials used in construction of housings, supports, etc. must be compatible with the mechanical loads that the structure will be subjected to (§9.8 of [IEC 60601-1](#)).

It should also be noted that some polymer materials commonly used in MR coils (e.g., PMMA) will snap, if not shatter, leaving pieces with sharp edges. It may be preferable to use tougher materials such as polycarbonate (PC) or FR4 (fire-retardant glass-reinforced epoxy laminate) which undergo plastic deformation (bend or delaminate) before breaking (if ever).

Because of the common use of polymers in MRI coil housings, further attention should be given to the heat deflection temperature (HDT), which describes the increased tendency of a material to deform as its temperature rises. Heat deflection temperature is measured according to the test procedures in [ASTM D648](#) or [ISO 75](#), and Ref. [2] recommends that materials with $HDT \geq 80^{\circ}\text{C}$ should be used (bear in mind that these conditions may also exceed the [Temperature Limits](#)).

4.2 Ignition Temperature and Flammability

Ignition, i.e., the starting of a fire, is caused by temporary or sustained temperatures that exceed the material's ignition temperature, which is measured according to [IEC 60695-2-13](#), [IEC 60695-11-10](#), [ASTM D1929](#), [ISO 871](#), [ISO 9772](#) and [ISO 9773](#). Reference [2] recommends using materials with ignition temperature $\geq 350^{\circ}\text{C}$. Many polymers satisfy this criterion, whereas PMMA, POM, some PVC, TPU and organic materials such as wood do not [9].

Flammability is the ability of a material to sustain burning after the ignition source is removed, and it must be given consideration, especially if any of the following are present:

- a. high voltages ($>50\text{V}$)
- b. fields that can induce sparks
- c. high temperatures ($>300^{\circ}\text{C}$)

Non-flammable materials (e.g., rated V0 according to [UL 94](#)) should be used, especially for parts that are near to, or come into contact with, high-power or high-voltage circuits and components. If flammable materials cannot be avoided, the associated risks must be assessed and mitigated (e.g., very small amounts, containment, etc.). If the flammability of a material is not known, or provided by the manufacturer, a flammability test ([UL 94](#), [IEC 60695-11-10](#)) is performed.

4.3 NMR Signal

Visible ^1H NMR signals are emitted by many polymers including soft plastic and rubber, but also some hard plastics. Even if outside the field of view, these signals can appear as artefacts folded into the image, and could be misinterpreted as pathological structures in the anatomy. Therefore the NMR signals emitted by coil materials at the Larmor frequency of the nucleus or nuclei of interest should be negligible. If absolutely zero ^1H signal is required then (per)fluorinated polymers (e.g., PTFE) can be used.

Some materials (e.g., polyamide (nylon)) can absorb water due to storage conditions, humidity, cleaning, etc. If this cannot be prevented by using appropriate materials or other design choices, waterproofing may need to be added.

Reference [2] recommends acquiring a short echo time (TE) image with a field of view large enough to cover the whole coil to identify potential signal sources. Alternatively, samples of the materials used in construction could be scanned individually. Information is also available in the literature [10], [11], although it should be noted that polymers of the same family (e.g., polyethylene) can vary widely between manufacturers and manufacturing runs. Therefore testing individual batches of material may be necessary.

Finally, there are anecdotal reports of signal crosstalk from nuclei with similar g (e.g., ^1H and ^{19}F)¹. In a ^{19}F measurement, signal from ^1H could be detected from regions of lower B_0 field (e.g., from the dielectric in the cables exiting the bore). In such cases the absence from the cables of *both* nuclei would need to be ensured.

4.4 Magnetism

Ferromagnetic materials introduce forces that can lead to projectile hazards as well as deteriorating image quality due to B_0 distortion (see, e.g., [NEMA MS 2](#)). Therefore, ferromagnetic materials should be avoided whenever possible, but, unfortunately, they are often present in a wide variety of components and assemblies such as cables, connectors, passive and active electronic components (typically as plating on conductors). Even alloys such as brass and austenitic stainless steel, which are nominally not ferromagnetic, are often found to be ferromagnetic. Brass can contain ferromagnetic impurities and stainless steel becomes ferromagnetic after cold working.

Small amounts of ferromagnetic materials may be acceptable in parts/components/devices if ALL of the following are true (see also [Ferro-magnetism of Components](#)):

- a. In the static magnetic field for which the assembly is intended, the magnetic force and torque are tolerable by the overall mechanical design (e.g., negligible);
- b. the magnetic force and torque do not damage the part and its support, including long-term fatigue of the device, solder or crimping joints, or other means of attachment;
- c. Additional hysteresis losses in the ferromagnetic material (by gradient switching and/or RF pulses) are accounted for in the overall heating analysis;
- d. The maximum magnetic moment of the ferromagnetic part is sufficiently small to produce a negligible B_0 distortion in the imaging region (depends on the application, pulse sequence, etc.; e.g., <1 ppm).

¹ In principle this could happen between any nuclei with different γ .

It must be noted that the effects in a, b, and d above depend on B_0 , and all (a–d) depend on the amount (volume or mass) of ferromagnetic material present. Therefore it is not sufficient (or, indeed, practical) to specify a maximum susceptibility (c) or permeability (μ) because, given a large enough amount, even a paramagnetic material can have measurable adverse effects (primarily d).

4.4.1 Testing for Magnetic Materials

Standard tests for torque and force on magnetic materials in the MRI environment include [ASTM F2052](#) and [ASTM F2213](#), respectively.

Standard tests for the presence of ferromagnetic materials also exist in the aerospace and connector industries ([NASA – GSFC S-311-P-10](#), [IEC 60512-24](#), [EIA-364 series TP-54A](#) and [TP-88](#)). However, these standards have not been adopted for MRI applications even though there is a need for standardization in the industry. In the few cases where information on magnetism is provided by component and device manufacturers, it is typically limited to maximum susceptibility or permeability.

Fortunately, some manufacturers have realized that it is more useful to provide magnetic moment. One goes as far as specifying complete magnetic moment vs. H field curves (e.g., [Ma-Com MA4P7461F-1072T](#)).

The MRI community would benefit if more manufacturers would adopt this practice. Until this becomes common, measurement methods such as those listed below will be used instead to assess the presence of ferromagnetic materials. Be advised that testing for magnetism of an unknown component or device using the field from an MRI scanner can be **very dangerous**. All MRI site safety procedures (e.g., [ACR MR Safety Manual](#)) must be followed at all times.

1. **Using a handheld magnet:** It is recommended to employ a strong rare-earth magnet (e.g., magnetization specification N40 or better) for this test. The mechanical force exhibited to the device under test (DUT) is proportional to its magnetization, the strength of the external flux density and its gradient. Therefore, ideal test magnets produce a strong magnetic field with a strong gradient – for instance a rod magnet. Be aware that such magnets can produce forces that are potentially dangerous for the person as well as for the device. Therefore starting with a small test magnet is advised. The DUT is best hung with string from the ceiling, while the magnet is slowly approached. If the device is attracted to the magnet, it is ferromagnetic. If implemented correctly this approach is sensitive enough to detect the small repulsion from a diamagnetic object.
2. **B_0 mapping:** Reference [2] recommends testing a new coil by acquiring a B_0 map of a uniform phantom and comparing it with the B_0 map from a standard coil to identify artefacts due to magnetic materials. Methods for B_0 mapping are described in [AAPM Report No. 100](#) and in the [ACR MRI QC Manual](#), as well as numerous journal publications. Light devices (e.g., <5 g) with weak magnetism can be tested similarly in the scanner. The device is placed at the position where it will be employed in the final construction. A preferably spherical phantom is positioned covering the imaging volume. Shimming and f_0 adjustment routines must be turned off. Then a B_0 map is acquired first with the device in position, then without. The action limit on the difference between the two maps should be set depending on the system (e.g., field and gradient strengths) and performance requirements for the intended use of the device (e.g., spectroscopy vs. imaging pulse sequences). The effect of the device should also be small enough that, if available on the scanner, automatic calibration routines (tip angle, f_0 , shimming, etc.) are still able to function reliably.
3. **Magnetic moment measurement:** With precautions similar to those of #2 above, it is possible to measure the magnetic moment of small parts quantitatively using the phase of MRI signals similarly to the methods described in [12], [13].

4.5 RF Permittivity and Losses

Materials also interact with the RF fields that are present, especially in locations with strong fields such as RF coil enclosures and high-power circuits. The RF interaction of a material with $\mu \approx \mu_0$ is dominated by the complex permittivity (dielectric constant) of which the imaginary part (alternatively the conductivity or loss tangent) describes losses that result in heating of the material. The loss tangent of common materials can range from below 10^{-3} (e.g., PTFE) to above 10^{-2} (e.g., wood) and much higher for carbon fibre composites.

The tolerable amount of loss is highly dependent on application. Losses can lead to degradations in SNR as well as RF heating of the material, therefore Temperature Limits must not be exceeded.

The relative permittivity of most common materials is below 5, resulting in minimal changes to the RF fields relative to those in free space. However, if extensive volumes of high-permittivity materials are used to manipulate RF fields intentionally (see §II.C.2.1.5), they should be incorporated into simulations including their properties to determine the resulting RF fields.

5 Labelling and Instructions

It is good practice to design devices to operate in the way that users expect them to (see the usability standards IEC 62366-1 and IEC 62366-2). Additionally, for many devices, information will need to be provided to the user to ensure correct use (see, e.g., §7 of IEC 60601-1 and §23 of Annex II of EU Medical Device Regulation 2017/745). The types of information provided include:

- Safety warnings (weight, electrical risks, etc.)
- Instructions for use (IFU) and maintenance (handling and operating instructions, connections, storage conditions, user manual, etc.)
- Identification of the equipment (name, identification number, manufacturing date, etc.)
- Range of application (system manufacturer, field strength, etc.)

It is good practice to attach appropriate labels to site-built RF hardware. Labels can be written in the language in use at the institution. There are also many standard graphical symbols (ISO 7010 for general symbols, IEC 60417 general equipment labels, ISO 15223-1 and IEC 60878 for medical device labels) that can be used to provide some of the above information quickly in a universally-accepted format.

Instructions for use for MR equipment are discussed in detail in §201.7.9.2.101 of IEC 60601-2-33, while for medical devices in general see §7.9.2 of IEC 60601-1, and §23.4 of Annex II of EU Medical Device Regulation 2017/745.

B. Safety of Electronics

- 1 Electrical Construction and Layout3
 - 1.1 Basic Design Considerations3
 - 1.1.1 Printed Circuit Board (PCB) designs.....3
 - 1.1.2 Attention to Parasitic Oscillations4
 - 1.2 Grounding4
 - 1.3 Protection from Electrostatic Discharge (ESD)5
 - 1.4 Ferro-magnetism of Components5
 - 1.4.1 Magnetic materials relevant for electrical device operation5
 - 1.4.2 Magnetic materials not relevant for electrical device operation5
- 2 Protection from Electrical Shock Hazards6
 - 2.1 Requirements.....6
 - 2.2 Common Means of Protection.....6
 - 2.3 Exposed Connectors.....7
 - 2.4 Grounding and Isolation Schematic7
 - 2.5 Insulation Testing Method.....7
- 3 Potentially Dangerous Devices and Toxic Materials8
 - 3.1 Requirements.....8
 - 3.1.1 Electronic Components Requiring Special Considerations Regarding Toxicity8
 - 3.1.2 Electro-optical Components8
 - 3.1.3 RF and HF Emitting Devices.....8
 - 3.1.4 Sound Pressure Emitting Devices.....8
 - 3.2 Validation and Testing Methods.....9
- 4 Voltage, Current and Power Rating Verification9
 - 4.1 Requirements.....9
 - 4.1.1 Voltage Ratings of Components9
 - 4.1.2 Current Ratings of Components.....10
 - 4.1.3 Power Ratings of Components10
 - 4.2 Validation and Testing Methods.....11
 - 4.3 Validation Through Electromagnetic Simulations.....13

4.4	Setting Safe Operational Limits: Coil Files.....	13
5	SAR Exposure.....	13
5.1	Requirements.....	13
5.2	Coil Detuning.....	14
5.2.1	Validation and Testing Methods.....	16
5.2.1.1	Bench Testing.....	16
5.2.1.2	Scanner Testing.....	16
5.3	Cable Current Protection: Padding, Cable Traps and Chokes.....	16
5.3.1	Validation and Testing Methods.....	20
5.3.1.1	Bench Testing.....	20
5.3.1.2	Scanner Testing.....	20
5.4	Disconnected Coils and Accessories.....	20
6	Auxiliary Device Considerations.....	21
6.1	Requirements for Medical Power Supplies.....	21

The recommendations in this chapter apply to the electronics of all RF coils and associated RF devices, including:

- Transmit, transceive, and receive coils and arrays
- Tuning and matching circuitry
- Cables
- Cable traps
- Scanner interfacing electronics

The chapter contains:

- Requirements
- Limiting values
- Recommendations for testing procedures

The main goals of this chapter are to provide guidance, means for managing risks and documenting safety to:

- Prevent electrical shock hazard to technicians, operators, and subjects in particular.
- Prevent overheating or ignition.
- Prevent critical break-downs during operation.
- Prevent risk escalation from potential malfunctions.

1 Electrical Construction and Layout

1.1 Basic Design Considerations

MRI RF coils are resonant structures with an inductance (L) and a capacitance (C), which are tuned to a certain resonance frequency (usually the Larmor frequency of interest). Basic layouts and various designs for MRI RF coils or NMR probes are found in a large number of specific articles and books. A comprehensive list cannot be provided in this guide, but some general references on the topic include [8], [14]–[20] as well as numerous articles (parts A–D) in [21].

To guarantee the highest possible level of protection for research subjects and operators, along with ensuring the intended function, the IEC 60601-1 standard defines both general and technical requirements for manufacturers, and therefore serves as a reference guide for safety in medical electrical equipment and systems.

Section 4.7 of IEC 60601-1 requires Single Fault Safety, i.e., that at least two means of protection (IEC 60601-1, §8.5.1) be provided for both subject and user (operator) from hazards like electrical shock (§8). Specifically, if one means of protection fails (i.e., a single-fault condition, SFC), additional means of protection must remain effective for the service life of the equipment, or the initial fault is detected so that corrective action can be taken.

For MRI coils and their supporting electronics (e.g., PIN diode bias, preamp power supply), it is important to consider carefully the (air) clearances, creepage distances, outer insulation and reduced leakage currents or unwanted electrical discharges (see Protection from Electrostatic Discharge (ESD)).

Outer insulation (housing, discussed in detail in Part II.A, Electrical Insulation is the most common method of providing protection from electrical hazards. If needed (e.g., to provide air openings for cooling) the standard further defines:

- **Clearance distance:** The shortest distance between two contacts outside a solid insulation body.
- **Creepage distance:** The shortest distance between two contacts along the surface of an insulation body.

For exact values for clearance and creepage distances as means of protection, refer to the appropriate sections in IEC 60601-1, §8.9 Table 12 (patient protection) and Table 13 (operator protection).

The clearance distance is intended to protect against high field strengths that can generate an electric arc in air between the two contacts. This can damage individual components (e.g., ICs, capacitors, connectors), but also endanger the well-being of patients (subjects) and operators, may cause burns, peripheral nerve stimulation and even cardiac arrest.

Creepage distances protect against the tendency of insulation to deteriorate gradually due to dust or dirt deposits, as well as moisture which, e.g., can condense onto any component following changes in temperature. This can result in flow of leakage currents on the surface of the insulation or component body, resulting in a partial or complete loss of insulating function. The consequence may be an electric shock, with similar effects as mentioned above.

1.1.1 Printed Circuit Board (PCB) designs

Devices for MRI can include many electrical and mechanical components and modules. While IEC 60601-1 is much broader and applies to all electrical medical devices, the IPC-2221B standard is a

generic standard for the design of PCBs (e.g., rigid, flexible, MCM-L), and is used for design layout, parts lists, materials, mechanical and physical and electrical properties, thermal management and much more. Clearances between electrical conductors to prevent arcing are discussed in §6.3 of [IPC-2221B](#). Table 6-1 provides guidelines for the minimum spacing between electrical conductors (internal and external) for given DC and peak AC voltages. Bear in mind that this spacing can be closer than the clearance and creepage distances defined above when they are *not* providing a means of protection.

Furthermore, the standard provides general assembly and placement guidelines (§8), including minimum clearances between component leads or components with metal cases and any other conductive path.

1.1.2 Attention to Parasitic Oscillations

During design and construction of RF hardware that includes active (amplifying) devices, it is prudent to search for any parasitic oscillations caused by unintended coupling between electronic components (e.g., input and output of preamplifiers). This can lead to loss of MR signal (degraded amplification) or functionality (e.g., detuning).

Oscillations are identified using a sniffer probe connected to the input of a spectrum analyser. Because of intermodulation and other nonlinear effects all parasitic oscillations should be eliminated. Those within a few percent (e.g., 10%) of the Larmor frequency will especially affect the MR signal or saturate devices further down the receive chain.

1.2 Grounding

Most MR systems require special attention to ground connections and grounding points. Creating ground loops can cause severe malfunctions or harmful effects (e.g., heating, eddy currents, etc.), due to voltages induced in these ground loops by gradient pulses. Connections between DC and RF grounds, and between ground signals in connectors should therefore be avoided or engineered carefully. This can happen, e.g., between transmit (Tx), receive (Rx), coil ID code or PIN diode grounds ([Figure 2](#)).

To measure the heating and vibration (forces) introduced in ground loops due to strong gradient pulses (gradient eddy currents), it is recommended to switch off the RF transmit/receive and apply a dedicated high-power gradient sequence, and measure the heating using an MR compatible infrared thermometer (see Part II.A, [MR-compatible Temperature Probes](#)). Bear in mind that gradient coil design and certain scan parameters (FOV, slice thickness, TR, TE, number of slices, slice orientation) have an effect on the induced eddy currents.

The MRI vendor may have further advice, requirements, or recommendations. Additional information regarding gradient-induced heating and vibrations can be found in the active implantable medical device (AIMD) test standard ([ISO/TS 10974](#), Annex A).

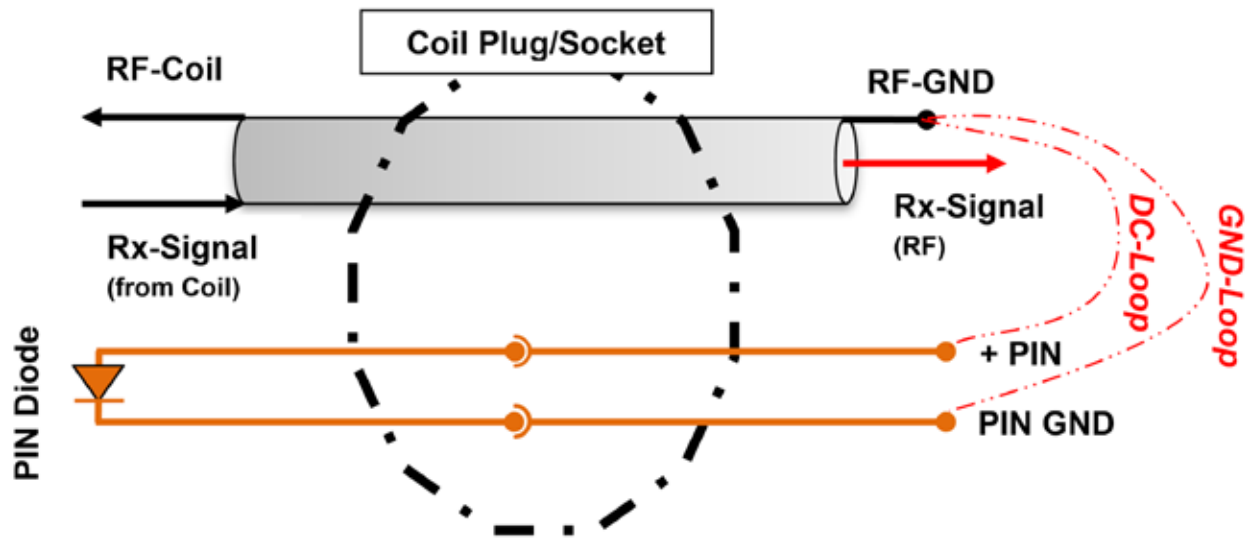


Figure 2: examples of ground loops.

1.3 Protection from Electrostatic Discharge (ESD)

The performance characteristics of most electronic devices are guaranteed only if the device is never exposed to an ESD event during its life cycle. This includes the manufacturing process as well as assembly and operation. Therefore, it is prudent to include ESD protection in signal-level circuits wherever possible to prevent damage to sensitive devices like RF preamps and logic circuits. Protection is recommended at all connections, especially those accessible by the operator and those used for routine operation and maintenance. Standard testing procedures for ESD immunity include those of [IEC 60601-1-2](#) and [IEC 61000-4-2](#). The MRI system's manufacturer and [FDA Guidance 19011](#) should be consulted for specific requirements.

1.4 Ferro-magnetism of Components

Many electronic devices and components are not MR-compatible since they contain ferro- or ferri-magnetic materials. The use of ferro-magnetic material in electrical and electronic components can be divided into two subcategories:

1.4.1 Magnetic materials relevant for electrical device operation

The material is deployed due to its magnetic properties, such as for increasing inductance in ferrite cores; blocking (choking) high frequency signals as in ferrite beads; transformer cores for RF, power electronics, isolators, etc.

Such materials cannot generally be employed close to MRI scanners. In the bore or its fringe field, the device would likely be operated out of its specifications (i.e., saturation of the material in the presence of a static field) and, generally, all labelling and specifications (e.g., permeability) from the vendor are invalid in this situation.

1.4.2 Magnetic materials not relevant for electrical device operation

This includes materials introduced as diffusion or oxidation barriers (e.g., nickel underplating) or as mechanical components (e.g., plated or clad steel). The safety issues and other effects of these

materials are described in detail in the Magnetism section of §II.A.

2 Protection from Electrical Shock Hazards

2.1 Requirements

The subject, but also MR technicians and personnel, must be protected from electrical shock hazards at all times. The most common scenario where this can happen is a break-through of high voltages from the mains by a failure in the power supply or a surge event while connecting lines to the device. The voltage supplies and signal lines provided by the scanner manufacturer do provide adequate protection and should be utilized whenever possible. However, if the experimental setup does require additional conductive cabling or even external power or signal sources, then those added components must be very carefully safety validated both against possible electrical shock hazards and RF hazards like common-mode currents. Specifically, it is essential that cables (including those for low-frequency or DC signals) be fitted with appropriate high frequency cable traps (see §II.B.5.3), particularly if they pass through parts of the RF body transmitter. Cables running the length of the RF transmitter should be avoided entirely since they pose significant risk to the subject and likely will negatively influence MR data stability and quality. As a general rule, direct contact of such lines with the subject must be prevented - i.e., by routing cables at a safe distance or by creating physical barriers. Since the inherent isolation of a subject's skin in the scanner can be compromised (e.g., by ECG leads, venous or arterial lines, skin lesions, etc.), the discharge current must be limited when touching a connection. These requirements (e.g., for a ground connection) are more strict than for general consumer-grade devices.

The design review shall document which safety features are engineered into the system and should demonstrate that foreseeable malfunctions do not endanger the subject or operator.

2.2 Common Means of Protection

Electrical shock hazards are described in detail in §8 of IEC 60601-1. In some cases, the standard defines different requirements for methods of operator protection (MOOP) and methods of patient protection (MOPP). Some specific means of protection that are often considered for coils and other RF devices include:

1. The isolation barrier must exhibit a dielectric strength according to Table 6 in §8.8.3 of IEC 60601-1.
2. Connections to multiple reference grounds (ground loops) must be avoided at all cost (see Grounding). All connections to mains grounds must be isolated (potential separated). A protective ground connection must be provided (§8.6) to all non-energized metal parts of the housing and installation (metallic housing box, rack etc.) to protect from fault currents by shunting them to ground through a low-impedance path.
3. If a connection to the mains and other external power sources are provided, the subject must be protected against discharge currents in case of an isolation breakdown to the mains voltage by at least two independent means of protection. Furthermore, the discharge capacitance must be medical grade. It is hence recommended to deploy only medical grade power supplies (see Requirements for medical power supplies) offering both features.
4. Overvoltage protection (e.g., using varistors) must be provided to all parts that could be energized by a voltage break-through or surge.
5. Parts of the device that the subject can touch must be fully isolated to limit currents through the subject. According to Table 3 in §8.7 of IEC 60601-1, the maximum allowed current discharged over

the subject depends on the type of device. Typical MRI scanners are classified (§8.3 of Annex A) as type B devices (only unintended delivery of current to the body) and BF devices if there is an intentional electrical connection such as ECG or EEG electrodes.

2.3 Exposed Connectors

Non-mated or exposed connectors can pose a potential safety hazard due to leakage currents. Even if the probability of touching an exposed connection is negligible, there are limits imposed on the voltage to earth and the stored energy, as described in [IEC 60601-1](#), §8.4.2.

Connectors should have two means of protection to ensure the leakage current limits of [IEC 60601-1](#), §8.4 are not exceeded. These means of protection can include solid insulation, creepage distances and air clearances, and protective earth connections.

2.4 Grounding and Isolation Schematic

A grounding and isolation schematic ([Figure 3](#)) describes how the grounds are connected to the infrastructure and how the isolation barrier acts as a means of protection to the subject and operator. All electrically conductive components, cables, and surfaces are shown in the schematic with their connections to power supplies and signal lines, including protection components such as diodes, fuses and varistors. The schematic furthermore documents the isolation barriers provided by the power supplies, isolators and housing.

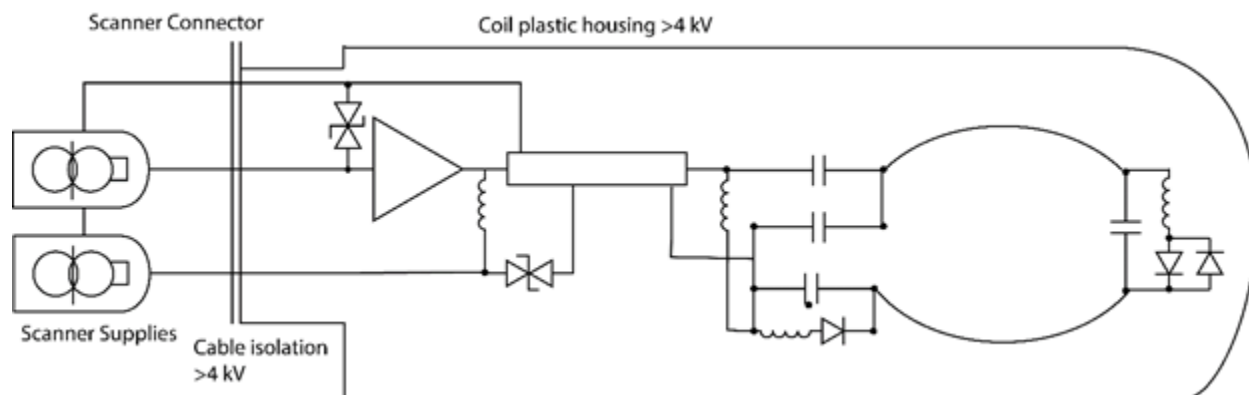


Figure 3: Example of a grounding and isolation overview.

2.5 Insulation Testing Method

The dielectric strength of insulation that has a safety function is tested as described in §8.8.3 of [IEC 60601-1](#). A typical test would be performed by connecting all conducting pins of the coil connector (grounds, signal and metallic alignment pins) to one terminal of the high-voltage test supply. The coil is wrapped in aluminum foil and connected to the second terminal of the test supply. A test voltage according to Table 6 of §8.8.3 is applied between the connector and the aluminum foil. The insulation fails if there is a rapid increase of sustained uncontrolled current flow (i.e., breakdown).

3 Potentially Dangerous Devices and Toxic Materials

3.1 Requirements

Materials built into the device must be non-flammable, non-toxic and not decompose into or evaporate toxic products to which humans can be exposed (see §II.B). Also, potential emission of hazardous levels and intensities of light and sound pressure waves must be considered.

3.1.1 Electronic Components Requiring Special Considerations Regarding Toxicity

Components such as batteries, electrolytic, tantalum or super-capacitors contain hazardous substances and are prone to bursting, and therefore require separate considerations for safe operation. The following are typical situations that can lead to ignition or generation of toxic gases, and must be excluded by appropriate design strategies such as:

1. Reverse polarity protection.
2. Overvoltage protection.
3. Protection from excessive charging currents.
4. Overheating protection.

3.1.2 Electro-optical Components

The risk for eye damage, potential burns and ignition of fire induced by electro-optical components such as light bulbs, LEDs and lasers needs to be considered according to the power and wavelength emitted.

For lasers and LEDs it is recommended to adhere to the revised classification system ([ANSI Z136.1](#)). Special considerations are required for laser light exceeding class 3B even if guided in an optical fiber. In particular the case of open optical connections and a (partially) broken fiber must be considered. Class 4 lasers require further safety systems such as a key switch and safety interlock.

3.1.3 RF and HF Emitting Devices

Devices emitting RF and HF power (besides MR transmitter coils), such as radio, WiFi, Bluetooth, wireless power devices etc., must be included into the SAR safety validations to avoid excessive tissue heating by direct emissions as well as by coupling to the RF transmission pulses of the scanner.

3.1.4 Sound Pressure Emitting Devices

Strong sound pressure waves can have highly adverse health effects. For temporary exposures the risk of damaging the auditory organs and causing tissue disruptions/cavitation or overheating needs to be considered. RF devices may add acoustic noise by interactions with the gradient fields, e.g., through ground loops and currents induced in RF shields. These interactions must also be minimized for other reasons like signal quality.

Reference [22] provides an extensive, detailed review of acoustic noise exposure in MRI, as well as reviewing various standards and regulations applicable in numerous jurisdictions. If acoustic noise needs to be considered in detail (e.g., a design that enhances existing scanner noise or creates additional noise), [IEC 60601-1](#) specifies a limit of 80 dBA of exposure over 24h, which is increased by 3 dB for every halving of the exposure time. This means that for a duration of, say, 1h, the maximum increases to 94 dB. [IEC 60601-2-33](#) §201.9.6 also indicates an absolute maximum unweighted sound

pressure of 140 dB relative to 20 nPa, measured according to NEMA MS 4. Section 201.7.9.2.101, part d) includes guidance on instructions for use relevant to acoustic noise, and specifically requires that hearing protection must be worn if sound pressures ≥ 99 dBA are possible.

If considerable amounts of ultrasound waves are emitted into the body, additional considerations must be made regarding safety with respect to tissue heating and cavitation. Section 9.6 of IEC 60601-1-1 covers acoustic energy and further discussion is found in [23].

3.2 Validation and Testing Methods

Schematics, bill of materials and devices must be inspected for potentially dangerous components. If these components cannot be avoided, their safety mitigation must be documented.

It must be verified that the components operate within their tolerances and temperature range. The worst-case exposure of the human subject and technical personnel to the hazards in §II.B.3.1 must be documented and, if potentially exceeding safety limits, validated experimentally.

4 Voltage, Current and Power Rating Verification

4.1 Requirements

For a safe and long-term stable operation of the device, it is of crucial importance that all components in the design are operated within their specified limitations. Although the components might operate over their rated values in the short term, degradation over extended periods of time cannot be excluded. Since long term tests cannot typically be performed for research devices, staying within the specified limits is highly recommended.

4.1.1 Voltage Ratings of Components

The design must specifically ensure that all components are operated within the specified voltage ratings.

In typical receive coil designs only the components in the detuning circuits are subjected to high voltages. For a typical LC tank circuit this includes the capacitor, the inductor, the diode/switching element and the feed chokes. The voltage across the RF high impedance section of the receive coil can be estimated via the total induced voltage at full power transmission ($B_{1,max}$). For a loop coil of area A operating at frequency f , Faraday's law yields:

$$V_{max} = 2\pi f B_{1,max} A. \quad II.1$$

Note that, at resonance, the current in the inductor and capacitor is Q times the current driven by this voltage in the conductance of the circuit (Q is quality factor of the LC circuit). Therefore, L and C must be rated for this higher current.

For transmitter and transceiver coils, every component is likely subjected to high voltages and must be analyzed. Voltages are best analyzed using a circuit simulation, but in some cases the peak transmit currents (and thus voltages) can be estimated from the expected RF B_1 fields using analytical formulas (e.g., Biot-Savart law).

Furthermore, components such as capacitors, diodes, transistors and resistors employed outside the RF circuitry (e.g., in the biasing) must be rated at least according to the voltage applied in the worst-case scenario.

4.1.2 Current Ratings of Components

Components must similarly be operated within their current ratings. In particular, power supply components such as regulators, current sources, etc. must be operated within their current limits. Even if the power can be handled, internal electro-migration effects might impair their long-term performance.

Passive components like capacitors also have a limited current carrying capacity which is analyzed analogously to their voltage handling capabilities.

4.1.3 Power Ratings of Components

In addition to limited current and voltage capabilities, all components can only dissipate a limited amount of power. This amount further depends on the thermal grounding (cooling) that is provided. Typically, these properties are expressed in terms of a maximum operating temperature in the device and thermal heat conduction out of the device. In a linear approximation, the temperature of a device that is cooled through a heat conductor given by

$$\Delta T = T_{device} - T_{cooler} = \Theta P_{dissipated}, \tag{II.2}$$

where T is the temperature of the device and the cooler, P is the dissipated power in the device at the top of the cascade and Θ is the thermal conductance of the thermal bridge that is considered ([Figure 4](#)).

Using Equation ([II.2](#)), the temperature estimation can be cascaded up to device internal parts that can typically not be accessed using thermometers or thermographs. Note however, that the assumption is based on the ambient temperature of the device that is typical inside the housing. This temperature must ultimately be verified by measurement.

The dissipated power in the device is generally calculated as the difference of power that goes into the device and the power that it re-emits. For most linear, two-terminal devices, the dissipated power can be estimated by the current x voltage product at its terminals.

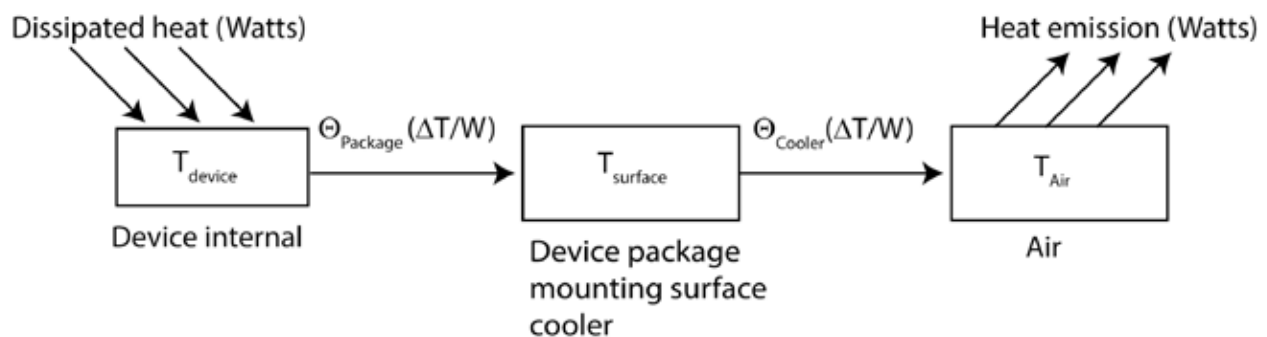


Figure 4: Thermal heat conduction diagram.

Heat dissipation from blocking circuits and preamplifiers can produce significant heat that can increase the surface temperature of a coil's housing (see [Surface Temperature Limits](#)). The estimated heat

dissipation in active and passive detuning circuits and other coil components (such as preamplifiers) can be estimated before testing a coil on the scanner [24].

4.2 Validation and Testing Methods

An important concern regarding the voltage rating is the RF voltage induced by high power RF pulses which might induce arcing or breakdown of dielectric insulations. The resulting discharges pose risks to the subject and the coil as well as to other components of the system that can be irreversibly damaged. Therefore, the voltage handling capabilities must be tested by exposing the device (transmitter or receiver) to at least the maximum rated peak power or B_1 , respectively (Figure 5). It is advised to consult the vendor’s recommendations on the (excess) power for testing since this is related to available power and the safety measures/concept implemented on the MRI platform. In the case of a transmitter to be tested, the power is sent to the port; in the case of a receiver, the surrounding transmitter must be set to produce the maximum peak B_1 possible. Ideally a triangular pulse is played out reaching to the peak power (Figure 6). Amplitude linearity and break-downs can then be directly assessed on the response curve. Alternatively, a series of block pulses with increasing amplitudes can be employed. A pick-up loop is placed inside the coil and its output is recorded using an oscilloscope or a spectrum analyzer with time domain demodulation function (Figure 5).

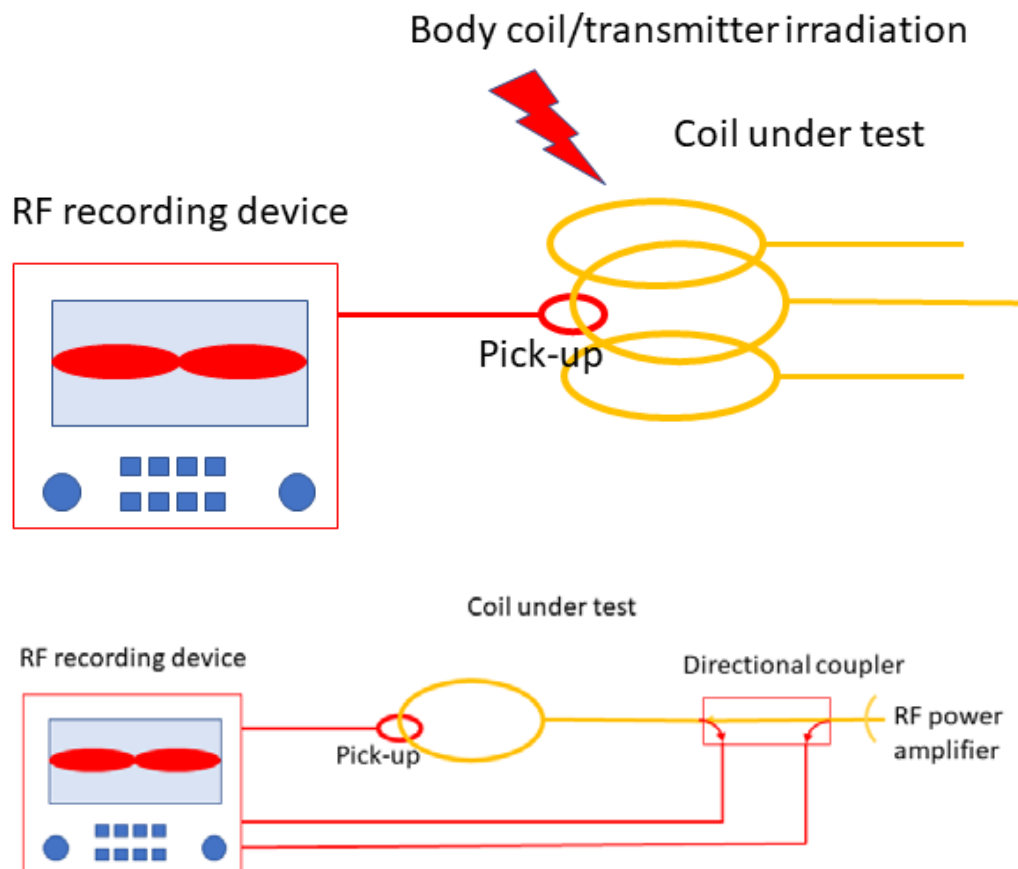


Figure 5: Setups for RF power withstanding tests, a) for devices (e.g., receive-only coils) that are not connected to the transmit chain, and b) for devices that are.

To test the linearity of the system the RF pulse is recorded with an RF-capable oscilloscope or spectrum analyzer with time-domain demodulation function. For receiver coils and other devices the measurement input is captured using a pick-up loop, while for transmit coils, the measurement input is obtained using a directional coupler in the transmit chain (see [Figure 5](#)). The baseline linearity and stability of the RF transmission chain should first be measured without the device under test (DUT) present in the bore or the transmission chain.

With the DUT present, the amplitude of the signal from the pick-up coil or directional coupler ideally follows the exact envelope of the applied test pulse without compression and remains stable over many repetitions. If the signal is compressed significantly, the biasing voltages of the active detuning circuits may be insufficient. Jagged, spiking or unstable traces are a suggestive sign for arcing or voltage breakthrough in the coils. The test should be aborted to avoid damaging components and the RF transmission chain: such a device cannot be put into service. Arcing can also be located visually by spotting its corona or signs of burns around or on the components following the test. It is worth noting that operating under such conditions can endanger the device by generating excessive voltage and current transients as well as heating. Furthermore, broadband signals can be produced which can bypass protective circuits of the system. The insulation of devices exposed to such arcing events can be irreversibly damaged. As a consequence, the affected device no longer meets its specifications and should be replaced. The test should be performed over an extended amount of time (e.g., 20 min) to account for thermal- and wear-induced insulation failures.

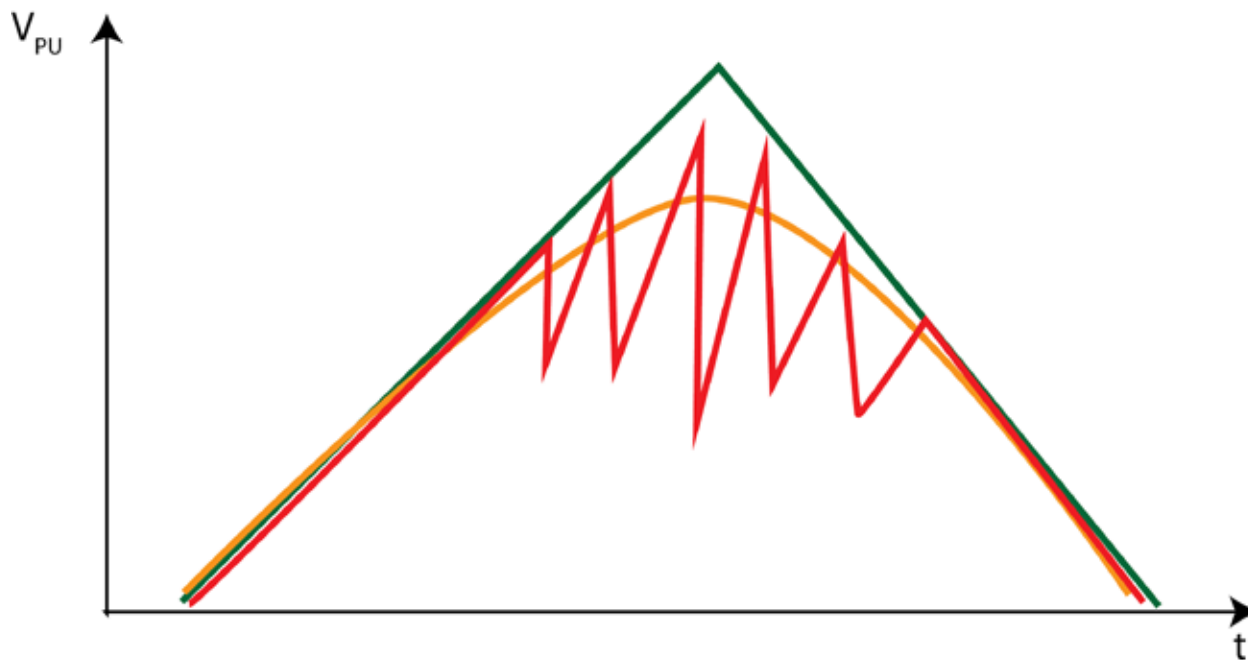


Figure 6: Amplitude traces of signals acquired during a voltage handling test. Green is the ideal response to a high power triangular pulse. Orange shows a typical compression behavior. Red indicates severe arcing.

Power rating of components and devices is typically validated by ensuring operation in a safe range of temperatures. For this, the device is first operated for 20 min without application of external RF pulses. In this time the local temperature of the critical devices is monitored (see [MR-compatible Temperature](#)

Probes). Thereafter, the device is exposed to full RF transmit duty cycle for another 20 min after which the temperature is measured again.

The temperature can thereby be measured using thermographs if the covers can be removed quickly enough. Otherwise, local sensors that do not interfere with the RF fields (e.g., optical or high impedance thermo-probes) can be employed (see MR-compatible Temperature Probes).

It must be emphasized that the measured surface temperature must be low enough to ensure a safe internal temperature of the device (see Internal Temperature Limits).

4.3 Validation Through Electromagnetic Simulations

Electromagnetic simulations (see §II.C) are important in the final validation of the proper operation of the RF coil and are used to evaluate location and tissue-specific RF power deposition. By comparing the simulated B_1 maps - ideally under consideration of the measured losses in the cables, power splitters, and all the components before the coil ports in the simulations - with the experimentally acquired B_1 maps, proper operation of all the coil components, particularly the decoupling circuits of the receive insert and the tuning and matching of the transmit coil as well as all the components in the transmit path can be assured.

It is recommended that the comparison between simulations and experimental data be performed in a phantom and that the exact phantom geometry and material properties be carefully measured. Specific details on simulations and validation are provided in §II.C.

4.4 Setting Safe Operational Limits: Coil Files

Many vendors allow for coil-specific files to be created that include relevant safety information for the applicable coil. Once the hardware power operational limits are determined by the components of the coil, bench tests, and the tests in the scanner, these limits should be programmed (with conservative Safety Margins) into the coil files in the MRI scanner. The format of the files is vendor-specific and usually includes short- and long-term power limits that can be applied to the coils. These limits are distinct from the Online SAR Supervision thresholds and are specific to protect the hardware from high power exposure. Where applicable, the correct biasing scheme (polarity) of PIN diodes should also be included in the coil file to ensure correct operation during both transmission and reception. It should also be verified by a specific test that the system correctly recognizes the coil, and that appropriate errors are generated if an incompatible configuration (e.g., only one connector is mated in a coil that requires multiple connections, or incompatible coils are plugged in simultaneously) is detected. Vendor guidelines, when applicable, should be followed to determine required parameters for the coil file and other files and settings that control coil combinations and exclusions. When coil files are written, their correct usage should be described in the coil's manual.

5 SAR Exposure

5.1 Requirements

In no event may the subject be exposed to SAR levels that could cause tissue damage or burns. The global and local SAR exposure produced by transmitter coils for producing the RF excitation field is the topic of the RF Safety section (see also NEMA MS 10); however, in principle every conducting material can carry RF currents and hence must be considered (as do materials that support displacement

currents). A particular concern is the cabling connecting the coil and the behavior of receive arrays during transmit operation. This is because these components are typically not included in the field calculations and SAR estimations of the transmitter. The electronics must hence ensure that in no event, large RF currents can flow on these structures, since they could in turn alter the RF electromagnetic field of the transmitter and induce high SAR values in near-by tissue, including outside the volume of the transmitter. To counter these effects, cable currents are suppressed by RF traps and currents on receive coils are blocked by detuning circuits (see §II.B.5.3 below).

These considerations apply to coils as well as other inserts and accessories that are used with increasing popularity, especially in research sites. Indeed, the transmit RF field is readily modified by the presence of devices such as high-permittivity dielectrics, metamaterials, EEG electrode caps, TMS coils, HIFU transducers, etc. The RF safety of operating such devices in the MR scanner can be analyzed by performing risk analysis, RF simulations and measurements, as well as introducing mitigations like RF traps where appropriate. Use tests and procedures appropriate to the specific device and situation.

5.2 Coil Detuning

Receive coils that are not active during the transmission phase must be detuned [25]–[28] by blocking the current on the coil conductor using a high impedance. This is typically achieved by introducing a parallel-resonant trap (tank circuit) in series with the current on the coil conductor [26]. This trap circuit can be actively switched (by controlling the DC terminal voltages of a PIN diode, transistor, or MEMS switch) ON (in resonance) and OFF (non-resonant). Typically, this circuit is combined with a capacitor on the coil (for tuning) or its matching circuit ([Figure 7](#)). Reference [29] provides guidelines on the required blocking impedance (at 64 MHz) as a function of the surface area enclosed by the coil element. The impedance required at other frequencies can be extrapolated by accounting for the frequency dependence of Faraday induction.

If the circumferential length of the coil is significant with respect to a quarter of a wavelength, multiple traps may need to be distributed around the coil.

Coil detuning is an important example of the need to ensure there are at **least two independent mechanisms** for detuning of the coil and that the failure of the primary must be detectable (see [Single Fault Safety](#) and [Basic Design Considerations](#)).

A typical implementation ([Figure 7](#)) employs a low-voltage driven active detuning. To detect the failure of the primary PIN diode, the forward current and the reverse voltage are monitored. As a fallback measure, a passive detuning circuit is employed [26], [27]. The diode pair switches on if the voltage across their terminals is high enough. Relatively fast acting PIN diodes, or a combination of PIN and Schottky diodes, can be used here.

Alternatively, the secondary detuning can be established by employing a fuse [30]. Since the fuse is not reversible, a failure of the primary circuit, leading to the destruction of the fuse, will be detected by an impaired coil sensitivity (low SNR and/or distorted pattern); hence, monitoring the diodes in the first circuit directly is not required. Note that the fuse must burn at a low enough RF current while also being able to withstand the voltage across its terminals (typically the same as derived in the [Voltage Ratings of Components](#) section above). Otherwise the fuse might not blow or be shorted again by an arc.

It is recommended that the tuning of both the transmit and receive coil, with and without activating the detuning circuits, be recorded using a network analyzer. Changes in tuning can be evaluated throughout the testing period of the coil to verify the integrity of the circuits.

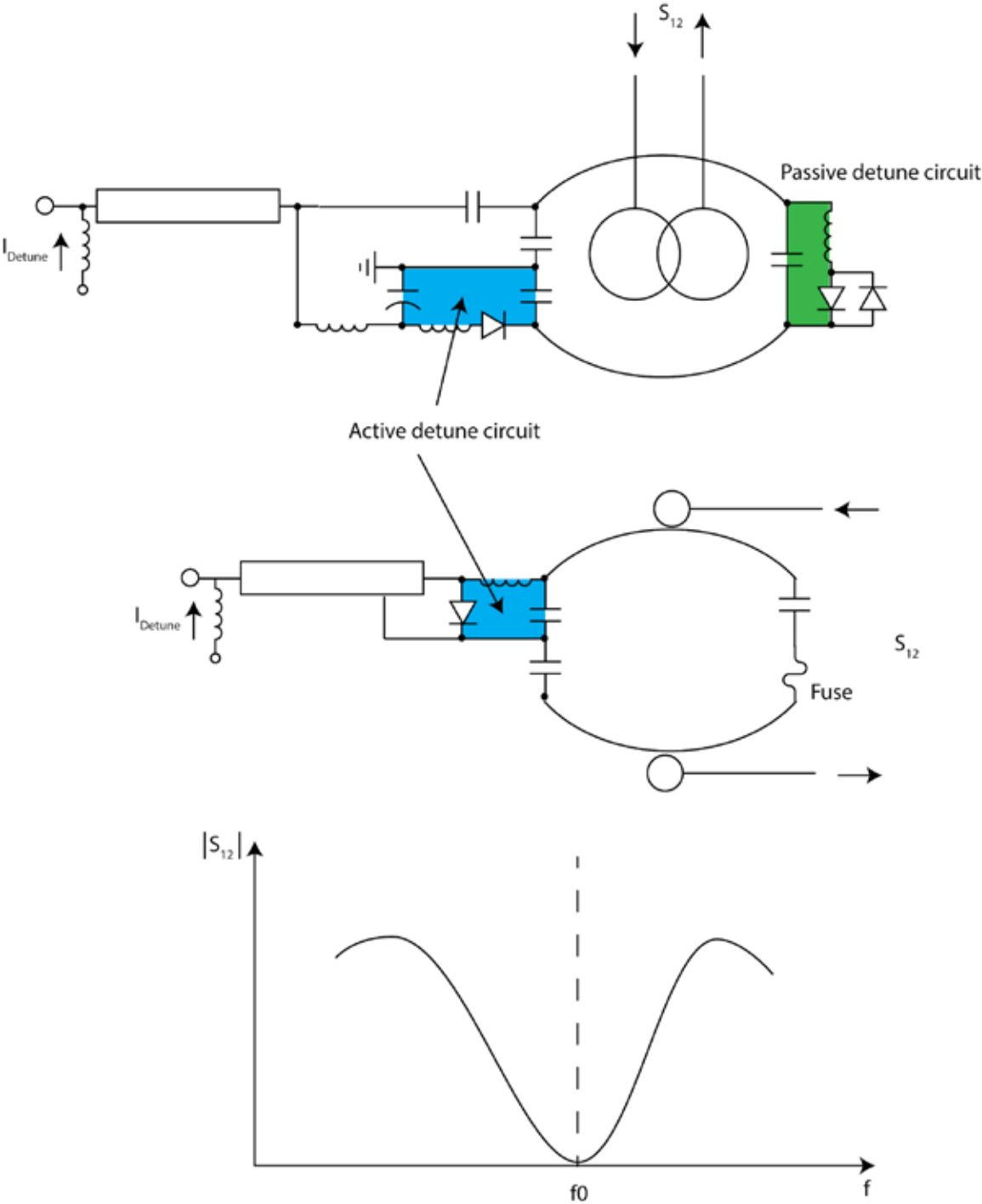


Figure 7: Two frequently employed low-voltage detuning topologies, including example placements of the VNA pickup probes and measured S_{12} response curve. The blue and green areas mark the circuit meshes that form a parallel resonance during transmission, whose high impedance blocks the current in the coil.

5.2.1 Validation and Testing Methods

5.2.1.1 Bench Testing

The effectiveness of the detuning is tested by measuring the current that can be coupled into the coil conductor [30]–[32]. For this, two pick-up loops are used, one to transmit and one to receive ([Figure 7](#)). The coupling between the two loops is measured using a VNA and it should only be minimally altered by the presence of the coil. Ideally, the two pick-up loops are decoupled from each other in free space, either by adjusting their overlap or by making them small and physically separated. Then the pick-up loops are brought close to the coil and the coupling is measured. A trace similar to that depicted in [Figure 7](#) indicates that almost no current flows at the frequency of operation.

Passive detuning circuits can be tested similarly by temporarily shorting the crossed diodes.

5.2.1.2 Scanner Testing

On the scanner the detuning is tested by validating that the distribution and uniformity of the excitation are not significantly altered by the receive coil. For this an image or B_1^+ map of a low conductivity and dielectric phantom (e.g., oil) filling the subject space is acquired using the volume transmitter as a transceiver. This measurement is repeated with the coil under test present and compared to the B_1^+ map obtained in absence of the coil. There should be minimal differences between the two maps (see [29]). In addition to altering the excitation field, ineffective detuning of the receive coil can also cause a large change in the RF power or voltage required to produce a given flip angle. This value should therefore be recorded with and without the coil under test.

Ineffective detuning can likewise result in local heating of receive-coil components. Methods for determining surface temperature rises during scanning and their respective limits are described in [Surface Temperature Limits](#) in §II.A. Local temperatures should be measured with infrared thermography to ensure significant heating of components has not occurred. Thermocouples or other local sensors can alternatively be used to assess the temperature rise at predetermined positions. Detailed methods for characterizing RF coil heating are described in [NEMA MS 14](#).

5.3 Cable Current Protection: Padding, Cable Traps and Chokes

Cables, coaxial RF lines, DC supply or control signal lines, can carry substantial, unwanted RF currents as common modes or so-called sheath waves ([Figure 8](#)) [8], [31]–[35]. Coil imbalance or exposure to the field of the transmitter is a typical cause of common-mode currents for single-channel transmitters. Common-mode coupling from another transmitter port, typically originating from potential differences between the grounds, as in quadrature birdcage coils and transmit arrays, can also cause common-mode RF currents to flow on the electrical cabling. The cabling of receiver arrays can pick up high RF currents as a result of the high electric fields produced by the transmitter. These electric currents need to be suppressed to guarantee a stable and safe operation [31], [32]. Furthermore, the subject needs to be protected against the strong SAR and associated burns that can be caused by currents flowing on conductors or cables routed near to, or in contact with the subject [8], [36]. Strong capacitive coupling between cables and subject is a well-known cause of MRI injuries and can be avoided, e.g., by placing them farther than ~1 cm from the subject through appropriate routing, or by covering the cable with foam padding when that distance cannot be guaranteed by other means.

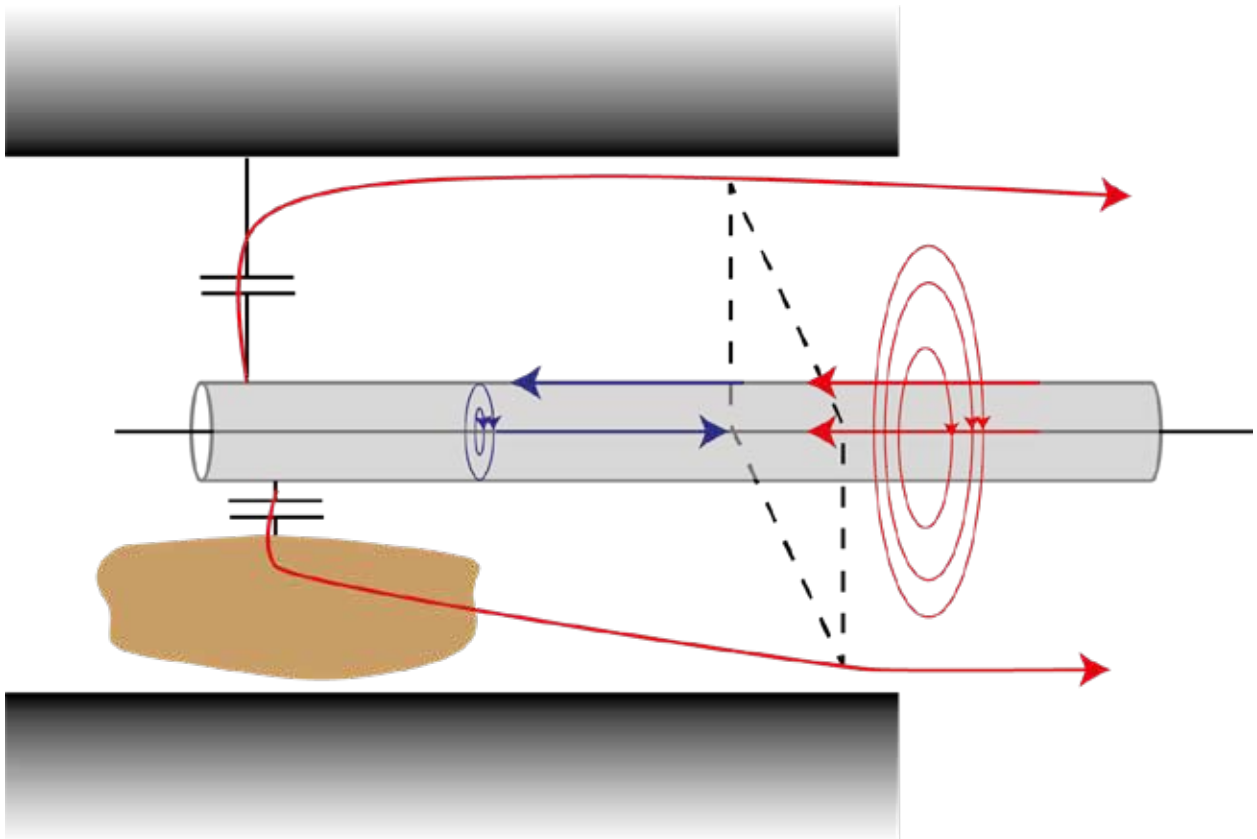


Figure 8: Schematic of common mode currents. A coaxial cable or signal lines can carry two spatial modes. The balanced mode in which the inflowing current on one conductor equals the outflowing on the other (blue arrows). There is no net current flowing through sectional planes of the cable (dashed rectangle). In contrast, the common mode or sheath waves (red arrows) have a return current path outside the cable (including through the subject). Consequently, there is a net current flowing through the sectional test plane and also a corresponding magnetic field (red circles) outside the cable.

Common-mode currents can be suppressed by introducing high impedance sections for RF currents [37]. For supply and low-speed signal lines (frequency $\ll f_0$) choke inductors can be employed (e.g., [Figure 9.5](#)). Their inductance generates a net high impedance for high frequencies:

$$|Z| = \omega L. \quad \text{II.3}$$

For most efficient implementation, RF chokes are chosen that have a self-resonant frequency close to the RF frequency, maximizing the net impedance to RF currents.

On high-frequency lines, the common modes are blocked by using the field external to the cable to induce a high impedance. These “RF traps” or “cable traps” offer narrowband blocking abilities [18], [38] and take advantage of the fact that the balanced modes do not have strong fields outside the cable, so they are essentially unaffected in contrast to the common mode currents. Cable traps are ubiquitous in commercial RF coils and are a necessity in most custom RF hardware, including both transmit and receive coils. The required inductance, L , can be created by coiling the coaxial cable, then forming a

parallel resonance by connecting a capacitor ([Figure 9.1](#)). The blocking impedance can be expressed as

$$|Z| = Q\omega L, \quad \text{II.4}$$

where Q is the quality factor of the resonance. In this type of trap the resonator is galvanically coupled to the cable [18], [31], [32]. Since the resonant circuit can also pick-up external fields, the coiling is often arranged to suppress the generation of external fields, i.e., in a figure 8 or a toroidal configuration. Shielding can also be employed to reduce the coupling of the trap to the transmitter field.

Sleeve or bazooka traps ([Figure 9.2](#)) [18], [38] offer very good shielding properties. However, because of the low inductance and very high Q they are relatively narrow band and therefore must be tuned with care.

A third type of traps relies on inductive coupling to a tank circuit. These traps are most often employed to block current on multi-conductor cables. These floating traps can be realized either by coiling an outer shield or sleeve of the cable ([Figure 9.3](#)) [39], or by surrounding the cable by a resonant cylinder ([Figure 9.4](#)) [39]. Note that current flowing differentially on lines within the shield are not suppressed in this configuration.

Cable traps are typically placed at the connection port(s) of the coil and in regions where high shield currents may exist (for example, in regions exposed to high electric fields). Cable traps should be placed at regular intervals (typically between $l/10$ and $l/20$) along cables exposed to the transmit field.

Another important consideration is the required voltage handling of the trap. In principle, the voltage across an effective trap is the line integral of the maximum electric field along the cable, which can exceed several kV in many cases.

For multi-tuned coils, cable traps are required to block common-mode currents at each frequency of interest [40], [41].

Finally, it should be verified that appropriate isolation and creepage distances (see §8.9 of [IEC 60601-1](#)) between conductors that are on opposite sides of an insulating barrier are maintained, and that no solder, flux, or other foreign materials can ignite or cause arcing are present.

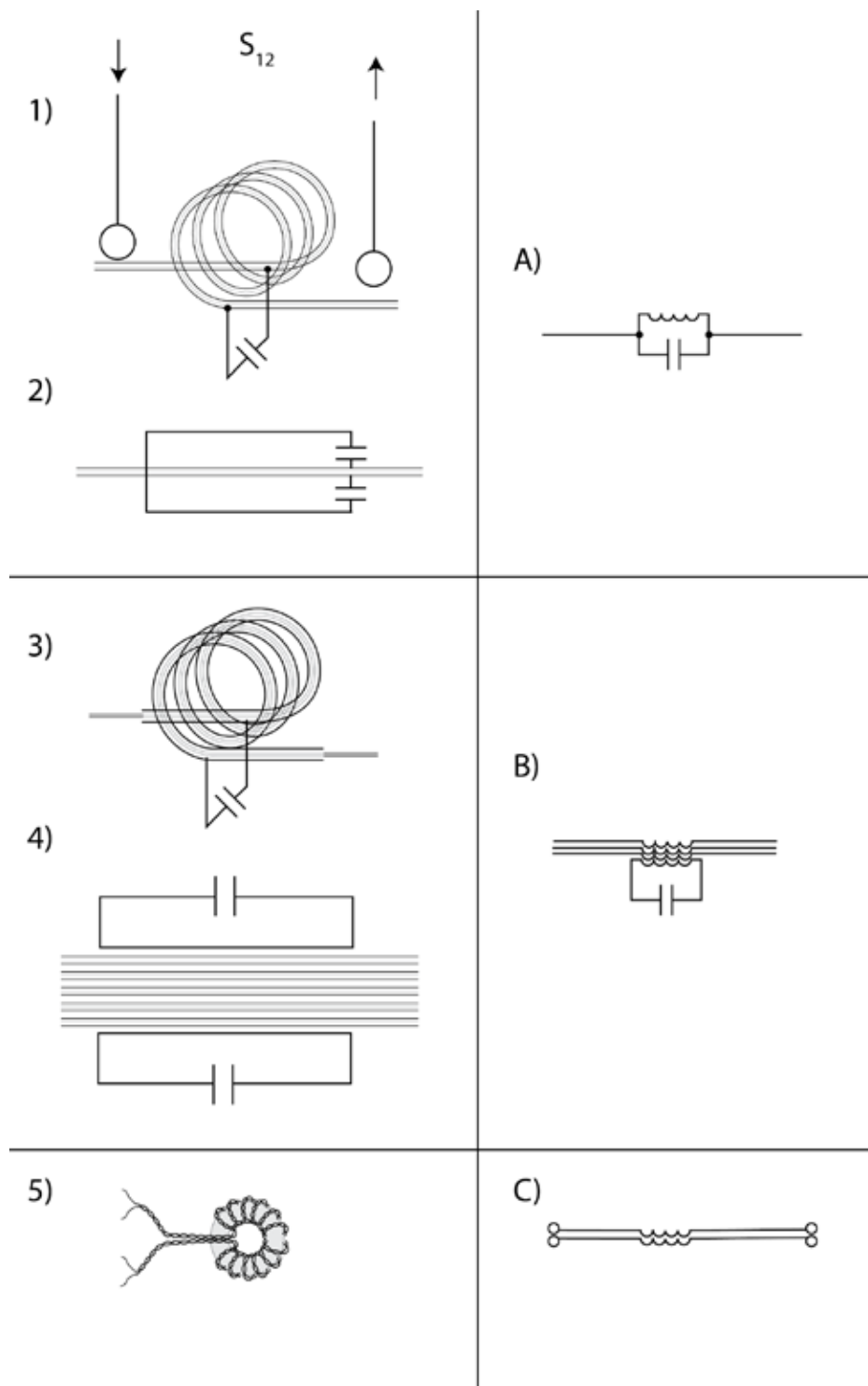


Figure 9: Basic topologies of cable-current suppression units. Implementations are shown on the left with their schematic representation on the right. Top row shows implementations of a parallel-resonant circuit on a (coaxial) RF line (A). These circuits can be implemented by coiling the cable and resonating it with a parallel capacitor (1). Bazooka balun (2). Floating sleeve coil trap (3), floating pod trap (4), RF choke mainly employed for DC and low-speed signal lines (5).

5.3.1 Validation and Testing Methods

5.3.1.1 Bench Testing

Practical coil implementations involve many cables with unknown coupling between them and other structures; therefore, the placement [31], [32], [37] and tuning [42] of cable traps represents a difficult task. To reduce coupling of RF power to cabling, it is recommended that cables be routed in regions of low electric fields and cable traps be placed in cable locations that are exposed to the highest electric field. The tuning and efficiency of cable traps can be evaluated by using either small, well balanced pick-up loops to scan along the cables, or by using current probes on either side of the cable trap [31], [32]. The dip in transmission induced by the traps when exposing the coil to an external field or driving its port should be clearly visible [31], [32].

An indication of severe cable currents can also be gained if the scattering parameters of the coil are unstable with respect to touching and rearranging the cables.

5.3.1.2 Scanner Testing

The RF signal distortion (B_1) induced by the cable is measured by placing the cables next to a phantom and imaging with a B_1 -sensitive sequence. Strong cable currents will show distortions near the location of the cable, while these distortions will be absent without the cables.

Alternatively, the cables can be scanned with a highly isolated pick-up loop connected to a power meter while the scanner runs a low power sequence.

Heating of cable traps may occur during the application of a high-power sequence; therefore, the temperature of cable traps should be measured following a 20-minute acquisition at maximum SAR levels, as described in §4.2. Ineffective cable traps may result in heating of cabling; therefore, the temperature of cabling should likewise be assessed. Additional padding may be required if there is heating of cables that are in close proximity to the subject.

5.4 Disconnected Coils and Accessories

A possible single-fault failure mode is to have unconnected or partially-connected coils or arrays (receive-only, as well as transmit), resulting in multiple hazards. In some cases, vendors may monitor for unconnected coils (e.g., by detecting conditions in the transmit chain such as detuning, high power reflections, etc.), but this condition can be difficult to detect with certainty. Therefore incorporation of fail-safe circuits such as secondary detuning (i.e., using passively switched diodes or fuses as described in §II.B.5.2) may help mitigate the hazard in the event of an unconnected coil. Additional measures may be needed.

The system vendor's recommendations and testing procedures should be followed to design for, and evaluate the safety of a disconnected coil. NEMA MS 14 also provides guidance for evaluating the hazards due to unconnected or partially connected coils. In addition to local heating (SAR hot spots) in the subject, unconnected coils can cause heating of the coil itself. Worst-case heating of the coil and, ideally, the subject, should be measured when driving the coil with the maximum permissible power. The worst-case heating may likely, but not necessarily, occur with an unloaded coil, or one loaded with a light load.

Additional hazards can result from adaptor cables or boxes that are often used in research sites to connect site-built coils. These devices have multiple interfaces that can potentially be disconnected

(e.g., system connection and one or more coil connections). It is prudent to analyze and test for all possible combinations of connected and disconnected interfaces.

Similar methods can also be employed to analyze the effects of other inserts and accessories described in §II.B.5.1.

6 Auxiliary Device Considerations

6.1 Requirements for Medical Power Supplies

The standard applicable in most countries, IEC 60601-1, introduces specific requirements for power supplies that are deployed in medical equipment. Note that, because it is considered an integral part of the system, the power supply cannot individually be given IEC 60601-1 compliance. If power supplies are required in addition to those already available on the scanner, attention must be paid to ensure that compliance is maintained. Besides EMI considerations, the key requirements for power supplies are isolation, as well as operator and patient protection.

Isolation, creepage and air clearances must comply with the requirements of §8 of IEC 60601-1 (briefly summarized here in §2.2), including values listed in Tables 6, 12, and 13. These include requirements for single- and double-layer protections towards the operator (MOOP) and towards the patient (MOPP).

The power supply rails provided by the coil connector of the scanner can be assumed to fulfil these requirements if the scanner is a licensed medical device.

The isolation provided by the entire device towards the operator and patient (subject) remains relevant (see Common Means of Protection), and choosing the right supply can only be considered the first step. It must be considered that additional filters (e.g., to penetrate the system's RF cage) and inline components alike can significantly alter isolation and other relevant safety parameters.

In summary, a medical grade power supply (specifically, rated for type B applied parts if there is no intended electrical contact with the subject) should be used for powering devices that are used in, or connected to, the MRI scanner if its internal supplies are not sufficient.

C. RF Safety

Page II.C.*

1	Regulations	2
1.1	Tissue Temperature Limits.....	2
1.2	SAR Limits	3
1.3	Total Energy Limit	4
2	Numerical Modelling - Goals and Requirements	4
2.1	Electromagnetic Modelling of Hardware	5
2.1.1	Considerations for Single Channel Transmit (sTx) Systems	5
2.1.2	Considerations for Multichannel Transmit Systems (pTx)	6
2.1.3	Considerations for Receive-only Probes	6
2.1.4	Considerations for Multinuclear Probes	6
2.1.5	Miscellaneous Devices	7
2.2	Body Models	7
2.2.1	Heterogeneous Models	7
2.2.2	Simplified Models	8
3	Computation of RF Field and Temperature Distribution	10
3.1	Electromagnetic Field Solver	10
3.1.1	Boundaries	11
3.1.2	Essential Simulation Data and Post-processing	12
3.2	Post-processing: SAR Averaging.....	12
3.3	Thermal Simulations	12
3.3.1	Diffusion Equation	13
3.3.2	Pennes' Bioheat Equation	14
4	Experimental Validation	15
4.1	Phantoms.....	15
4.2	Bench Measurements	16
4.3	B1 + Mapping.....	17
4.4	Validation Using S-parameters and B1 + Fields	17
4.5	Near-field Probes	19

4.6 MR Thermometry	19
5 Online SAR Supervision	20
5.1 Single-channel Transmission	21
5.2 Parallel Transmission.....	21
6 Safety Margins	24
6.1 Safety Margin for Inter-subject Variability	25
6.2 Safety Margin for RF System Imperfections	26
6.3 Safety Margin for Modelling Errors.....	27
7 Documentation of Simulations and Validations	27

The recommendations in this chapter address hazards caused by tissue heating due to exposure to the radiofrequency (RF) fields used in human MR examinations. The RF fields used for spin excitation inevitably create RF eddy currents in the human body which dissipate energy as heat, and the subsequent temperature increase can cause physiological stress and ultimately result in tissue damage. The regulations and techniques described in this chapter were developed to assist in minimizing the risk of thermal injury due to RF fields used in MR scanning. Thermal injury due to contact heat sources is discussed in §II.A.3.

1 Regulations

IEC 60601-2-33 is the internationally-recognised standard for regulating the safety of commercial MR equipment. Among the MR device standards currently recognised by the United States Food and Drug Administration (FDA Guidance 340), solely IEC 60601-2-33, which the FDA recognises in near-entirety, delineates RF safety requirements (see FDA Recognized Consensus Standards, FDA Guidance 793). Similarly, European Union’s EU Directive 2013/35 largely echoes the safety limits specified by IEC 60601-2-33. The telecommunications world uses closely-related standards such as IEEE C95.1.

IEC 60601-2-33 defines three “operating modes” depending on the ability of the scanner’s outputs (RF, gradient, and B_0) to cause physiological stress to patients. In the normal operating mode, none of the outputs have a value that can cause physiological stress for healthy subjects. In the first level controlled operating mode, one or more outputs can reach a value that can cause physiological stress to patients and thus must be administered only under medical supervision. In the second level controlled operating mode, one or more outputs can reach a value that may cause a significant risk to patients, and thus ethics approval is explicitly required. The IEC standard therefore clearly assigns an increasing risk of injury to increasing scanner outputs.

1.1 Tissue Temperature Limits

Tissue temperature is directly related to tissue damage. Temperature limits established by IEC for different regions and operating modes are given in Table 7.

Table 7: Limits for maximum body core temperature, maximum local tissue temperature, and maximum body core temperature elevation (from Table 201.104 of IEC 60601-2-33).

	Maximal body core temperature in °C	Maximal local tissue temperature in °C	Maximal body core temperature elevation in °C
Normal Operating Mode	39	39	0.5
1 st Level Controlled Operating Mode	40	40	1
2 nd Level Controlled Operating Mode	> 40	> 40	> 1

1.2 SAR Limits

Because temperature is challenging to measure in real time over large enough areas of the anatomy, IEC 60601-2-33 specifies that compliance with the temperature limits may also be reached by limiting the specific absorption rate (SAR). However, because of the complex relationship between SAR and temperature, SAR limits are typically more conservative than the temperature limits. Limits for global and local (10-g average) SAR in W/kg are given in Table 8 for both volume and local coils. A volume transmit coil is one designed to produce a homogeneous field over a specific part of the anatomy (e.g., body, head, joint), while all others are considered local transmit coils. The limits are defined for an averaging period of 6 minutes. Over any 10-s period, the limits must not exceed two times the 6-minute average values.

Table 8: Limits for global and localised SAR averaged over a time of 6 min (from Tables 201.105 and 106 of IEC 60601-2-33).

Operating mode	Normal	1 st Level Controlled	2 nd Level Controlled
Global SAR (W/kg)	Volume Transmit Coils		
Whole Body	2	4	> 4
Partial Body *	2 - 10	4 - 10	> 4 - 10
Head	3.2	3.2	> 3.2
Local SAR (W/kg)	Local Transmit Coils		
Head, Trunk	10	20	> 20
Limbs	20	40	> 40

* The partial body SAR limit is calculated by linearly interpolating between the maximum and minimum as a function of the ratio of the exposed patient mass (mass receiving 95% of the RF power) to the total mass (Figure AA.8 of IEC 60601-2-33).

1.3 Total Energy Limit

While temperature and SAR limits are designed to prevent RF burns, the body must also dissipate the absorbed energy to maintain core body temperature within the normal range. Therefore, IEC 60601-2-33 (Table 201.105) additionally specifies an upper limit of 14.4 kJ/kg (240 W·min/kg) for the specific absorbed energy (SAE, also known as specific energy absorption or dose) during the whole *examination*. The SAE is obtained by integrating global SAR (i.e., for volume coils) over time for the duration of the whole scan session. For frequencies above 400 MHz the International Commission on Non-Ionizing Radiation Protection (ICNIRP) also restricts local (10-g) SAE (see ICNIRP EMF Guidelines).

2 Numerical Modelling - Goals and Requirements

The goal of numerical simulations for RF safety assessments is to predict the spatial distribution and temporal evolution of physical quantities like electromagnetic (EM) field amplitudes, power dissipation density, and temperature. Measuring such quantities in living tissue can be technically challenging, and therefore generating an accurate computer representation is very valuable. The results of such simulations can then be used to determine safe sequence parameters and Thresholds for SAR Supervision (i.e., RF power limits).

To secure the predictive value of these numerical models, one evidently must include all relevant components and parameters of the physical configuration that affect the respective results, possibly accounting for residual uncertainties via Safety Margins. Most commercial simulation packages include CAD functionality to create accurate models of structures such as the RF probe and its surroundings, as well as the ability to import existing third-party 3D CAD files. Phantoms with dielectric properties similar to those of the body can provide a means for Experimental Validation of the numerical model of the RF probe through, e.g., B_1^+ maps, field or temperature measurements.

Detailed anatomical body models are then used to represent the in vivo scenario for a more realistic safety assessment. Based on these results, a maximum input power is then determined in case of a single channel system to satisfy the appropriate regulatory limits (i.e., IEC 60601-2-33). Appropriate settings (e.g., RF power limits and Thresholds for SAR Supervision) should then be applied on the MR system to ensure that SAR and temperature limits are not exceeded during in vivo scanning.

The accuracy of the numerical results will ultimately depend on the specific properties of the simulated configuration, the sensitivity of the numerical result with respect to model parameters and simplifications, and solver settings such as resolution and convergence tolerance (see IEEE 1597.2). Example features incorporated in simulation models for MR-related simulations may include

- Fine details of RF probe and mechanical housing;
- Lumped-element circuit components, e.g., capacitors;
- Cables, connectors, and cable traps (although in typical scenarios, when cable routing is outside the RF coil's sensitive region, the inclusion of cable traps in the EM model of the RF coil is unnecessary);
- Anatomical Body Models;
- Large structures, e.g., the RF screen and space surrounding the magnet.

2.1 Electromagnetic Modelling of Hardware

The simulation model should include a sufficiently accurate representation of the coil geometry including relevant conductors, lumped elements as well as feed structures and decoupling components. A reference plane or port(s) must be defined for all RF connections of the RF probe, from which point all components of the RF probe are to be included in the numerical model. Typically, the RF connection interface of the MR system is considered as a reference plane (which also makes the corresponding RF probe plug a convenient point to connect the probe to RF bench instrumentation), as most system manufacturers employ calibration procedures that compensate for attenuation and phase deviations between this point and the RF supervision hardware of the MR system. Alternatively, the attenuations and phase offsets can be determined experimentally, e.g., with B₁⁺ Mapping measurements.

In many cases, coaxial cables and additional hardware components that connect the RF probe to the RF connection interface, such as power splitters, transmit/receive switches, etc., do not need to be simulated in detail. However, their attenuations and phase shifts must be considered in the simulation model to avoid errors in the 3D field distributions. Further, the mechanical housing, patient table and their material properties may affect the electrical characteristics of the RF probe and may therefore need to be included.

The RF field distribution may also be affected by the RF screen or shield which lines the inner surface of the MR bore. In particular, for ultra-high-field (UHF) configurations with radiating probe elements, e.g., antenna topologies, the RF wavelength becomes comparable to the dimensions of the MR bore, which may cause its RF screen to act as a waveguide for RF waves propagating through the bore [43]. Orzada et al. simulated a 32-channel body coil for 7T, where they show high E-field exposure outside of the region of the body coil [44]. In this case, a model which includes the full RF shield and the full body model is necessary to account for wave propagation. Propagating RF waves can also deposit RF power in areas of the anatomy remote from the coil elements [45].

Conversely, in many scenarios, e.g., when dealing with shielded coils or local transmit coils, it is not necessary to include the whole MR bore, which is desirable to limit the computational resources required to perform the simulation. However, the validity of such model simplifications should be demonstrated either through additional simulations or through other validation procedures (c.f. §II.C.4).

A suitable reference phantom that produces electrical loading conditions similar to those imposed by the human body is essential to evaluate the RF probe performance. For this purpose, phantoms with minimal geometrical complexity but known electrical and thermal parameters can be used for validation steps. It is imperative that the physical spacing between the transmit coil and the dielectric load is modelled accurately to represent the actual set up. Detailed requirements for phantoms are presented in §II.C.4.1. Anatomical body models for safety assessments are presented in §II.C.2.2.

2.1.1 Considerations for Single Channel Transmit (sTx) Systems

sTx systems are driven by a single signal which can be modulated in amplitude. sTx RF probes can consist of either a single probe element or multiple probe elements driven by fixed relative phases and amplitudes. sTx systems can include traditional linear or quadrature probes, as well as combinations of multiple probe elements connected to a single excitation source through a fixed power distribution network. In all such cases, SAR is proportional to the total power accepted by the feed port (forward minus reflected power). In the quadrature and multi-element cases, the coupling, power attenuation,

and phase shifts between the elements should be incorporated into the model, as well as the effects of feeding and decoupling networks (e.g., coaxial cables, power splitters, capacitors, or inductors).

2.1.2 Considerations for Multichannel Transmit Systems (pTx)

Parallel transmit (pTx) systems transmit with multiple independent channels via an array of RF probes which allow a time-varying amplitude and phase on each channel. Thus, in multichannel transmit systems, SAR will be a function of the superposition of complex (real and imaginary) RF voltages, i.e., amplitude and phase, applied to individual array elements. In contrast to sTx probes, simulations for pTx probe arrays require individual excitations with multiple sources. The simulation must be carried out with all probe elements present. Decoupling networks need to be considered as described in §II.C.4.4.

2.1.3 Considerations for Receive-only Probes

Independent receive-only probe arrays are commonly employed instead of volume coils to improve image quality and shorten scan time. Although receive-only probe elements are typically detuned during RF transmission to electrically isolate them from the transmitting RF probe, local alterations in the transmit RF field and therefore local SAR can still be induced even in well-engineered implementations [46]. Detuning performance can be measured on the bench, e.g., with scattering parameter measurements on a network analyser [17], [30]; varying degrees of coupling can be added to the simulation model through techniques such as circuit co-simulation [47]. Because fine structures such as detuning circuits significantly increase the simulation effort, it is possible to replace them with an open-circuit [48] or high-impedance port [46]. If not including receive-only probes in the transmitting probe model, it should be proven experimentally that their influence is negligible, or appropriate Safety Margins should be incorporated to account for their omission. Global coupling effects can also be quantified experimentally by measuring the additional power required to achieve a nominal flip angle (e.g., 90°) in presence of the receive array relative to the power required with the transmit probe alone (see §II.B.5.2).

2.1.4 Considerations for Multinuclear Probes

Transmit probes that operate at two or more frequencies, known as multinuclear coils, are employed for non-proton MRI and MR spectroscopy (MRS) research applications, e.g., phosphorus-31 (³¹P) MRS, carbon-13 (¹³C) MRS, sodium (²³Na) MRI, and xenon-129 (¹²⁹Xe). Frequently, these coils maintain proton (¹H) functionality as well to allow basic scout imaging and B₀ shimming, and to deliver signal enhancement via techniques such as nuclear Overhauser effect and proton decoupling. Safety assessments must be performed for all frequencies utilised. Accordingly, all modelling and phantom experiments recommended for typical proton transmit coils must be performed for all transmit frequencies/nuclei. An illustrative example of modelling a dual-tuned ¹H/³¹P 3 T TEM coil is available in [49]. Ultimately, the resulting SAR-limiting safety parameters for each transmit frequency must be entered into the scanner console software to ensure subject safety.

Particular attention is advised for coils with considerable EM coupling between proton and multinuclear transmit elements. Many in-vivo multinuclear studies rely on geometric decoupling or mode orthogonality to isolate the proton and multinuclear probes, circumventing the need for decoupling circuitry (e.g., [50]); however, non-standard probe configurations may require trap circuits to be inserted on the lower-frequency element [41], [51]. A representative (e.g., lumped-circuit) model of the trap can

be incorporated in the EM model to accurately simulate inter-frequency decoupling performance [52]. Additionally, dissipation within the trap circuit can produce considerable temperature increases, which should be characterised experimentally (see §II.B).

2.1.5 Miscellaneous Devices

Miscellaneous devices and accessories may be situated in the MR probe environment, particularly in research settings. Such devices, including dielectric pads, metamaterial structures, EEG electrode caps, TMS coils, HIFU transducers, etc., may alter the RF field and therefore local SAR. Owing to the diverse number of possible configurations, considerations specific to electromagnetic modelling of miscellaneous devices cannot be listed in detail here. Similar to RF devices, simulations should include an appropriate level of detail. Procedures and standards suitable to the specific device and situation may be available elsewhere (e.g., the manufacturer).

2.2 Body Models

A numerical body model is a critical component of the RF simulation to obtain realistic SAR and tissue temperature distributions. Body models are discussed in Annex D.6 of [IEEE C95.3](#) as well as in the following sections.

2.2.1 Heterogeneous Models

At present, heterogeneous anatomical body models are available in a voxel-based and surface-based form. Surface-based models are free of staircasing errors intrinsic to voxelised models and can be converted into voxel-based representations.

Simulations should be performed for a variety of anatomical body models covering a suitable range of body physiques to achieve generalizable results. A statistical assessment of the intersubject variability can then demonstrate safety in a sufficient variety of subjects. If several positions of the body relative to the coil are possible, multiple simulations can be performed to assess the sensitivity of SAR with respect to body position. Examples of such studies can be found in the literature [53], [54], where a [Safety Margins](#) of 1.5 was suggested to account for local SAR intersubject variability in pTx head imaging at 7T.

The resolution required for spatial discretisation of the body model depends on the frequency of operation and a higher spatial resolution can be required for higher frequencies, to account for interaction of fine anatomical structures with the RF field at shorter wavelengths. For field strengths up to 3 T, a spatial resolution of 5 mm has been shown to be suitable for local SAR assessments [55], [56], whereas for higher field strengths a higher spatial resolution is generally recommended. The frequency dependence of electrical material parameters (dispersion) should also be taken into consideration by selecting the parameters appropriate for the RF frequency [57], or frequencies, in the case of multinuclear probes (see §II.C.2.1.4).

Heterogeneous body models are widely available through various resources, such as, the Virtual Family dataset [58] and the Visible Human Project [59] from which the [AustinMan and AustinWoman Models](#) were developed [60]. Typically, these models have been constructed in supine body position. Some software tools allow modifying the body posture to match the actual situation better, which can also serve to assess SAR variability with respect to body posture [54]. Further customisation may involve including configuration-specific and even subject-specific anatomical features [61]–[63]. Fully

customised body models can be generated from segmented MR images acquired at 1.5 or 3 T for the large usable FOV, optionally including the mechanical housing of the RF probe for better correspondence of the anatomical geometry. A suitable MR protocol for whole-body models is presented in [58] and [56] and a protocol specifically for head models with high tissue count in the brain in [64].

2.2.2 Simplified Models

Including the entire anatomical body model into the computational domain is not always necessary, and a truncated version of the body model can substantially reduce the computational cost of the analysis. As a general “rule of thumb”, the body model should extend sufficiently beyond the active region of the RF probe to prevent truncation effects on the RF field distribution (e.g., for a head coil at 7 T, a model that consists of only the head and shoulders can provide sufficiently accurate results [65]). Furthermore, a coarser spatial resolution may be considered in remote areas of the body outside the active region of the RF probe. However, as with the aforementioned computational domain considerations, best practices recommend demonstrating that the results are not affected by modelling simplifications, e.g., by performing a separate convergence analysis [66]. For example, one may examine the effects of modelling simplifications using the flowchart illustrated in [Figure 10](#).

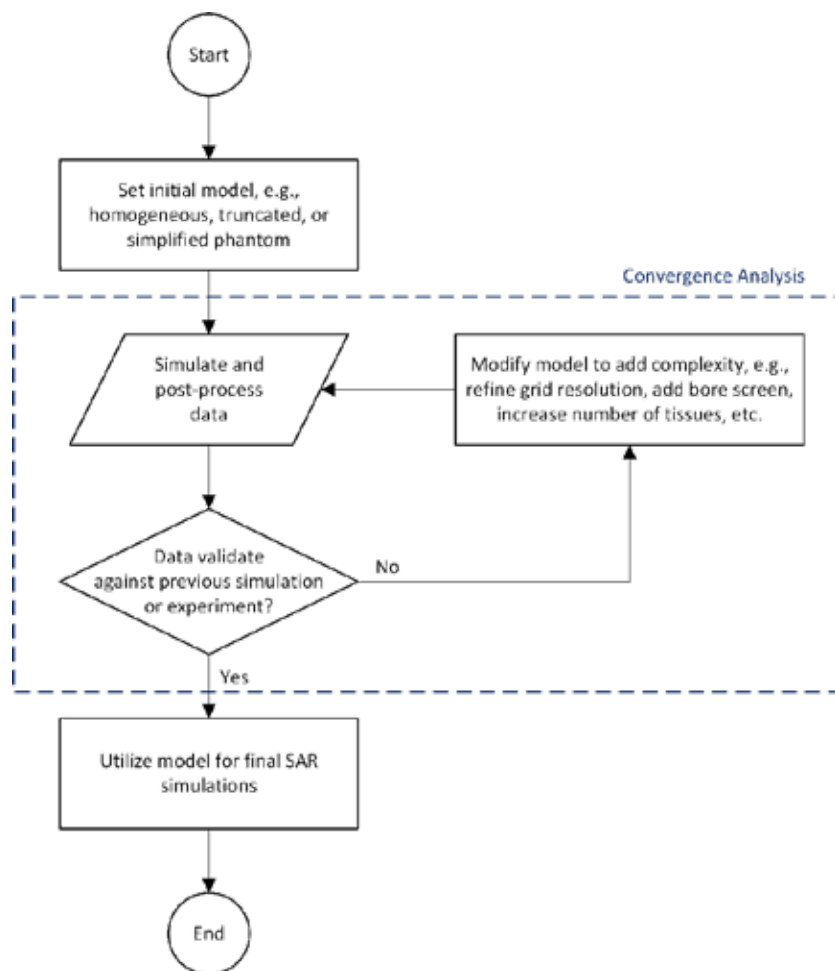


Figure 10: Example flowchart illustrating RF coil simulation strategy for analysing validity of common modelling simplifications.

For simulations that focus on a specific body part only (for example head-only), it can be computationally more efficient to simulate a truncated body model which includes only the region of interest. However, if the truncation is done at locations where strong RF fields are present, the EM-field distribution can be distorted. Wolf et al. compared simulations for a head-only coil using a full body model, a model truncated below the shoulders and a model truncated above the shoulders [65]. They demonstrated that for head-only coils, the neck and shoulders need to be included in the model to retain the same EM-distributions as for the full body model. Based on these results, they conclude that how far the model needs to be extended beyond the coil depends on the size of the coil and its radiation behaviour (which also depends on frequency). Additionally, a criterion is suggested to ensure that global SAR of the full and the truncated model are within a given difference or ratio.

The calculation accuracy depends on several factors, e.g., the frequency, the transmit excitation mode, the model's resolution, and the number of tissue classes. No one set of factors will be sufficient for all cases. As an example, Homann et al. found that a resolution of 5 mm and a distinction between fatty tissues, water-rich tissue and the lungs are sufficient for 3T body imaging. A comparison of fully-detailed body models with simplified muscle-lung-fat versions resulted in peak local SAR values that were within 8% agreement for an 8-channel transmit array driven in quadrature mode [56]. Yet in another study, Yetişir et al. found that reducing pregnant body models from 25 to 8 tissues (muscle, fat, lung, placenta, amniotic fluid, umbilical cord, foetal brain, and foetal body) caused a change in peak local SAR of 23% for pTx and 12% for birdcage mode excitation (Figure 11), and the location of peak local SAR across models changed more often for pTx [67]. These examples highlight that body model detail should be analysed and adapted for each study, and necessary Safety Margins to account for any simplifications should be incorporated into the overall safety margin.

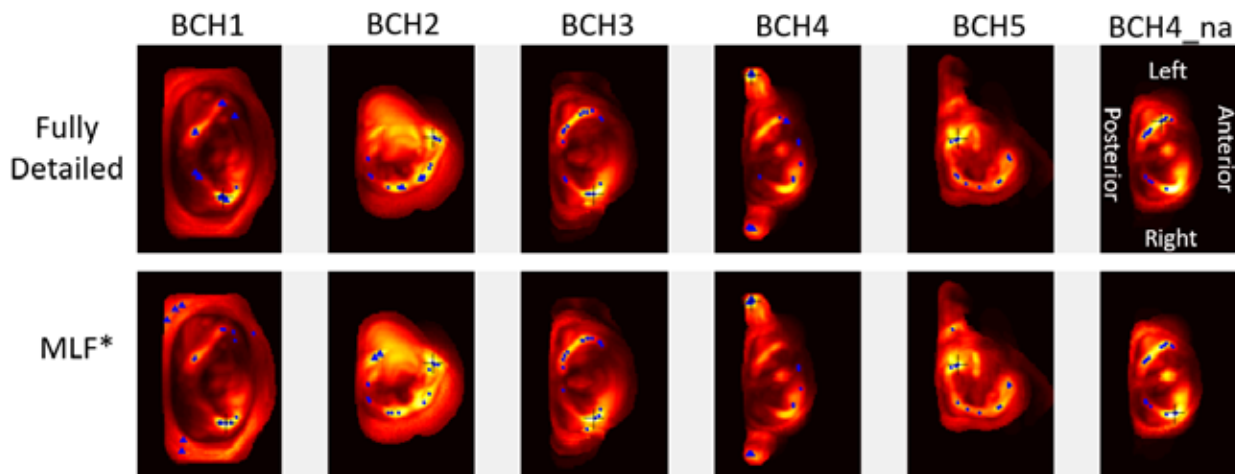


Figure 11: Location of maternal peak local SAR for 30 random RF shim settings for which muscle-lung-fat (MLF) models underestimated the SAR of fully detailed models (blue dots) overlaid on top of the maximum intensity projection of the local SAR map for birdcage mode excitation (peak local SAR of birdcage mode: black +). For BCH1, BCH2 and BCH4; 30, 16(all) and 30 random RF shim settings for which MLF models overestimated SAR are also included (blue triangles). In BCH4, overestimation usually occurs when peak local SAR is in the arms.

Homogeneous body models and phantoms do not provide realistic information and are typically not reliable for local SAR calculations. Nevertheless, homogeneous models could be utilised in cases where

only global SAR is of interest, by ensuring that the total power deposited in the homogeneous model is equal to the power deposited in a corresponding anatomical model. Simplified homogeneous phantoms may also be applicable in well-defined scenarios of local exposure such as near implants (see ASTM F2182), or at the body surface near local transmit coils, which typically produce the highest SAR in superficial tissues.

3 Computation of RF Field and Temperature Distribution

Numerical solvers are applied to calculate field distributions, specific absorption rate (SAR), tissue temperature and thermal dose from a numerical model representing the physical set up. At present, these quantities cannot be measured non-invasively and accurately *in vivo*. Thus, numerical simulations are the only means to estimate field and temperature distributions in the anatomy to allow for an RF safety assessment.

The following section explains the key requirements on the functionality of numerical simulation tools in the area of RF safety in MRI. These functions can be achieved by both commercial and self-developed software packages. An overview of commercially available implementations is given in [2], [68]. In case of self-developed software, additional verification and validation steps are recommended to ensure accuracy.

3.1 Electromagnetic Field Solver

Electromagnetic field solvers are applied to solve the full set of Maxwell equations in a 3D numerical domain. Various types of EM solvers can be used to calculate the 3D field distribution in the simulation domain. At present, the most commonly used numerical solvers in the field of simulations for MR use are the finite-difference time-domain (FDTD) method [69], [70], finite integration technique (FIT) [71] or the finite element method (FEM) [72]. Please note that this section does not aim to provide a comprehensive, detailed discussion and comparison of computational techniques; for more information, refer to the references provided, Annex B of [IEEE 1597.2](#), Annex D.6 of [IEEE C95.3](#), or others in the extensive computational electromagnetics literature.

To solve Maxwell's equations, a discretisation of the simulation domain is necessary, which requires a trade-off between accuracy and computational cost. FDTD and FIT are typically used with regular hexahedral, rectangular meshes that discretise the entire domain into volume elements (voxels). In the simplest implementation, the discretisation assigns a single material to each voxel, which for curved or angled structures results in a staircase approximation of the geometry and corresponding errors in the EM field solution. Increasing the spatial resolution can reduce such errors at the cost of a larger the number of voxels and, thus, memory demand and computation time. State-of-the-art FDTD and FIT software employs rectangular meshes with anisotropic spatial resolution as well as conformal meshes. The spatial discretisation chosen for a given problem must allow the inclusion of the geometrical details necessary to achieve the desired solution accuracy. When the accuracy is dominated by wavelength effects, such as modal distributions, it is generally considered sufficient to limit the maximum length of the voxel edges to one tenth of the smallest wavelength of interest [73]. In local SAR assessments involving anatomical structures, however, less than one twentieth of the wavelength is more appropriate. Specific rationale may depend on the body region and can be established by performing a stability analysis. FDTD and FIT are defined in the time domain and therefore excitation signals can be arbitrary. Frequency-domain results, useful to identify the resonant modes and coil tuning, are obtained

by applying a discrete Fourier transform to the time-domain signal. The memory demand of FDTD and FIT scales approximately linearly with the number of mesh cells, and simulation execution can often be performed by GPU resources, facilitating their use for large-scale problems [66].

FEM is commonly used with an irregular tetrahedral mesh, which offers greater flexibility and accuracy to model curved structures and fine details compared to the rectangular meshes used in FDTD and FIT. As with FDTD and FIT, the entire computational domain needs to be discretised, but, because the cell size is readily adapted to the dimensions of the features in the model, FEM typically requires a smaller number of tetrahedral cells compared to the number of FDTD voxels for the same structure. The FEM algorithm is also well-suited for resonant structures because it is formulated in the frequency domain. However, memory usage of FEM is significantly higher compared to FDTD when incorporating detailed human models, restricting FEM to problems of smaller dimensions or reduced details [66].

Other solvers can be used only to a limited extent. E.g., surface-based methods such as those based on the method-of-moments can be used for homogeneous phantoms but suffer from prohibitive computational costs when heterogeneous body models are considered. Nonetheless, surface-based solvers can prove useful to model and validate an RF probe model adjacent to a homogeneous phantom, and results from surface-based solvers can also be used to corroborate those of FDTD, FIT, and FEM [74].

Numerical accuracy requires an appropriate choice of simulation parameters, including mesh density, convergence criteria and boundary conditions [75], [76]. Simulation stability and accuracy can be checked by performing a power budget, i.e., comparing the total power entering the computational domain (forward minus reflected power) to the sum of the dissipated and radiated power.

3.1.1 Boundaries

RF simulations done with the FDTD or FEM method can require large amounts of memory to calculate the electromagnetic field at all points in the domain. To reduce the amount of memory needed, both the domain in which the model is simulated as well as the Body Models can be truncated (see also §II.C.2.2.2).

Appropriate boundary conditions must be set at the surfaces surrounding the simulation domain (e.g., the scanner bore and two openings). Absorbing boundary conditions (ABCs) [77] are used to model free space behaviour. An implementation of ABCs that is often used in MRI is the perfectly matched layer [78], [79] in which incoming waves are fully absorbed at the boundaries. To model a domain that is surrounded by conducting materials, perfectly conducting boundary conditions can be set. Collins et al. used perfectly conducting boundary conditions to model the RF screen and cryostat for a 1.5T MRI system, and showed significant effects on SNR compared to a situation without RF screen and magnet casing present [80]. Then again, Collins et al. also showed the local coil RF shield meshing and design can significantly alter SAR distribution while only marginally affecting magnetic field amplitude within the coil [81], suggesting greater importance of the coil shield compared to the bore shield for inclusion in the simulation mesh. Supporting this conclusion, Wolf et al. included a large RF-shield (64 cm diameter) in a simulation model of a head-only coil with a local RF shield [65]; they showed that the presence of the large RF-shield had minor effects on the SAR distribution in the body and none on the field distribution inside the head coil.

3.1.2 Essential Simulation Data and Post-processing

Simulation tools should be able to determine, evaluate or export different parameters and quantities that are necessary for experimental validation steps. For example:

- The component values (e.g., capacitances) necessary to tune the loaded coil to the Larmor frequency
- Scattering parameters and frequency response
- distributions of electric and magnetic fields, B_1^+ , SAR, and temperature
- For B_1^+ : note the circular polarisation for B_1^+ and B_1^- is dependent on the orientation of the static magnetic field. Both polarisations must be considered if the static field direction is unknown or if the coil is intended to be used in both head-first and feet-first scenarios
- For Q-Matrix and VOP compression: electric field distributions produced by each transmit element in an array, as well as material properties within the body model

3.2 Post-processing: SAR Averaging

[IEC 60601-2-33](#) defines local SAR as that “averaged over any 10 g of tissue of the body”. Simulations typically have a much finer spatial resolution and therefore post-processing (spatial averaging) is required to calculate this quantity to compare with the limits in [Table 8](#). Spatial averaging of SAR has the purpose of approximating the effect of thermal diffusion, which in tissue is a complex function of thermal conductivity, tissue heterogeneity and perfusion. Various biophysical modelling studies have aimed to optimise the correlation between spatially averaged SAR and temperature distributions under steady-state exposure, effectively aiming to reproduce the relevant thermal diffusion length by a localised heat source in tissue [82]–[84]. Further rationale for the use of 10 g as an averaging mass was given by ICNIRP in 1996 [85] and [IEEE C95.1](#), 2005 edition, in view of specific concerns about localised heating of the eye and other body parts with a similar mass.

[IEC/IEEE 62704-1](#) prescribes the algorithm that should be used to grow a cubic averaging volume containing the required tissue mass at each location within the body model, taking special care of locations where the averaging volume extends beyond the exterior surface of the body. At these locations, maximum averaged SAR values from nearby locations are propagated outwards instead of performing an average over a smaller mass of tissue. Although this approach can introduce errors, notably SAR overestimation at surfaces, which are less likely to correlate with temperature, it is considered a conservative approach for frequencies below 3 GHz (see [IEEE C95.1](#)). Since establishment of the [IEC/IEEE 62704-1](#) standard, various research efforts have explored alternative procedures to further improve the spatial correlation between a SAR-derived metric and the temperature increase [86]–[90].

3.3 Thermal Simulations

Thermal solvers aim to calculate temperature by solving the pertinent heat transfer equation in 3D with the non-averaged voxel-based SAR distribution as the heat-source. One advantage of temperature data is that it allows the application of [Tissue Temperature Limits](#), which have direct physiological meaning, instead of the limits on applied SAR, which have an indirect effect. For head exposure, heating of the eyes is of particular importance (see [91]–[93] for details) because of the absence of blood flow in the vitreous humor. The second advantage of temperature is that unlike SAR, it can be measured directly, and therefore is very useful for [Experimental Validation](#).

The solution of the heat transfer equation in combination with a homogeneous phantom can be used for model validation steps. For in-vivo safety assessments, the RF-induced temperature increase must also account for bio-heat transfer mechanisms such as thermoregulation. The most widely used bio-heat transfer equation was proposed by Pennes [94]. This is an area of active research where it is challenging to provide specific recommendations [95]. The following sections introduce the basic concepts and some representative results.

3.3.1 Diffusion Equation

In presence of only diffusion, the increase in temperature, $T(r)$, in a phantom is obtained by solving the heat diffusion equation with spatial power deposition, $SAR(r)$, as the input,

$$\rho C_p \frac{\partial T}{\partial t} = \nabla \cdot (k \nabla T) + \rho SAR, \quad \text{II.5}$$

where ρ is the mass density (kg/m³), C_p is the specific heat capacity (J/kg/°C) and k the thermal conductivity (W/m/°C). During an MR imaging sequence, short RF pulses are typically pulsed periodically) with inter-pulse intervals on the time scale of tens of milliseconds (see Appendix C.3). Because of the much longer thermal transfer times and low heat diffusivity, the SAR during a sequence can be conveniently averaged over the sequence repetition time and applied as a constant input in the thermal simulations [96], [97].

By including appropriate boundary conditions (e.g., Dirichlet, Neumann) and initial conditions, the heat diffusion equation can be solved analytically for simple geometries, while for complex geometries numerical solutions are required. Commercial software packages are available to solve this equation, as well as more complex versions like the Pennes' Bioheat Equation.

Different numerical methods exist to solve such problems but, given the low thermal diffusivity in tissues $\alpha = k/(\rho C_p)$, the Euler method has proved effective and simple. If T_n is the absolute temperature at instant n , at the next instant it is:

$$T_{n+1} = T_n + \alpha \Delta T_n dt + \frac{SAR}{C_p} dt, \quad \text{II.6}$$

where dt is the discretisation time step. The latter should be small enough given the spatial resolution to ensure numerical stability [98]. When a SAR calculation is to be validated, the initial slope of the measured temperature yields the SAR:

$$\left. \frac{\partial T}{\partial t} \right|_{t=0} = \frac{SAR}{C_p}. \quad \text{II.7}$$

Although the details of implementation of the boundary conditions do not play a significant role given the low diffusivity in tissues, it can still affect quantitatively the results near the boundaries.

Figure 12 below presents an in vitro comparison of simulated temperature versus measured temperature with MR thermometry for an 8-channel pTx probe array, for 2 excitation modes at 7 T. The results highlight that SAR and heating patterns are highly dependent on excitation phases, and it is recommended that at least two such complementary patterns be implemented for validation.

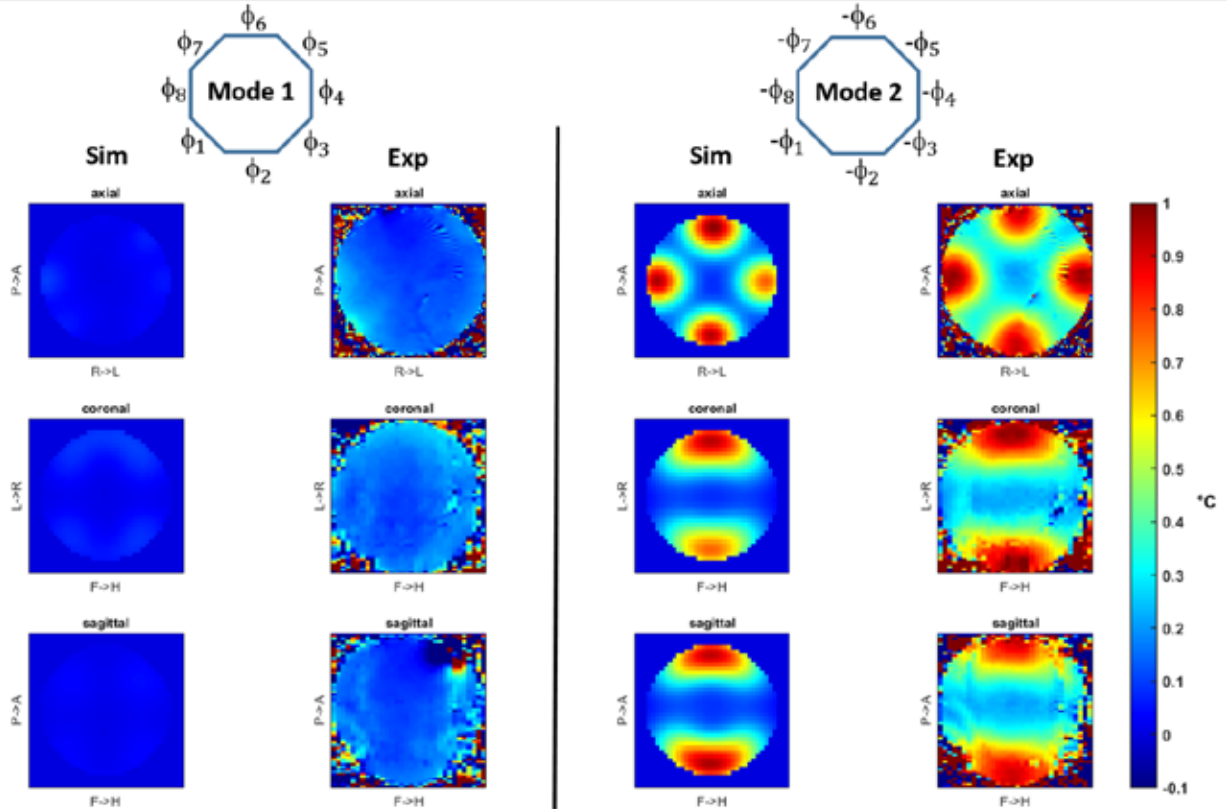


Figure 12: Comparisons of simulated versus measured temperature rises in vitro at 7 T for an 8-channel RF probe array. Two modes of excitation are presented.

3.3.2 Pennes' Bioheat Equation

To simulate the evolution of tissue temperature for in vivo studies, the gold standard today remains Pennes' bioheat transfer equation [94], ubiquitously used in the mobile phone industry [98]. In addition to diffusion (Eq. (II.5)), the bioheat equation incorporates additional terms for perfusion and metabolism:

$$\rho(r)C_p(r)\frac{\partial T(r)}{\partial t} = \nabla \cdot (k(r)\nabla T(r)) + \rho(r)SAR(r) + Q(r) - P(r)(T(r) - T_b), \quad \text{II.8}$$

where Q is the metabolic rate (W/m^3), P is the perfusion coefficient ($W/m^3/^\circ C$), while T_b is the blood temperature. Considering exam or sequence durations, worst-case values can be determined by solving the above equation in the steady-state regime, i.e., when the left hand-side is equal to 0. In practice, this can be achieved for instance by setting a homogeneous initial temperature and integrating the equation for a sufficiently long RF exposure time (~ 1 hour) to reach equilibrium. In this model, the blood temperature $T_b(r)$ is typically assumed to be spatially and temporally constant and equal to the body core temperature ($37^\circ C$); this allows the $(T(r) - T_b)$ term in Eq. (II.8) to be recast as temperature rise ($\Delta T(r)$).

Equation (II.8) can also be solved by using Euler's method. Example results of such simulations can be found in [88], [99]–[101], [93], [102]–[104]. Losses from heat convection, sweat, clothing etc. can also be added to the model [99].

For the small core temperature rises compliant with [IEC 60601-2-33](#) guidelines (1°C, see §II.C.1.1), thermal tissue parameters can be considered constant over the RF heating period. They can, however, change when undergoing sufficient heat stress as the result of a thermoregulatory response, leading for instance to an exponential increase of skin perfusion with temperature, although with a more than two-fold variability in the exponent across literature [99], [105]. Pennes' model continues to be debated also because blood temperature is assumed invariant, and thus refinements have been proposed [106], [107]. In [108], it was shown that Pennes' model slightly overestimated the temperature compared to a more advanced model that included temperature variations through discrete vasculature. In that particular example, the simpler Pennes' model constituted a more conservative scenario. Furthermore, a study on mesh resolution by Wang et al. suggests coarse resolution results in a more conservative temperature rise scenario, when compared to temperature rise results with finer mesh resolution [109].

A generic bioheat transfer thermal model by Shrivastava et al. [107] was also proposed with a two-pool description (blood and tissues) to take into account variations of blood temperature. Experiments performed on anaesthetised swine yielded good agreement with the theory [110], notably with the disappearance of a plateau predicted by Pennes' model, even after hours of RF heating. Interestingly, other measurements also on anaesthetised swine suggest the appearance of a plateau at some probe locations after around 10 minutes [104]. The effect of anaesthesia (known to affect thermoregulation) remains to be investigated.

4 Experimental Validation

The experimental validation of a simulation model is a basic component of any RF safety assessment, and hence, it should be performed on one or more test setups prior to the final calculation of the RF field exposure in heterogeneous body models. To ensure repeatability, the validation is carried out using an experimental setup with a phantom model. General practices for validation of EM simulations are described in [IEEE 1597.2](#).

4.1 Phantoms

The most common and straightforward validation approach is to use a phantom with a simple geometry that approximates the body region exposed by the RF probe and presents a typical body load to the RF probe. More complex phantoms such as anthropomorphic phantoms with multiple compartments with different dielectric properties can also be constructed, in which case the phantom casing can be 3D-printed, for example. In both cases the geometry must be well known (e.g., CAD model) so that it can be reproduced accurately in the model. In addition, the phantom needs to be relatively similar in its dielectric and, possibly, thermal properties compared to the concerned body part. In general, it is desirable to be as accurate as possible with respect to the target tissue region; however, for validation purposes a reasonable deviation may be considered if this results in improved measurement properties (stability, sensitivity, etc.). Furthermore, the phantom material should be MR visible with adequate SNR for MR based validation techniques (i.e., [B₁⁺ mapping](#), [MR Thermometry](#)) and, preferably, a single resonance line. Hence, water-based phantoms are typically preferred. In case of validation techniques that rely on measurements with near-field or temperature probes, accessibility to the interior of the phantom is an additional consideration.

Filling materials include tissue-simulating liquids and gels (TSL) that can be mixed to produce the desired dielectric properties ([IEC/IEEE 62209-1528](#) specifies target dielectric properties in Table 2 and

recipes in Annex F). Common TSLs for MRI are provided in standards such as [AAPM Report No. 100](#) and [ACR Large Phantom](#). Other solutions include water, sugar and sodium chloride (NaCl) [111]; water, Polyvinylpyrrolidone (PVP) and NaCl [112], [113] (see also the [NIH Dielectric Phantom Recipe Generator](#)); or water, denatured ethanol (C₂H₆O) and NaCl [114]. While the amount of sugar, PVP or ethanol defines the permittivity, NaCl is added to adjust the conductivity. It is highly recommended to measure both material properties at the operating frequency, for example using an open-ended coaxial dielectric probe. Using measured values will facilitate achieving a proper match between measured fields and simulation. To improve MR visibility, a relaxation agent such as cupric sulphate (CuSO₄), nickel chloride (NiCl₂), gadolinium, etc. can be considered to modify its T_1 (and T_2), bearing in mind that ionic compounds will also modify the conductivity. Moreover, sodium azide (NaN₃) can be added as an antiseptic to improve shelf life and robustness over time (see the [Martinis Center Anthropomorphic Phantoms](#) page), but require special care in terms of handling and disposal.

To avoid flow and thermal convection that influences MR measurement and thermal modelling accuracies, a high viscosity of the medium is desirable. Gelling agents include agar, agarose, porcine gelatine, hydrophilic organic polymers (e.g., TX-150 and TX-151 from Oil Center Research, USA), and carbomers (e.g., Carbopol® 980, and Carbopol® 974P from Lubrizol, USA), among others [115] (see also NEMA MS 10). It should be noted that these materials also affect the MR relaxation times.

When performing [MR thermometry](#), both a short T_1 relaxation time and minimum spectral side peaks are desirable. For more realistic MR thermometry measurements and thermal distributions, oil-in-gelatin dispersion phantoms show some promising results for multicomponent phantoms [116], [117]. Bear in mind that using fat in your thermal phantoms poses additional challenges for PRF thermometry that might affect measurement accuracy [118]. To increase the temperature sensitivity of the phantom for higher accuracy temperature measurements, the phantom can be doped with TmDOTMA- [119], [120]. Additional details on MR thermometry are presented in §II.C.4.6.

4.2 Bench Measurements

Bench measurements can be employed to validate quantities accessible using a vector network analyser (VNA). These measurements include connecting one or more ports of the RF probe directly to the VNA to measure and validate the impedance spectrum of the RF probe. Additionally, basic near-field probes (E or H) can also be connected to the VNA, obtaining qualitative measurements proportional to the corresponding field. These probe measurements can identify resonance frequencies and provide basic information on relative distributions of fields and currents (see §II.B for additional measurements that can be performed with a VNA on the bench).

The comparison between measured and simulated RF probe characteristics allows a first consistency check to ensure that simulated loading, tuning, and coupling conditions are consistent with the physical setup. When the values for lumped elements (capacitances, inductances) needed to tune the numerical model show a substantial deviation from their physical values, it is recommended to review the numerical setup and to address the cause of such deviations. In case of RF probe arrays, diagonal (S_{ii}) and off-diagonal scattering parameters (S_{ij}) should also be evaluated and compared with simulated characteristics. It is best practice, especially for unshielded coils operating in weak loading conditions, to perform bench measurements with the test setup inserted within a conducting cylindrical bore to fully mimic the MR scanner environment. Similar to the comparison of the lumped element values, the line width of the resonances (i.e., quality factor (Q)) should be similar between measurement and simulation.

All bench measurements must be documented and may be needed in the subsequent validation steps (e.g., to allow a proper power normalisation).

4.3 B_1^+ Mapping

Comparing the simulated excitation profiles of a transmit probe with measured B_1^+ maps is a direct validation of the simulations and allows to identify a wide variety of discrepancies. Besides a qualitative agreement of the $|B_1^+|$ distribution, a quantitative comparison can be achieved by comparing the average and maximum B_1^+ sensitivity for a given input power. Various B_1^+ mapping techniques exist, and their availability will depend on the specific MR system and field strength considered [121]. In sTx and quadrature cases, the absolute B_1^+ phase can be approximated as half of the transceive phase as obtained from a spin echo phase image, after removing residual phase components from gradient-field-induced eddy currents [122], [123]. Common B_1^+ mapping techniques include the Actual Flip angle Imaging (AFI) method [124] and the Bloch-Siegert approach [125].

Additional levels of validation in transmit arrays can be obtained by performing comparisons of different excitation patterns, and by evaluating the excitation profiles within different slices (e.g., close to the coil element, deep within the phantom) [126]. Methods to estimate the absolute transmit phase include those described in [127] and [128]. In [129] the AFI method [124] was applied for the validation of a surface transmit/receive coil array, while in [130] the Bloch-Siegert approach [125] was used for a 16-channel cardiac array and a torso phantom. Another popular method is the dual refocusing angle acquisition mode (DREAM) [131] applied for the validation of an 8-channel Tx/Rx dipole array in [132], for example. For the validation of high transmit channel counts and in large body phantoms, B_1^+ mapping based on the TIAMO technique seems advantageous [133].

A proper power calibration (e.g., $B_1^+/\sqrt{\text{power}}$) performed at a suitable reference plane within the RF transmit chain is required for a quantitative comparison of the measured and simulated transmit sensitivity. Note, that for B_1^+ measurements the reference plane is typically the probe plug, whereas for simulations it is typically the feeding point. Hence, attenuation and insertion losses in cables and transmit/receive switches or any kind of RF components between the probe plug and feeding point must be measured and accounted for.

4.4 Validation Using S-parameters and B_1^+ Fields

In addition to the diagonal scattering parameters (S_{ii}) for all channels in an array, coupling coefficients (S_{ij}) between channels should also be compared between the simulation and the measurements to ensure faithful representation of the coupling mechanisms. Moreover, in addition to comparing the amplitude of the B_1^+ field maps for all channels, the phase maps between channels should also be compared (Figure 13). For RF pulse design and SAR evaluations, verifying the relative phases with respect to a reference channel is enough and thus spares the user from reconstructing absolute phases [134].

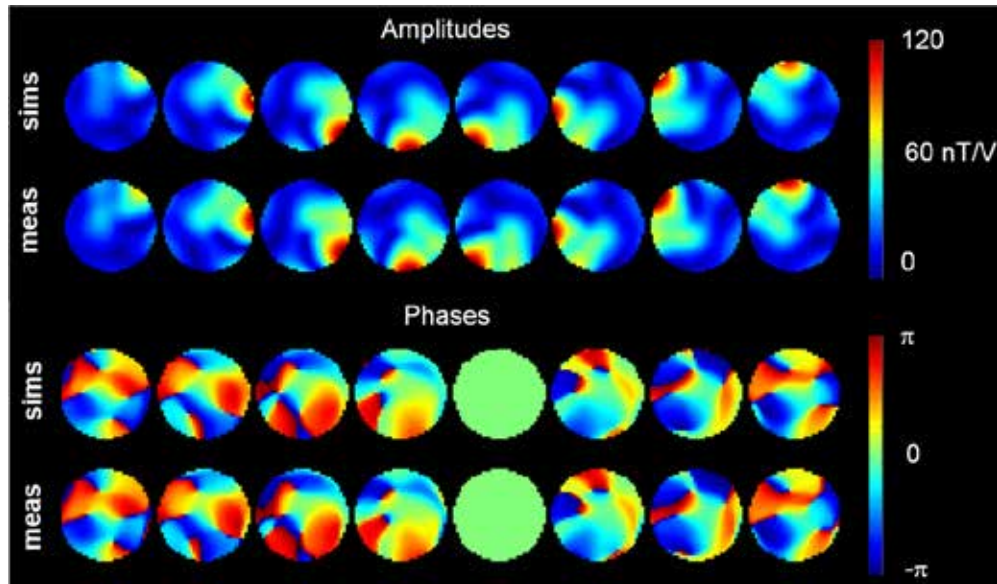


Figure 13: Simulated and experimental transmit field maps of an 8-ch transmit head array inside a homogeneous spherical phantom. Top row: magnitude, bottom row: phase.

If a calibration step is employed to match simulated and measured S-parameters and B_1^+ fields as described above, it is good practice to experimentally validate the simulated B_1^+ fields using two different phantoms with different shapes, sizes and/or dielectric properties [135]. This ensures that the simulation captures the load sensitivity of the coil and the fitting of the simulation data is not specifically optimised for a single scenario.

It may be challenging and time-consuming to match the S-parameters and B_1^+ fields closely between measurement and simulation, because of inaccuracies in coil modelling, existence of additional hardware such as Tx-Rx switch boxes that are difficult to model, or under strong inter-element coupling. In this case, co-simulation [47], fitting [136], [137], and/or optimization [138] approaches can be implemented to decrease the discrepancy between the simulated and measured S-parameters and B_1^+ fields in a practical way. In the co-simulation approach, lumped elements in the coil are treated as virtual ports during the 3D EM simulation. Then, the values of the lumped elements are optimised in an RF circuit simulation environment to match the simulated S-parameters to the measured S-parameters. Several studies combined co-simulation and active decoupling [136], [137], [139] by simulating ideal decoupling, i.e., simulating each channel of the coil while isolated, matched, and tuned; subsequently, a linear combination of the simulated fields may be calculated to match S-parameters or measured B_1^+ fields. In case of residual mismatch in B_1^+ fields due to cable losses, and phase shifts in the additional hardware between the coil and the scanner, optimised global scale factors and global phase offsets can be applied to each channel [140], [141]. Finally, the decoupling circuits themselves may be included in a hybrid circuit-spatial domain simulation model, and results optimised for agreement with measured B_1^+ fields, S-parameters, and physical coil components [142].

For both single channel and parallel transmission cases, the residual mismatch between the simulated and measured B_1^+ fields should be accounted for via Safety Margins. The difference for pTx coils is that several RF pulse configurations should be considered when calculating such a Safety Margins.

Assuming the worst-case scenario can lead to an overly conservative safety margin. Ferrand et al. [135], [140] describes an approach to calculate a safety margin based on a given error in the simulated electric fields, deduced from the root mean square error between measured and simulated B_1^+ fields while assuming Gaussian errors. They showed that using a probabilistic approach prevents an overly conservative safety margin while still ensuring, with a specified probability (e.g., 99.9%), that SAR limits will not be exceeded for an 8 channel transmit array for head imaging.

4.5 Near-field Probes

Spatial information about the RF field of the transmit probe can also be obtained through direct measurements using near-field probes during pulsed or continuous wave excitation. These measurements can be performed either within the MR magnet or outside in an external setup (e.g., anechoic chamber). Near-field probes can either measure the magnetic ($|H|$) field inside or outside the TSL, or perform dosimetric (SAR, or rather $|E|$ field) measurements inside the TSL (see [IEC/IEEE 62209-1528](#)). As illustrated by Collins et al., two coil simulations can result in similar $|B_1|$ distributions but with striking differences in SAR distributions [81]. Accordingly, validation using both $|H|$ and $|E|$ field probes can impart greater confidence in experimental validation [90].

Existing technologies permit measuring either the field magnitude of all three field components simultaneously, or the magnitude and phase of one particular component. Overall, this approach allows a high accuracy and dynamic range but requires a dedicated test setup including a computer-controlled probe positioning system [143], probes calibrated to the TSL and frequency range of interest, (MR conditional) data acquisition systems, as well as a signal generator and power amplifier when considering an external measurement setup. Again, a proper power normalisation (e.g., $\frac{B_1^+}{\sqrt{P}}$), referring to a suitable reference plane within the RF transmit chain, is a requirement for a quantitative comparison between measurement and simulations.

4.6 MR Thermometry

MR thermometry may serve as a useful tool for experimental validation of modelling results. There are various types of MR thermometry techniques that use different temperature-sensitive MR parameters to quantify either relative or absolute temperatures [118], [144]. For the purpose of this work, we will focus on the gradient-echo (GRE) based proton resonance frequency (PRF) shift method, which has a fast acquisition, high resolution, and relatively high accuracy ($< \pm 0.5$ °C) that can be readily implemented on most MR systems.

The PRF method is based on a linear increase in electron shielding of water, which decreases the chemical shift. Consequently, temperature changes can be deduced from changes in the phase of basic gradient-echo (GRE) images, which is in particular advantageous for high field MRI, since the GRE phase signal is relatively immune to B_1^+ and B_1^- inhomogeneities. As the PRF method measures relative temperature changes (not absolute temperatures), at least two time points are needed, i.e., prior to RF heating and after RF heating. The simplest way to calculate the temperature change is using the following equation based on a single echo GRE sequence and these two time points:

$$\Delta T = \frac{\Delta\varphi}{\alpha\gamma B_0 TE} = \frac{\varphi_f - \varphi_i}{\alpha\gamma B_0 TE}, \quad \text{II.9}$$

where variables are denoted as: gyromagnetic ratio γ , PRF coefficient α , static magnetic field strength B_0 , echo time TE , final phase φ_f , and initial phase φ_i .

The PRF coefficient α can be considered constant in the temperature range relevant for RF validation and has the value of -0.01 ppm/°C for pure water [145]. Published PRF coefficients for phantom materials show a wider variety depending on the doping agent used for adjustment of the dielectric properties. If literature values are not available, or must be verified, it is possible to experimentally determine α for the constructed phantom by using Fluoroptic® probes (see §II.A.3.1 and NEMA MS 10) positioned inside the phantom [146], [147].

A few bias mechanisms may deteriorate the measurement accuracy of the PRF method. As the method is based on the phase of the MR signal, other sources of phase change such as drift of the main magnetic field B_0 will also influence the results. A typical drift of 0.02 ppm/h may already introduce a temperature bias of 2°C after one hour. Additional spatial terms in the static field drift may also be present due to hardware instabilities in the gradient and/or shim system. These terms can be corrected by using, e.g., reference oil samples around the phantom [148]. If the field drift is repeatable, the accuracy of the background field drift correction can be assessed by simply performing an additional experiment without RF heating. Other sources of phase bias include temperature-induced changes in electrical conductivity, which can lead to changes in the phase of the GRE signal independent of TE (because conductivity affects RF phase). When needed, these effects can be corrected by applying a dual echo technique [118], [149]. Typically, however, they are negligible, and a single-echo technique can provide sufficient accuracy for RF probe validation. Generally, MR thermometry measurement is less sensitive to bias mechanisms when applied heating exceeds 3 °C [150].

5 Online SAR Supervision

Most modern MRI systems are capable of producing SAR and temperatures in the subject that exceed the IEC limits. The scanner can typically estimate the SAR for each sequence depending on timing parameters, RF calibrations, etc., but safety must be ensured even if the estimate is incorrect or if there is a failure during the scan (i.e., Single Fault Safety). It is prudent to perform regular quality assurance (QA) to ensure that the components of the transmit chain (including RF amplifiers and coils) behave properly.

The SAR supervisor or monitor is a device that uses the principle of energy conservation to measure, in real time, the time-averaged power dissipated in the subject. These measurements are compared to the SAR Limits, and the scan is stopped immediately if those limits are exceeded (both the 6-minute and 10-second averages). Certain manufacturers have also implemented the Total Energy Limit (specific absorbed energy—SAE, or specific energy dose—SED; see §II.C.1.3) [151].

Because the SAR monitor can only measure power, a conversion must be made between power and corresponding SAR for each experimental setup. The conversion allows the relevant IEC SAR Limits (both local and global) to be converted to the required power thresholds (see Appendix C for detailed calculations). Simulations are especially relevant to determine the power limits for local SAR, which is usually expressed through the ratio of 10-g SAR to global SAR. The two modes of transmission are discussed separately below because of their different complexity levels.

5.1 Single-channel Transmission

In single-channel transmission, one operates with a volume or surface probe with a single RF channel and therefore pulse shape. The calculation begins with the definition of SAR at location r for 100% duty cycle at unit waveform amplitude is given by:

$$SAR(r) = \frac{\sigma}{2\rho} \|\vec{E}(r)\|^2, \quad \text{II.10}$$

where σ is the electrical conductivity in S/m, ρ is the mass density in kg/m³, \vec{E} is the time-harmonic electric field vector peak amplitude (with components along the x , y and z axis) corresponding to a unitary input in V/m. When the electric field is modulated by an input RF waveform, the previous formula becomes:

$$SAR(r) = \frac{\sigma}{2\rho} \|\vec{E}(r)\|^2 \frac{1}{T} \int_0^T |s(t)|^2 dt, \quad \text{II.11}$$

where T is the averaging time window and $s(t)$ is the complex-valued RF waveform. Conveniently, the outcome is that the SAR for a given body load is directly proportional to the time-averaged power of the RF pulse. This greatly simplifies exam supervision, as a conservative estimate of the average power is already established by monitoring the forward power, e.g., by using a directional coupler and power meter. Another approach is to determine the accepted power by monitoring both the forward and reflected powers.

Although analytical models have been employed to model local SAR at low fields [152], full-wave numerical simulations are required at higher fields to establish a relation between input power and peak 10-g SAR, incorporating additional Safety Margins to account for various uncertainties (dielectric properties, position in the coil, intersubject variability, etc.).

Finally, one should observe that these equations assume that all power is dissipated in the subject, ignoring losses in the RF probe, RF chain and radiation. This assumption may be improved through simulations and validation measurements (for instance bench measurements or B_1^+ mapping) to characterise these losses.

5.2 Parallel Transmission

Parallel transmission (§II.C.2.1.2) makes use of an array of RF transmitters independently controllable in amplitude and phase over time. The previous SAR formula now becomes:

$$SAR(r) = \frac{\sigma}{2\rho} \frac{1}{T} \int_0^T \left\| \sum_{k=1}^N s_k(t) \vec{E}_k(r) \right\|^2 dt, \quad \text{II.12}$$

where N denotes the number of transmit channels and $s_k(t)$ denotes the complex-valued RF waveform on the k^{th} channel. Unlike the single channel mode, the superposition of the time-dependent amplitudes and phases of the different waveforms play an important role. This formula can be recast using quadratic forms leading to SAR or Q matrices [153]:

$$\begin{aligned}
SAR(r) = \frac{1}{n} \sum_{j=1}^n S_j^\dagger & \left[\frac{\sigma}{2\rho} ([E_{X,1}^* \ : \ E_{X,N}^*] [E_{X,1} \ \cdots \ E_{X,N}] \right. \\
& + [E_{Y,1}^* \ : \ E_{Y,N}^*] [E_{Y,1} \ \cdots \ E_{Y,N}] \\
& \left. + [E_{Z,1}^* \ : \ E_{Z,N}^*] [E_{Z,1} \ \cdots \ E_{Z,N}] \right) S_j = \frac{1}{n} \sum_{j=1}^n S_j^\dagger Q(r) S_j,
\end{aligned} \tag{II.13}$$

where S_j is the column vector containing the complex values corresponding to the different channels at the j^{th} time step. Global SAR can again be assessed by invoking energy conservation, similar to the case of single-channel transmission. By measuring forward ($P_{forward}$) and reflected powers (P_{ref}) on all channels, the dissipated power is

$$\sum_{k=1}^N P_{forward,k} - \sum_{k=1}^N P_{ref,k}, \tag{II.14}$$

which yields an upper-bound of the global SAR after division by the exposed mass [154]. Despite the merit of such an approach in terms of estimating global SAR, estimating the corresponding local SAR here would require assuming worst-case constructive interference conditions, which would be very restrictive. Numerical simulations have, for instance, reported worst-case peak 10-g SAR over global SAR ratios on the order of 20 to 60 [93], [155] depending on the RF probe array and excitation conditions. If minimum supervision of the experiment is pursued, safe usage may still be established by incorporating very conservative Safety Margins [156], [157]. The more information about the actual experiment that can be incorporated into the local SAR estimate, the less conservative these margins need to be; highly conservative margins lead to a drastic underexploitation of parallel transmission technology.

Additional information about the actual experiment can be obtained by real-time monitoring of the amplitudes and phases, e.g., with directional couplers, and to relate this information to local SAR based on a pre-calculated set of numerical body models [156]. Monitoring local SAR this way was a challenge initially due to the high number of Q matrices involved. This number can range from tens of thousands to a few million per body model depending on the size of the body exposed and the resolution of the simulations. Virtual Observation Points (VOPs) [158] were proposed to drastically compress the number of Q matrices at the cost of an overestimation factor, making this approach tractable. Some variants are able to reach higher levels of compression [159], [160]. Some MR vendors allow incorporating these VOPs into the scanner's safety monitoring system to enable local SAR supervision. Within this framework, it is therefore advised to keep the number of VOPs reasonable (~1000 or less) to allow for SAR computation in real-time in high-duty-cycle sequences. The higher the number of transmit channels, the higher the overestimation factor in general needs to be, to reach this target due to the higher spatial diversity in the RF transmit fields. The directional couplers also introduce additional uncertainties (typically $\pm 10\%$ in power, $\pm 5^\circ$ in phase) leading to additional Safety Margins that should be taken into account [161], [162]. An alternative to directional couplers is to use pick-up loops in close proximity to the RF transmit coils [137], [139], [156], which can be furthermore exploited to perform active decoupling (through feedback) and leads to better match with the simulated conditions [137], [139]. One additional advantage of using pick-up loops is that the physical field values are being monitored, as opposed to the transmitted RF signals, which avoids uncertainties due to instabilities in

the RF probe and its feed circuit. When using directional couplers, it is implicitly assumed that the RF probe array is functioning properly and without drift, which needs to be confirmed by regular quality control checks but cannot be guaranteed in real time. Some information can be gained by measuring reflected powers and thus detect potential faults [154], [163].

For simplicity, supervision can also be performed on powers only, ignoring phase and amplitude information. We provide here some guiding principles on how to calculate the thresholds. From a numerical set of Q matrices, it is possible to determine the worst-case scenario based on the largest eigenvalue. By denoting this eigenvalue λ_{\max} (in kg^{-1}), then the maximum total power limit allowed is $10/\lambda_{\max}$ and $20/\lambda_{\max}$ for the 6-min time-average normal and first level IEC modes of operation, respectively [164]. Relying on this principle assumes that the total power is monitored. It can be also quite conservative as it is very unlikely that the worst-case waveform, i.e., the eigenvector corresponding to the largest eigenvalue, is played during the whole RF pulse and sequence. Power limits on each individual channel can also be enforced. Dividing the total power derived above by the number of channels ensures compliance but it is even more conservative, since the worst-case scenario given a total power can be all the energy going in a couple of channels. One possibility is to perform a numerical search of the worst-case scenario given a set of equal power limits among channels [164].

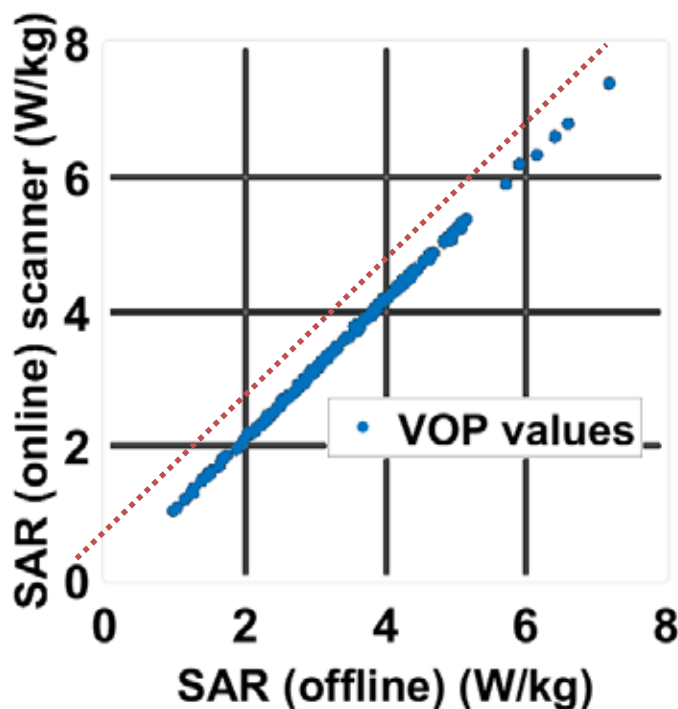


Figure 14: SAR online values calculated by the scanner based on measured waveforms versus SAR offline values calculated based on the model. Results were obtained on a Siemens scanner (Siemens Healthcare, Erlangen, Germany) equipped with a Nova 8Tx-32Rx coil (Nova Medical, Wilmington, MA, USA).

Regardless of the origin of the local SAR model, i.e., provided by the probe manufacturer or created in-house for home-made probes, its validation and application in the MR system remains the responsibility of the user. This requires a thorough understanding of the VOP format needed for the scanner (channel ordering, phase conventions etc.) and post-processing steps required, for instance when incorporating

possible safety factors. In [Figure 14](#), the offline and online (returned by the scanner) values for each VOP are plotted against each other for a random waveform [162]. The two can differ slightly, for instance due to system instabilities and imperfections. Instead, the online computation performed by the scanner measures the waveforms in real-time and performs the 6-min and 10-s sliding window integrations, thereby taking into account possible non-ideal behaviours of the RF amplifiers.

Finally, it should be noted that, although the tools presented here involved SAR monitoring, temperature remains more important biologically than SAR. Using the same formalism as above, temperature VOPs, thus compatible with the same monitoring tools, have also been proposed [165].

6 Safety Margins

Establishing appropriate safety margins is necessary to account for inevitable discrepancies between calculated SAR values and those occurring in reality. Discrepancies can occur for a variety of reasons, including

- variation in the anatomy between subjects and within the same subject at different points in time;
- measurement uncertainty of various quantities (e.g., RF power, physical dimensions, permittivity and conductivity, etc.);
- modelling approximations;
- construction tolerances and component drift (thermal as well as due to ageing).

Appropriate safety margins can be determined from a detailed analysis of the scanning scenario. Note that the margins are not necessarily constant when important variables such as the Larmor frequency, transmission scheme, or anatomical region are changed. Consequently, it is difficult to provide safety margin values that can be applied generally.

One area of particular interest is the simulated local SAR distribution, which can be used to predict peak local SAR at the scanner. Peak local SAR prediction can be based on VOPs (for pTx systems) and/or the average power input at the scanner (for single channel systems). However, the simulated peak local SAR is not necessarily identical to the peak local SAR in the scanner. This can result in an underestimation of peak local SAR during the MRI exam, which is an unsafe situation. To prevent underestimation of peak local SAR, the simulated SAR can be multiplied by a safety margin to give a corrected peak SAR value to be used for peak local SAR assessment at the scanner:

$$pSAR_{corr} = pSAR_{sim} * \text{Safety margin}. \quad II.15$$

If the relative uncertainty in peak SAR estimation $\frac{\Delta pSAR}{pSAR_{sim}}$ is known, the safety margin can be calculated as follows and vice-versa [166]:

$$\text{Safety margin} = 1 + \frac{\Delta pSAR}{pSAR_{sim}}. \quad II.16$$

Three separate sources of error can be identified between simulations and measurements, resulting in a [Safety Margin for Inter-subject Variability](#), a [Safety Margin for RF System Imperfections](#), and a [Safety Margin for Modelling Errors](#) [162]. These errors may be assessed by separate procedures, as outlined in the sections below. When the inaccuracies from different error sources are known, they can be combined into a total safety margin obtained by multiplication (i.e., error propagation):

$$\begin{aligned}
\text{Safety margin} = & \left(1 + \frac{\Delta pSAR_{intersubj.var}}{pSAR_{sim}} \right) * \left(1 + \frac{\Delta pSAR_{RFsys.imperf}}{pSAR_{sim}} \right) \\
& * \left(1 + \frac{\Delta pSAR_{model.error}}{pSAR_{sim}} \right).
\end{aligned} \tag{II.17}$$

However, if we assume that the errors are randomly distributed (e.g., according to a normal distribution) and uncorrelated, the total relative uncertainty can be calculated by adding the different uncertainties in quadrature (root sum-of-squares) [166]:

$$\frac{\Delta pSAR}{pSAR_{sim}} = \sqrt{\left(\frac{\Delta pSAR_{intersubj.var}}{pSAR_{sim}} \right)^2 + \left(\frac{\Delta pSAR_{RFsys.imperf}}{pSAR_{sim}} \right)^2 + \left(\frac{\Delta pSAR_{model.error}}{pSAR_{sim}} \right)^2}. \tag{II.18}$$

The final safety margin can then be calculated. The probabilistic approach of propagating error into a safety margin is, in general, less conservative than multiplying individual safety factors because the latter assumes that the errors cannot compensate for one another.

6.1 Safety Margin for Inter-subject Variability

The effect of inter-subject variability, i.e., the mismatch between the subject in the scanner and the body model used to predict SAR or temperature, might be different for single channel and parallel transmission. The safety margin needed to take inter-subject variability into account is more complex to calculate for pTx excitations because of the necessity to consider several RF pulse configurations. To assess inter-subject variability of local SAR, simulations can be done on multiple human models [167]. For pTx systems, the difference in inter-subject variability for different RF shims or waveforms also must be considered.

De Greef et al. [53] analysed the SAR created at 7T by an 8 channel stripline volume coil in 6 different prevalent head models and found that, by assigning the Ella model from the Virtual Family as a so-called generic head model, optimisation of RF shimming excitation modes using the generic model SAR combined with a safety factor of 1.4 is sufficient to account for variation across the remaining 5 head models. Le Garrec et al. [54] carried out a probabilistic analysis of the intersubject variability of SAR due to changes in head length, head breadth and translations in Z and Y dimensions. They found that a safety margin of 1.5 was enough at 7T to ensure <1% probability of exceeding SAR limits in the Caucasian adult population. Sadeghi-Tarakameh et al. assessed the four different shimming scenarios of an 8-channel transmit/receive head coil for 10.5T and, rather than establishing a multiplicative safety factor based on intersubject variability, determined the measured RF cable loss of 3.9 dB between the amplifiers and coil feeds was sufficient on its own to safely limit power [168].

For body imaging, because the body shape and dimensions are more variable than those of the head, larger safety margins are typically required. Both Ipek et al. [169] and Meliado et al. [63] found safety margins >1.8 are needed to account for the large variation of SAR in prostate imaging at 7T using 8-channel surface transmit arrays driven in RF phase- shimmed conditions.

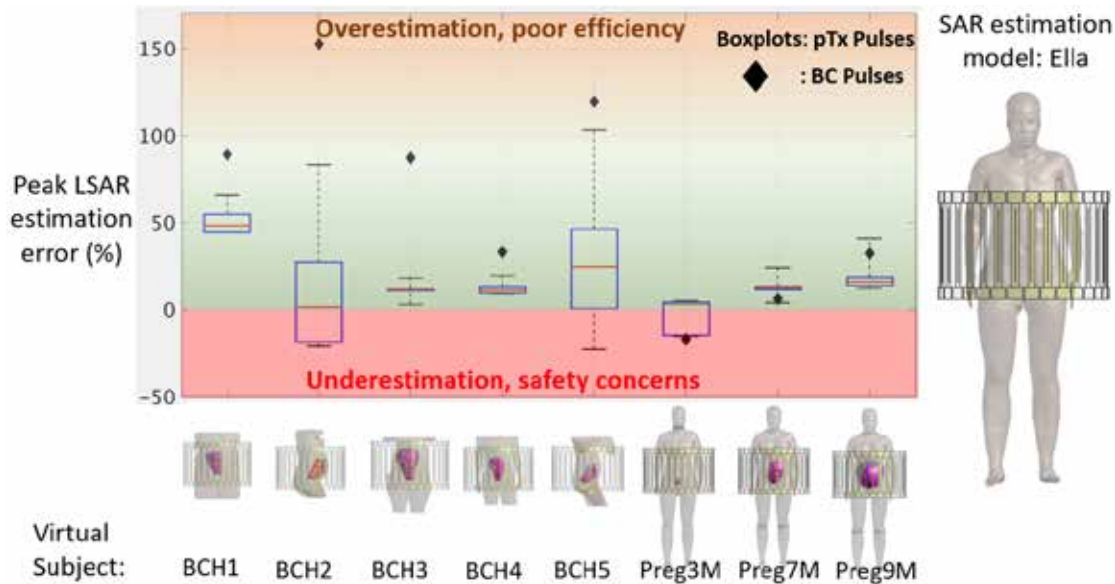


Figure 15: Estimation error for when a non-pregnant female body model (Ella) is used to estimate the peak local SAR of various pregnant “virtual subjects” (horizontal axis) for various RF excitation modes (BC: birdcage-standard, pTx: parallel transmission).

For pregnant body imaging, where the body shape and posture vary arguably the most among all imaging scenarios, Yetişir et al. (Figure 15) reported a maximum peak local SAR estimation error of 153% (corresponding to a safety margin of 2.5) at 3T due to the mismatch between the subject and the SAR body model for a 2-port 32-rung birdcage body coil [170]. They also compared quadrature operation, RF shimming and 2-spoke RF excitation modes and found that for more than half of the body models, the maximum SAR estimation errors were higher for the quadrature mode compared to pTx modes.

In summary, the safety margin for inter-subject variability depends on the excitation mode (single channel vs. parallel transmission, RF shimming vs full pTx, etc.), imaging site (head, prostate, knee, etc.) as well as the RF probe configuration (volume vs surface, number of channels, loop vs dipole etc.). Hence, a separate safety margin should be determined for each specific scenario.

6.2 Safety Margin for RF System Imperfections

Imperfections in the hardware of the RF transmit chain and Online SAR Supervision system can be accounted for by additional safety margins. On the scanner, RF waveforms measured in real time (e.g., using directional couplers or pickup loops) are used to estimate the actual SAR. The first margin accounts for these RF power measurement uncertainties, which translate directly into uncertainties in measured SAR. For sTx systems the safety margin for measurement uncertainty is readily calculated using Eq. (II.17) above.

For pTx systems, VOPs [158] are used to monitor local SAR in real time on the scanner and/or during RF pulse design. Due to intrinsic measurement uncertainties (e.g., 10% power, 5° phase), an additional safety factor should be adopted by multiplying the VOPs, as in Eq. (II.13) above.

The difference between designed and measured RF waveforms is a second system imperfection, although it does not typically impact subject safety. These differences can be accounted for by a safety

margin calculated by playing several different RF pulses on the scanner and quantifying the maximum difference between the peak local SAR measured online by the SAR supervisor and that calculated offline using the designed RF waveforms ([Figure 16](#)).

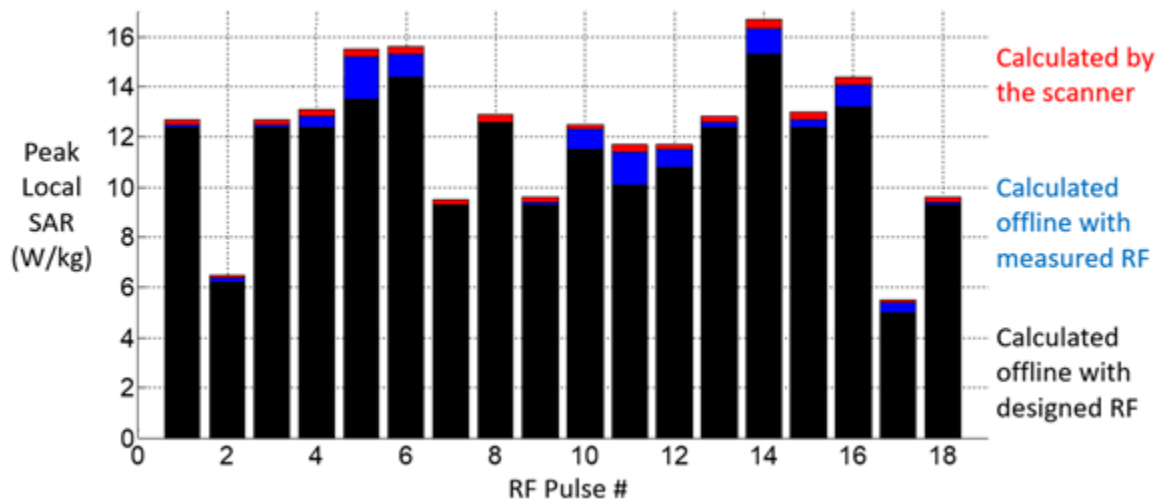


Figure 16: Discrepancy between the peak local SAR values calculated by one scanner using measured RF waveforms, calculated offline using measured RF waveforms, and calculated offline with designed RF waveforms, for 18 different RF pulses. <2% difference between read and blue is due to short test RF pulses played by the scanner before each sequence.

6.3 Safety Margin for Modelling Errors

In addition to inter-subject variability and RF system imperfections, there can be imperfections in the RF simulation model. After carefully matching the simulations and measurements, the modelling error can be assessed by quantifying the remaining error. From the remaining absolute discrepancies in B_1 magnitude, Boulant et al. calculated a peak local SAR relative error of 0.25 for an 8-channel head coil at 7T [162]. Similarly, when both B_1 and temperature maps are available, the larger error of the two may be set as the modelling inaccuracy; in this manner, Steensma et al. determined a relative modelling error of 0.52, given the greater SAR error from experimental MR thermometry for an 8-channel prostate array at 7T [166].

7 Documentation of Simulations and Validations

Following successful modelling and RF safety assessment, it is necessary to clearly document all completed procedures and analyses. Should modelling studies need to be completed in the future, owing either to a coil modification or a subject's unique anatomy, it is necessary to include all relevant simulation and validation details as well as initial results so that new personnel may reproduce the procedures. Example simulation details (see also) and software files that should be recorded and archived include:

- Model for RF and thermal simulations in combination with imported 3D structures
- Specific version of the simulation software

- Simulation settings and parameters (e.g., details of mesh generation or discretization grid, solver parameters)
- Human model version, grid size, and tissue properties database
- Data file format, e.g., HDF5, ASCII, DICOM

Example validation data to be documented include:

- For B_1 maps: imaging data in a standard format (e.g., DICOM), RF power logs, MR-System data
- Field probes: type, vendor, calibration certificate, measurement parameters
- Phantom information including dimensions, material, dielectric and relaxation properties

Some relevant information can also be found in [FDA Guidance 1807](#).

Part III

Page III.*

Acknowledgements.....	1
Author Contributions.....	1
References	2
Standards.....	2
Online Resources.....	8
Scientific Literature and Books.....	9
Appendices.....	22
A. Common Failure Modes for RF Coils.....	22
B. Example of Risk Analysis.....	23
C. Calculation of Sequence SAR and Supervision Thresholds	25
D. Summary of Relevant Standards, Government and Industry Publications	32

Acknowledgements

We thank the ISMRM and Dr. Daniel Sodickson (ISMRM president 2017–2018) for supporting this initiative from its inception. Valuable input, feedback and encouragement was also provided by Simone Winkler, Roberta Frass-Kriegl, Johan van den Brink, Brodi Roduta Roberts, and Vyacheslav Volotovskyy.

Author Contributions

All Authors contributed to the writing of specific sections of these recommendations. Further credit goes to CATvdB, DOB, JR, JM-B for leading the efforts to develop the 4 major chapters; ND and CATvdB for founding the initiative; ND, JR, TF, WB, KG played essential roles in editing and assembling the complete document.

References

Standards (see also Appendix [D](#))

AAPM Report No. 100

Acceptance Testing and Quality Assurance Procedures for Magnetic Resonance Imaging Facilities; AAPM Report No. 100; American Association of Physicists in Medicine, 2010.

ACR MRI QC Manual

ACR Magnetic Resonance Imaging Quality Control Manual; American College of Radiology, 2015.

ACR Large Phantom

Phantom Test Guidance for Use of the Large MRI Phantom; American College of Radiology, 2018.

ACR MR Safety Manual

ACR Manual on MR Safety; American College of Radiology, 2020.

ANSI Z136.1

American National Standards Institute; Laser Institute of America. American National Standard for Safe Use of Lasers; 2014.

ASTM D149

Test Method for Dielectric Breakdown Voltage and Dielectric Strength of Solid Electrical Insulating Materials at Commercial Power Frequencies; ASTM International, 2020.

ASTM D648

Test Method for Deflection Temperature of Plastics Under Flexural Load in the Edgewise Position; ASTM International, 2018.

ASTM D1929

Test Method for Determining Ignition Temperature of Plastics; ASTM International, 2020.

ASTM E595

Test Method for Total Mass Loss and Collected Volatile Condensable Materials from Outgassing in a Vacuum Environment; ASTM International, 2015.

ASTM F2052

Test Method for Measurement of Magnetically Induced Displacement Force on Medical Devices in the Magnetic Resonance Environment; ASTM International, 2015.

ASTM F2182

Test Method for Measurement of Radio Frequency Induced Heating On or Near Passive Implants During Magnetic Resonance Imaging; ASTM International, 2019.

ASTM F2213

Test Method for Measurement of Magnetically Induced Torque on Medical Devices in the Magnetic Resonance Environment; ASTM International, 2017.

ASTM D4565

Test Methods for Physical and Environmental Performance Properties of Insulations and Jackets for Telecommunications Wire and Cable; ASTM International, 2015.

EIA-364 Series

Electrical Connector Performance Test Standards; Electronic Components Industry Association (ECIA).

EU Directive 2013/35

Directive 2013/35/EU of the European Parliament and of the Council of 26 June 2013 on the Minimum Health and Safety Requirements Regarding the Exposure of Workers to the Risks Arising from Physical Agents (Electromagnetic Fields).

EU Medical Device Regulation 2017/745

Regulation (EU) 2017/745 of the European Parliament and of the Council of 5 April 2017 on Medical Devices, Amending Directive 2001/83/EC, Regulation (EC) No 178/2002 and Regulation (EC) No 1223/2009 and Repealing Council Directives 90/385/EEC and 93/42/EEC; 2017; Vol. 117.

FDA Guidance 340

Submission of Premarket Notifications for Magnetic Resonance Diagnostic Devices - Guidance for Industry and Food and Drug Administration Staff; 340; US Food and Drug Administration, 2016.

FDA Guidance 793

Criteria for Significant Risk Investigations of Magnetic Resonance Diagnostic Devices - Guidance for Industry and Food and Drug Administration Staff; 793; FDA, 2014.

FDA Guidance 1807

Reporting of Computational Modeling Studies in Medical Device Submissions - Guidance for Industry and Food and Drug Administration Staff, 1807, FDA, 2016.

FDA Guidance 19011

Magnetic Resonance (MR) Receive-only Coil - Performance Criteria for Safety and Performance Based Pathway - Guidance for Industry and Food and Drug Administration Staff; 19011; US Food and Drug Administration, 2020.

ICNIRP EMF Guidelines

International Commission on Non-Ionizing Radiation Protection (ICNIRP)1. Guidelines for Limiting Exposure to Electromagnetic Fields (100 KHz to 300 GHz): Health Physics 2020, 118 (5), 483–524.

IEC 60050-192

International electrotechnical vocabulary – Part 192: Dependability. International Electrotechnical Commission: Geneva, 2015.

IEC 60060 Series

High-Voltage Test Techniques; Part 1. International Electrotechnical Commission: Geneva, 2010.

IEC 60243 Series

Electric Strength of Insulating Materials - Test Methods; Part 1. International Electrotechnical Commission: Geneva, 2013.

IEC 60417

Graphical Symbols for Use on Equipment; International Electrotechnical Commission, 2002.

IEC 60512-24

Connectors for Electronic Equipment - Tests and Measurements - Part 24-1: Magnetic Interference Tests; International Electrotechnical Commission, 2010.

IEC 60529

Degrees of Protection Provided by Enclosures (IP Code); International Electrotechnical Commission, 2013.

IEC 60601-1

Medical Electrical Equipment – Part 1: General Requirements for Basic Safety and Essential Performance; IEC 60601-1 Ed. 3.2:2020; International Electrotechnical Commission: Geneva, Switzerland, 2020.

IEC 60601-1-2

Medical electrical equipment - Part 1-2: General requirements for basic safety and essential performance - Collateral Standard: Electromagnetic disturbances - Requirements and tests; IEC 60601-1-2:2014; International Electrotechnical Commission: Geneva, Switzerland, 2014.

IEC 60601-2-33

Medical Electrical Equipment — Part 2-33: Particular Requirements for the Basic Safety and Essential Performance of Magnetic Resonance Equipment for Medical Diagnosis; IEC 60601-2-33:2010; International Electrotechnical Commission: Geneva, Switzerland, 2010.

IEC 60695-2-13

Fire Hazard Testing. Glow-Wire Ignition Temperature (GWIT) Test Method for Materials Part 2-13, Part 2-13; International Electrotechnical Commission, 2014.

IEC 60695-11-10

Fire hazard testing; International Electrotechnical Commission. Fire Hazard Testing. Part 11-10: Test Flames – 50 W Horizontal and Vertical Flame Test Methods; International Electrotechnical Commission, 2013.

IEC 60812

Failure Modes and Effects Analysis (FMEA and FMECA); International Electrotechnical Commission: Geneva, Switzerland, 2018.

IEC 60878

Graphical Symbols for Electrical Equipment in Medical Practice; International Electrotechnical Commission, 2015.

IEC 61000-4-2

Electromagnetic Compatibility (EMC) - Part 4-2: Testing and Measurement Techniques - Electrostatic Discharge Immunity Test; International Electrotechnical Commission: Geneva, Switzerland, 2008.

IEC 61025

Fault Tree Analysis (FTA); International Electrotechnical Commission: Geneva, Switzerland, 2006.

IEC 62366-1

Medical Devices - Part 1: Application of Usability Engineering to Medical Devices; International Electrotechnical Commission, 2015.

IEC 62366-2

Medical Devices - Part 2: Guidance on the Application of Usability Engineering to Medical Devices; International Electrotechnical Commission, 2016.

IEC/IEEE 62209-1528

Measurement procedure for the assessment of specific absorption rate of human exposure to radio frequency fields from hand-held and body-mounted wireless communication devices – Part 1528: Human models, instrumentation, and procedures (Frequency range of 4 MHz to 10 GHz). International Electrotechnical Commission, IEEE Standards Association; 2020.

IEC/IEEE 62704-1

Determining the Peak Spatial-Average Specific Absorption Rate (SAR) in the Human Body from Wireless Communications Devices, 30 MHz to 6 GHz. Part 1; International Electrotechnical Commission, IEEE Standards Association; 2017.

IEEE C95.1

IEEE Standard for Safety Levels with Respect to Human Exposure to Electric, Magnetic, and Electromagnetic Fields, 0 Hz to 300 GHz. IEEE Standards Association; 2019.

IEEE C95.3

IEEE Recommended Practice for Measurements and Computations of Electric, Magnetic, and Electromagnetic Fields with Respect to Human Exposure to Such Fields, 0 Hz to 300 GHz. IEEE Standards Association; 2021.

IEEE 1597.2

IEEE Recommended Practice for Validation of Computational Electromagnetics Computer Modeling and Simulations. IEEE Standards Association; 2011. (Currently listed as *inactive* due to its age but not officially withdrawn).

IPC-2221B

Generic Standard on Printed Board Design; IPC International, 2012.

ISO 75

Plastics — Determination of Temperature of Deflection under Load — Part 1: General Test Method; ISO 75-1:2020; International Organization for Standardization: Geneva, Switzerland, 2020.

ISO 871

Plastics — Determination of Ignition Temperature Using a Hot-Air Furnace; ISO 871:2006; International Organization for Standardization: Geneva, Switzerland, 2006.

ISO 7010

Graphical Symbols — Safety Colours and Safety Signs — Registered Safety Signs; ISO 7010; International Organization for Standardization: Geneva, Switzerland, 2019.

ISO 9772

Cellular Plastics — Determination of Horizontal Burning Characteristics of Small Specimens Subjected to a Small Flame; International Organization for Standardization: Geneva, Switzerland, 2012.

ISO 9773

Plastics — Determination of Burning Behaviour of Thin Flexible Vertical Specimens in Contact with a Small-Flame Ignition Source; International Organization for Standardization: Geneva, Switzerland, 1998.

ISO/TS 10974

Assessment of the Safety of Magnetic Resonance Imaging for Patients with an Active Implantable Medical Device; International Organization for Standardization: Geneva, Switzerland, 2018.

ISO 10993-1

Biological Evaluation of Medical Devices — Part 1: Evaluation and Testing within a Risk Management Process; International Organization for Standardization: Geneva, Switzerland, 2018.

ISO 10993-10

Biological Evaluation of Medical Devices — Part 10: Tests for Irritation and Skin Sensitization; International Organization for Standardization: Geneva, Switzerland, 2010.

ISO 14971

Medical Devices — Application of Risk Management to Medical Devices; International Organization for Standardization: Geneva, Switzerland, 2019.

ISO 15223-1

Medical Devices — Symbols to Be Used with Medical Device Labels, Labelling and Information to Be Supplied — Part 1: General Requirements; International Organization for Standardization, 2016.

ISO 31000

Risk Management — Guidelines; International Organization for Standardization: Geneva, Switzerland, 2018.

NASA – GSFC S-311-P-10

Connectors, Electrical, Rectangular, Miniature, Polarized Shell, Rack and Panel, for Space Flight Use; NASA Electronic Parts and Packaging (NEPP) Program, Goddard Space Flight Center. National Aeronautics and Space Administration, 1992.

NEMA MS 2

Determination of Two-Dimensional Geometric Distortion in Diagnostic Magnetic Resonance Images; NEMA MS 2-2008 (R2014); National Electrical Manufacturers Association: Rosslyn, Virginia, 2008.

NEMA MS 4

Acoustic Noise Measurement Procedure for Diagnostic Magnetic Resonance Imaging Devices; NEMA MS 4-2010; National Electrical Manufacturers Association: Rosslyn, Virginia, 2010.

NEMA MS 8

Characterization of the Specific Absorption Rate (SAR) for Magnetic Resonance Imaging Systems; NEMA MS 8-2016; National Electrical Manufacturers Association: Rosslyn, Virginia, 2016.

NEMA MS 10

Determination of Local Specific Absorption Rate (SAR) in Diagnostic Magnetic Resonance Imaging; NEMA MS 10-2010; National Electrical Manufacturers Association: Rosslyn, Virginia, 2010.

NEMA MS 14

Characterization of Radiofrequency (RF) Coil Heating in Magnetic Resonance Imaging Systems; NEMA MS 14-2019; National Electrical Manufacturers Association: Rosslyn, Virginia, 2019.

UL 94

Standard for Tests for Flammability of Plastic Materials for Parts in Devices and Appliances; American National Standards Institute; Underwriters' Laboratories: Northbrook, Ill., 2013.

Online Resources

The following web sites and online resources are cited in this document; they are current and accessible at the time of writing. This list is by no means exhaustive and additional relevant information is, and will likely become, available online.

CC-BY-ND 4.0

<https://creativecommons.org/licenses/by-nd/4.0>

ISMRRM

<https://www.ismrm.org/>

ASQ Quality Glossary

<https://asq.org/quality-resources/quality-glossary/f#>

Opensourceimaging Wiki

<https://wiki.opensourceimaging.org/Hardware>

Ma-Com MA4P7461F-1072T

<https://cdn.macom.com/datasheets/MA4P7461F-1072T.pdf>

FDA Recognized Consensus Standards

https://www.accessdata.fda.gov/scripts/cdrh/cfdocs/cfStandards/detail.cfm?standard_identification_no=37168

Martinos Center Anthropomorphic Phantoms

https://phantoms.martinos.org/Main_Page

NIH Dielectric Phantom Recipe Generator

<https://amri.ninds.nih.gov/cgi-bin/phantomrecipe>

AustinMan and AustinWoman Models

<https://sites.utexas.edu/austinmanaustinwomanmodels>

AC6LA

<https://www.ac6la.com/swrloss.html>

Scientific Literature and Books

- [1] J. G. Delfino, D. M. Krainak, S. A. Flesher, and D. L. Miller, "MRI-related FDA adverse event reports: A 10-yr review," *Med. Phys.*, vol. 46, no. 12, pp. 5562–5571, Dec. 2019, doi: 10.1002/mp.13768.
- [2] J. Hoffmann *et al.*, "Safety testing and operational procedures for self-developed radiofrequency coils: Safety Procedure for Self-Developed RF Coils," *NMR Biomed.*, vol. 29, no. 9, pp. 1131–1144, Sep. 2016, doi: 10.1002/nbm.3290.
- [3] "System Safety Process Steps." U.S. Department of Transportation, Federal Aviation Administration, May 01, 2005. Accessed: May 31, 2021. [Online]. Available: https://www.faa.gov/regulations_policies/handbooks_manuals/aviation/risk_management/media/sprocdscrp.pdf
- [4] P. L. Jones, J. Jorgens, A. R. Taylor, and M. Weber, "Risk Management in the Design of Medical Device Software Systems," *Biomedical Instrumentation & Technology*, vol. 36, no. 4, pp. 237–266, Jul. 2002, doi: 10.2345/0899-8205(2002)36[237:RMITDO]2.0.CO;2.
- [5] S. Pilot, "What is fault tree analysis?," *Quality Progress*, vol. 35, no. 3, American Society for Quality, Milwaukee, United States, p. 120, Mar. 2002.
- [6] W.E. Vesely, F.F. Goldberg, N.H. Roberts, and D.F. Haasl, "Fault Tree Handbook," U.S. Nuclear Regulatory Commission, Washington, DC, NUREG-0492, 1981. Accessed: Jul. 23, 2020. [Online]. Available: <https://www.nrc.gov/reading-rm/doc-collections/nuregs/staff/sr0492/>
- [7] Clifton A. Ericson II, "Fault Tree Analysis," 1999. <http://www.cs.ucf.edu/~hlugo/cop4331/ericson-fta-tutorial.pdf> (accessed Jul. 23, 2020).
- [8] H. Fujita, "New Horizons in MR Technology: RF Coil Designs and Trends," *Magn Reson Med Sci*, vol. 6, no. 1, pp. 29–42, 2007, doi: 10.2463/mrms.6.29.
- [9] R. E. Lyon and M. L. Janssens, "Polymer Flammability," U.S. Department of Transportation, Federal Aviation Administration, Office of Aviation Research, Washington, DC, DOT/FAA/AR-05/14, May 2005. [Online]. Available: <https://www.fire.tc.faa.gov/pdf/05-14.pdf>
- [10] E. E. Babcock, J. T. Vaughan, B. Lesan And, and R. L. Nunnally, "Multinuclear nmr investigations of probe construction materials at 4.7 t," *Magn. Reson. Med.*, vol. 13, no. 3, pp. 498–503, Mar. 1990, doi: 10.1002/mrm.1910130317.
- [11] M. Marjanska, M. Waks, C. J. Snyder, and J. T. Vaughan, "Multinuclear NMR investigation of probe construction materials at 9.4T," *Magn Reson Med*, vol. 59, no. 4, pp. 936–938, 2008, doi: 10.1002/mrm.21566.
- [12] C. Barmet, N. De Zanche, L. S. Sasportas, and K. P. Pruessmann, "A model-free method for high-precision MR susceptometry," in *Proceedings of the International Society for Magnetic Resonance in Medicine, 15th Annual Scientific Meeting*, May 2007, p. 36.
- [13] Y.-C. N. Cheng, C.-Y. Hsieh, R. Tackett, P. Kokeny, R. K. Regmi, and G. Lawes, "Magnetic moment quantifications of small spherical objects in MRI," *Magnetic Resonance Imaging*, vol. 33, no. 6, pp. 829–839, Jul. 2015, doi: 10.1016/j.mri.2014.11.003.
- [14] J. Link, "The Design of Resonator Probes with Homogeneous Radiofrequency Fields," in *In-Vivo Magnetic Resonance Spectroscopy I: Probeheads and Radiofrequency Pulses Spectrum Analysis*, M. Rudin, Ed. Berlin, Heidelberg: Springer Berlin Heidelberg, 1992, pp. 3–31. doi: 10.1007/978-3-642-45697-8_1.
- [15] Axel Haase *et al.*, "NMR Probeheads for In Vivo Applications," *Concepts in Magnetic Resonance*, vol. 12, no. 6, pp. 361–388, 2000.

- [16]N. De Zanche, J. A. Massner, C. Leussler, and K. P. Pruessmann, "Modular design of receiver coil arrays," *NMR in Biomedicine*, vol. 21, no. 6, pp. 644–654, 2008, doi: 10.1002/nbm.1237.
- [17]M. A. Griswold, "Characterization of Multichannel Coil Arrays on the Benchtop," in *Encyclopedia of Magnetic Resonance*, R. K. Harris, Ed. Chichester, UK: John Wiley & Sons, Ltd, 2012, p. emrstm1141. doi: 10.1002/9780470034590.emrstm1141.
- [18]J. Mispelter, M. Lupu, and A. Briguet, *NMR probeheads for biophysical and biomedical experiments: theoretical principles & practical guidelines*, Second edition. London: Imperial College Press, 2015.
- [19]D. W. McRobbie, E. A. Moore, and M. J. Graves, *MRI from Picture to Proton.*, 3rd Edition. Cambridge, UK: Cambridge University Press, 2017. [Online]. Available: <https://www.cambridge.org/gb/academic/subjects/medicine/medical-imaging/mri-picture-proton-3rd-edition?format=PB>
- [20]B. Gruber, M. Froeling, T. Leiner, and D. W. J. Klomp, "RF coils: A practical guide for nonphysicists," *J. Magn. Reson. Imaging*, vol. 48, no. 3, pp. 590–604, Sep. 2018, doi: 10.1002/jmri.26187.
- [21]J. T. Vaughan and J. R. Griffiths, Eds., *RF coils for MRI*. Chichester, West Sussex: Wiley, 2012.
- [22]M. C. Steckner, "A Review of MRI Acoustic Noise and Its Potential Impact on Patient and Worker Health," in *eMagRes*, Wiley, 2020, pp. 21–38. doi: 10.1002/9780470034590.emrstm1628.
- [23]F. A. Duck, "Medical and non-medical protection standards for ultrasound and infrasound," *Progress in Biophysics and Molecular Biology*, vol. 93, no. 1, pp. 176–191, Jan. 2007, doi: 10.1016/j.pbiomolbio.2006.07.008.
- [24]J. Murphy-Boesch, "Heating of Coils and Parts in High-Field MRI," in *eMagRes*, Wiley, 2020, pp. 7–20. doi: 10.1002/9780470034590.emrstm1585.
- [25]E. B. Boskamp, "Improved surface coil imaging in MR: decoupling of the excitation and receiver coils," *Radiology*, vol. 157, no. 2, pp. 449–452, Nov. 1985, doi: 10.1148/radiology.157.2.4048454.
- [26]W. A. Edelstein, C. J. Hardy, and O. M. Mueller, "Electronic Decoupling of Surface Coils for NMR Imaging and Spectroscopy," Aug. 1985, vol. 2, pp. 1084–1085. doi: 10.1002/mrmp.22419850205.
- [27]J. S. Hyde, R. J. Rilling, and A. Jesmanowicz, "Passive decoupling of surface coils by pole insertion," *Journal of Magnetic Resonance (1969)*, vol. 89, no. 3, pp. 485–495, Oct. 1990, doi: 10.1016/0022-2364(90)90332-4.
- [28]H. Fujita, T. Zheng, X. Yang, M. J. Finnerty, and S. Handa, "RF Surface Receive Array Coils: The Art of an LC Circuit: RF Surface Receive Array Coils," *J. Magn. Reson. Imaging*, vol. 38, no. 1, pp. 12–25, Jul. 2013, doi: 10.1002/jmri.24159.
- [29]A. Kocharian, P. J. Rossman, T. C. Hulshizer, J. P. Felmler, and S. J. Riederer, "Determination of appropriate RF blocking impedance for MRI surface coils and arrays," *Magnetic Resonance Materials in Biology, Physics, and Medicine*, vol. 10, no. 2, pp. 80–83, 2000, doi: 10.1016/S1352-8661(00)00071-5.
- [30]B. Keil and L. L. Wald, "Massively parallel MRI detector arrays," *Journal of Magnetic Resonance*, vol. 229, pp. 75–89, Apr. 2013, doi: 10.1016/j.jmr.2013.02.001.
- [31]D. M. Peterson, B. L. Beck, G. R. Duensing, and J. R. Fitzsimmons, "Common mode signal rejection methods for MRI: Reduction of cable shield currents for high static magnetic field systems," *Concepts in Magnetic Resonance Part B: Magnetic Resonance Engineering*, vol. 19B, no. 1, pp. 1–8, 2003, doi: 10.1002/cmr.b.10090.

- [32] D. M. Peterson, "Impedance Matching and Baluns," in *Encyclopedia of Magnetic Resonance*, R. K. Harris and R. E. Wasylshen, Eds. Chichester, UK: John Wiley & Sons, Ltd, 2011, p. emrstm1112. doi: 10.1002/9780470034590.emrstm1112.
- [33] H. Barfuss *et al.*, "In Vivo Magnetic Resonance Imaging and Spectroscopy of Humans with a 4T Whole-Body Magnet," *NMR in Biomedicine*, vol. 3, no. 1, pp. 31–45, 1990, doi: 10.1002/nbm.1940030106.
- [34] B. L. Beck, D. M. Peterson, G. R. Duensing, and J. R. Fitzsimmons, "Implications of cable shield currents at 3.0 and 4.7 Tesla," in *Proceedings of the International Society for Magnetic Resonance in Medicine, 8th annual meeting*, Denver, 2000, p. 641.
- [35] D. M. Peterson, B. L. Beck, and G. R. Duensing, "Reduction of Cable Shield Currents Generated by High Field Body Coils at 3 Tesla and Above," in *Proceedings of the International Society for Magnetic Resonance in Medicine, 10th annual meeting*, Honolulu, HI, 2002, p. 850. [Online]. Available: <http://cds.ismrm.org/ismrm-2002/PDF3/0850.PDF>
- [36] M. F. Dempsey, B. Condon, and D. M. Hadley, "Investigation of the factors responsible for burns during MRI," *J. Magn. Reson. Imaging*, vol. 13, no. 4, pp. 627–631, Apr. 2001, doi: 10.1002/jmri.1088.
- [37] X. Yang, T. Zheng, and H. Fujita, "T/R Switches, Baluns, and Detuning Elements in MRI RF coils," presented at the Proceedings of the 14th Scientific Meeting, International Society for Magnetic Resonance in Medicine, Seattle, 2006.
- [38] *The ARRL Handbook for Radio Amateurs*, 78th ed. Newington, Conn.: American Radio Relay League, 2000.
- [39] D. A. Seeber, I. Jevtic, and A. Menon, "Floating shield current suppression trap," *Concepts Magn. Reson. Part B*, vol. 21B, no. 1, pp. 26–31, Apr. 2004, doi: 10.1002/cmr.b.20008.
- [40] A. G. Webb and N. Smith, "31P spectroscopy in human calf muscle at 7 tesla using a balanced double-quadrature proton-phosphorus RF coil," in *Proceedings of the International Society for Magnetic Resonance in Medicine, 18th annual meeting*, Stockholm, Sweden, 2010, p. 3818.
- [41] J. V. Rispoli, I. E. Dimitrov, S. Cheshkov, C. Malloy, S. M. Wright, and M. P. McDougall, "Trap design and construction for high-power multinuclear magnetic resonance experiments," *Concepts in Magnetic Resonance Part B: Magnetic Resonance Engineering*, vol. 46B, no. 4, pp. 162–168, 2016, doi: 10.1002/cmr.b.21345.
- [42] L. Eberler, J. Nistler, and V. Matschl, "How to tune a RF-trap?," in *Proceedings of the International Society for Magnetic Resonance in Medicine, 20th annual meeting*, Melbourne, 2012, p. 2726.
- [43] D. O. Brunner, N. De Zanche, J. Frohlich, J. Paska, and K. P. Pruessmann, "Travelling-wave nuclear magnetic resonance," *Nature*, vol. 457, no. 7232, pp. 994–998, 2009, doi: 10.1038/nature07752.
- [44] S. Orzada *et al.*, "A 32-channel parallel transmit system add-on for 7T MRI," *PLoS ONE*, vol. 14, no. 9, p. e0222452, Sep. 2019, doi: 10.1371/journal.pone.0222452.
- [45] W. Liu, C. Kao, C. M. Collins, M. B. Smith, and Q. X. Yang, "On consideration of radiated power in RF field simulations for MRI," *Magn Reson Med*, vol. 69, no. 1, pp. 290–294, Jan. 2013, doi: 10.1002/mrm.24244.
- [46] M. Malzacher, M. Davids, L. R. Schad, and J. Chacon-Caldera, "Evaluating the effects of receive-only arrays in specific absorption rate simulations at 3 and 7 T," *Magnetic Resonance Imaging*, vol. 53, pp. 7–13, Nov. 2018, doi: 10.1016/j.mri.2018.06.011.

- [47] M. Kozlov and R. Turner, "Fast MRI coil analysis based on 3-D electromagnetic and RF circuit co-simulation," *Journal of Magnetic Resonance*, vol. 200, no. 1, pp. 147–152, Sep. 2009, doi: 10.1016/j.jmr.2009.06.005.
- [48] N. Krishnamurthy, T. Zhao, and T. S. Ibrahim, "Effects of receive-only inserts on specific absorption rate, B_1^+ field, and Tx coil performance: Effects of Receive-Only Inserts," *J. Magn. Reson. Imaging*, vol. 39, no. 2, pp. 475–484, Feb. 2014, doi: 10.1002/jmri.24152.
- [49] W. Liu, "RF Field Modeling for Double-Tuned Volume Coils," in *Encyclopedia of Magnetic Resonance*, R. K. Harris, Ed. Chichester, UK: John Wiley & Sons, Ltd, 2011, p. emrstm1159. doi: 10.1002/9780470034590.emrstm1159.
- [50] G. Adriany and R. Gruetter, "A half-volume coil for efficient proton decoupling in humans at 4 Tesla," *J Magn Reson*, vol. 125, no. 1, pp. 178–184, Mar. 1997, doi: 10.1006/jmre.1997.1113.
- [51] M. Meyerspeer, E. S. Roig, R. Gruetter, and A. W. Magill, "An improved trap design for decoupling multinuclear RF coils," *Magn. Reson. Med.*, vol. 72, no. 2, pp. 584–590, Aug. 2014, doi: 10.1002/mrm.24931.
- [52] R. A. Lemdiasov, A. A. Obi, and R. Ludwig, "A numerical postprocessing procedure for analyzing radio frequency MRI coils," *Concepts Magn. Reson.*, vol. 38A, no. 4, pp. 133–147, Jul. 2011, doi: 10.1002/cmr.a.20217.
- [53] M. de Greef, O. Ipek, A. J. E. Raaijmakers, J. Crezee, and C. A. T. van den Berg, "Specific absorption rate intersubject variability in 7T parallel transmit MRI of the head," *Magn Reson Med*, vol. 69, no. 5, pp. 1476–1485, 2013, doi: 10.1002/mrm.24378.
- [54] M. Le Garrec, V. Gras, M.-F. Hang, G. Ferrand, M. Luong, and N. Boulant, "Probabilistic analysis of the specific absorption rate intersubject variability safety factor in parallel transmission MRI: Probabilistic Analysis of Specific Absorption Rate Intersubject Variability," *Magn. Reson. Med.*, vol. 78, no. 3, pp. 1217–1223, Sep. 2017, doi: 10.1002/mrm.26468.
- [55] C. M. Collins and M. B. Smith, "Spatial resolution of numerical models of man and calculated specific absorption rate using the FDTD method: A study at 64 MHz in a magnetic resonance imaging coil," *J. Magn. Reson. Imaging*, vol. 18, no. 3, pp. 383–388, Sep. 2003, doi: 10.1002/jmri.10359.
- [56] H. Homann, P. Börnert, H. Eggers, K. Nehrke, O. Dössel, and I. Graesslin, "Toward individualized SAR models and in vivo validation," *Magnetic Resonance in Medicine*, vol. 66, no. 6, pp. 1767–1776, 2011, doi: 10.1002/mrm.22948.
- [57] S. Gabriel, R. W. Lau, and C. Gabriel, "The dielectric properties of biological tissues: II. Measurements in the frequency range 10 Hz to 20 GHz," *Phys. Med. Biol.*, vol. 41, no. 11, pp. 2251–2269, 1996, doi: 10.1088/0031-9155/41/11/002.
- [58] A. Christ *et al.*, "The Virtual Family—development of surface-based anatomical models of two adults and two children for dosimetric simulations," *Phys. Med. Biol.*, vol. 55, no. 2, pp. N23–N38, Jan. 2010, doi: 10.1088/0031-9155/55/2/N01.
- [59] M. J. Ackerman, "The Visible Human Project," *Proc. IEEE*, vol. 86, no. 3, pp. 504–511, Mar. 1998, doi: 10.1109/5.662875.
- [60] J. W. Massey and A. E. Yilmaz, "AustinMan and AustinWoman: High-fidelity, anatomical voxel models developed from the VHP color images," in *38th Annual International Conference of the IEEE Engineering in Medicine and Biology Society (EMBC)*, Orlando, FL, USA, Aug. 2016, pp. 3346–3349. doi: 10.1109/EMBC.2016.7591444.

- [61] T. M. Fiedler, M. E. Ladd, and A. K. Bitz, "RF safety assessment of a bilateral four-channel transmit/receive 7 Tesla breast coil: SAR versus tissue temperature limits," *Med Phys*, vol. 44, no. 1, pp. 143–157, Jan. 2017, doi: 10.1002/mp.12034.
- [62] X. Li and J. V. Rispoli, "Toward 7T breast MRI clinical study: safety assessment using simulation of heterogeneous breast models in RF exposure," *Magn Reson Med*, vol. 81, no. 2, pp. 1307–1321, Feb. 2019, doi: 10.1002/mrm.27395.
- [63] E. F. Meliadó, C. A. T. van den Berg, P. R. Luijten, and A. J. E. Raaijmakers, "Intersubject specific absorption rate variability analysis through construction of 23 realistic body models for prostate imaging at 7T," *Magn. Reson. Med*, vol. 81, no. 3, pp. 2106–2119, Mar. 2019, doi: 10.1002/mrm.27518.
- [64] N. Makris *et al.*, "MRI-based anatomical model of the human head for specific absorption rate mapping," *Med Biol Eng Comput*, vol. 46, no. 12, pp. 1239–1251, Dec. 2008, doi: 10.1007/s11517-008-0414-z.
- [65] S. Wolf, D. Diehl, M. Gebhardt, J. Mallow, and O. Speck, "SAR simulations for high-field MRI: How much detail, effort, and accuracy is needed?: Simplified SAR Simulations for High Field MRI," *Magn. Reson. Med.*, vol. 69, no. 4, pp. 1157–1168, Apr. 2013, doi: 10.1002/mrm.24329.
- [66] J. M. Kabil and A. Gopinath, "Numerical Simulation for MRI RF Coils and Safety," in *eMagRes*, Wiley, 2020, pp. 127–142. doi: 10.1002/9780470034590.emrstm1568.
- [67] F. Yetisir, E. A. Turk, P. E. Grant, L. L. Wald, and E. Adalsteinsson, "The effect of tissue detail in pregnant body models on local SAR prediction accuracy at 3 T," in *Proceedings of the International Society for Magnetic Resonance in Medicine, 27th annual meeting*, Montreal, 2019, p. 4162.
- [68] T. M. Fiedler, M. E. Ladd, and A. K. Bitz, "SAR Simulations & Safety," *NeuroImage*, vol. 168, pp. 33–58, Mar. 2018, doi: 10.1016/j.neuroimage.2017.03.035.
- [69] K. Yee, "Numerical solution of initial boundary value problems involving maxwell's equations in isotropic media," *IEEE Trans. Antennas Propagat.*, vol. 14, no. 3, pp. 302–307, May 1966, doi: 10.1109/TAP.1966.1138693.
- [70] A. Taflove, *Advances in computational electrodynamics: the finite difference time domain method*. Boston: Artech House, 1998.
- [71] T. Weiland, "A Discretization Method for the Solution of Maxwell's Equations for Six-Component Fields," *Electronics and Communications AEU*, vol. 31, no. 3, pp. 116–120, 1977.
- [72] Jianming Jin, *Electromagnetic Analysis and Design in Magnetic Resonance Imaging*. New York: CRC Press, 1999.
- [73] T. S. Ibrahim, R. Lee, B. A. Baertlein, Y. Yu, and P.-M. L. Robitaille, "Computational analysis of the high pass birdcage resonator: finite difference time domain simulations for high-field MRI," *Magnetic Resonance Imaging*, vol. 18, no. 7, pp. 835–843, Sep. 2000, doi: 10.1016/S0730-725X(00)00161-2.
- [74] R. Stara *et al.*, "Validation of Numerical Approaches for Electromagnetic Characterization of Magnetic Resonance Radiofrequency Coils," *PIER M*, vol. 29, pp. 121–136, 2013, doi: 10.2528/PIERM12122113.
- [75] A. F. Peterson, S. L. Ray, and R. Mittra, *Computational methods for electromagnetics*. New York, NY: IEEE Press, 1998.
- [76] Dan Jiao and Jian-Ming Jin, "A general approach for the stability analysis of the time-domain finite-element method for electromagnetic simulations," *IEEE Trans. Antennas Propagat.*, vol. 50, no. 11, pp. 1624–1632, Nov. 2002, doi: 10.1109/TAP.2002.803965.

- [77]G. Mur, "Absorbing Boundary Conditions for the Finite-Difference Approximation of the Time-Domain Electromagnetic-Field Equations," *IEEE Trans. Electromagn. Compat.*, vol. EMC-23, no. 4, pp. 377–382, Nov. 1981, doi: 10.1109/TEMC.1981.303970.
- [78]Y. Duan, T. S. Ibrahim, B. S. Peterson, F. Liu, and A. Kangarlu, "Assessment of a PML Boundary Condition for Simulating an MRI Radio Frequency Coil," *International Journal of Antennas and Propagation*, vol. 2008, pp. 1–10, 2008, doi: 10.1155/2008/563196.
- [79]J.-P. Berenger, "A perfectly matched layer for the absorption of electromagnetic waves," *Journal of Computational Physics*, vol. 114, no. 2, pp. 185–200, Oct. 1994, doi: 10.1006/jcph.1994.1159.
- [80]C. M. Collins, W. Liu, M. B. Smith, and Q. X. Yang, "Dissipation of Radiated RF Power in Magnet Room: Implications for SNR Considerations," in *Proceedings of the 11th Scientific Meeting, International Society for Magnetic Resonance in Medicine*, Toronto, Canada, 2003, p. 714.
- [81]C. M. Collins, S. Z. Li, and M. B. Smith, "SAR and B-1 field distributions in a heterogeneous human head model within a birdcage coil," *Magn Reson Med*, vol. 40, no. 6, pp. 847–856, Dec. 1998, doi: 10.1002/mrm.1910400610.
- [82]A. Hirata and T. Shiozawa, "Correlation of maximum temperature increase and peak SAR in the human head due to handset antennas," *IEEE Transactions on Microwave Theory and Techniques*, vol. 51, no. 7, pp. 1834–1841, Jul. 2003, doi: 10.1109/TMTT.2003.814314.
- [83]A. Hirata, M. Fujimoto, T. Asano, J. Wang, O. Fujiwara, and T. Shiozawa, "Correlation between maximum temperature increase and peak SAR with different average schemes and masses," *IEEE Transactions on Electromagnetic Compatibility*, vol. 48, no. 3, pp. 569–578, Aug. 2006, doi: 10.1109/TEMC.2006.877784.
- [84]A. Razmadze, L. Shoshiashvili, D. Kakulia, R. Zaridze, G. Bit-Babik, and A. Faraone, "Influence of Specific Absorption Rate Averaging Schemes on Correlation between Mass-Averaged Specific Absorption Rate and Temperature Rise," *Electromagnetics*, vol. 29, no. 1, pp. 77–90, Jan. 2009, doi: 10.1080/02726340802530088.
- [85]International Commission on Non-Ionizing Radiation Protection, "Health issues related to the use of hand-held radiotelephones and base transmitters," *Health Phys*, vol. 70, no. 4, pp. 587–593, 1996.
- [86]R. L. McIntosh and V. Anderson, "SAR versus VAR, and the size and shape that provide the most appropriate RF exposure metric in the range of 0.5-6 GHz," *Bioelectromagnetics*, vol. 32, no. 4, pp. 312–321, May 2011, doi: 10.1002/bem.20642.
- [87]A. Kuehne, F. Seifert, and B. Itterman, "GPU-Accelerated SAR Computation with Arbitrary Averaging Shapes," in *Proceedings of the International Society for Magnetic Resonance in Medicine, 20th annual meeting*, Melbourne, 2012, p. 2735.
- [88]S. Oh, Y.-C. Ryu, G. Carluccio, C. T. Sica, and C. M. Collins, "Measurement of SAR-induced temperature increase in a phantom and in vivo with comparison to numerical simulation: SAR-Induced Temperature Rise," *Magn. Reson. Med.*, vol. 71, no. 5, pp. 1923–1931, May 2014, doi: 10.1002/mrm.24820.
- [89]S. Pisa, M. Cavagnaro, and J. C. Lin, "The Influence of Averaging Schemes and Exposure Duration on the Correlation Between Temperature Elevation and RF Power Absorption Metrics in MRI Scans [Health Matters]," *IEEE MICROW MAG*, vol. 17, no. 7, pp. 14–22, Jul. 2016, doi: 10.1109/MMM.2016.2551482.
- [90]A. Destruel, K. O'Brien, J. Jin, F. Liu, M. Barth, and S. Crozier, "Adaptive SAR mass-averaging framework to improve predictions of local RF heating near a hip implant for parallel transmit at 7 T," *Magn. Reson. Med*, vol. 81, no. 1, pp. 615–627, Jan. 2019, doi: 10.1002/mrm.27379.

- [91] F. G. Shellock and J. V. Crues, "Corneal temperature changes induced by high-field-strength MR imaging with a head coil.," *Radiology*, vol. 167, no. 3, pp. 809–811, Jun. 1988, doi: 10.1148/radiology.167.3.3363146.
- [92] B. J. Barber, D. J. Schaefer, C. J. Gordon, D. C. Zawieja, and J. Hecker, "Thermal effects of MR imaging: worst-case studies on sheep.," *American Journal of Roentgenology*, vol. 155, no. 5, pp. 1105–1110, Nov. 1990, doi: 10.2214/ajr.155.5.2120944.
- [93] A. Massire *et al.*, "Thermal simulations in the human head for high field MRI using parallel transmission," *J. Magn. Reson. Imaging*, vol. 35, no. 6, pp. 1312–1321, Jun. 2012, doi: 10.1002/jmri.23542.
- [94] H. H. Pennes, "Analysis of Tissue and Arterial Blood Temperatures in the Resting Human Forearm," *Journal of Applied Physiology*, vol. 1, no. 2, pp. 93–122, Aug. 1948, doi: 10.1152/jappl.1948.1.2.93.
- [95] K. R. Foster, M. C. Ziskin, Q. Balzano, and G. Bit-Babik, "Modeling Tissue Heating From Exposure to Radiofrequency Energy and Relevance of Tissue Heating to Exposure Limits: Heating Factor," *Health Physics*, vol. 115, no. 2, pp. 295–307, Aug. 2018, doi: 10.1097/HP.0000000000000854.
- [96] J. Nadobny, M. Szimtenings, D. Diehl, E. Stetter, G. Brinker, and P. Wust, "Evaluation of MR-Induced Hot Spots for Different Temporal SAR Modes Using a Time-Dependent Finite Difference Method With Explicit Temperature Gradient Treatment," *IEEE Trans. Biomed. Eng.*, vol. 54, no. 10, pp. 1837–1850, Oct. 2007, doi: 10.1109/TBME.2007.893499.
- [97] Z. Wang, M. B. Smith, and C. M. Collins, "Dependence of Temperature Increase on Pulse Sequence with Equivalent Time-Average SAR," in *Proceedings of the 15th Scientific Meeting, International Society for Magnetic Resonance in Medicine*, Berlin, 2007, p. 3247.
- [98] J. Wang and O. Fujiwara, "FDTD computation of temperature rise in the human head for portable telephones," *IEEE Trans. Microwave Theory Techn.*, vol. 47, no. 8, pp. 1528–1534, Aug. 1999, doi: 10.1109/22.780405.
- [99] P. Bernardi, M. Cavagnaro, S. Pisa, and E. Piuze, "Specific absorption rate and temperature elevation in a subject exposed in the far-field of radio-frequency sources operating in the 10-900-MHz range," *IEEE Trans. Biomed. Eng.*, vol. 50, no. 3, pp. 295–304, Mar. 2003, doi: 10.1109/TBME.2003.808809.
- [100] Z. Wang, J. C. Lin, W. Mao, W. Liu, M. B. Smith, and C. M. Collins, "SAR and temperature: Simulations and comparison to regulatory limits for MRI," *J. Magn. Reson. Imaging*, vol. 26, no. 2, pp. 437–441, Aug. 2007, doi: 10.1002/jmri.20977.
- [101] Z. Wang, J. C. Lin, J. T. Vaughan, and C. M. Collins, "Consideration of physiological response in numerical models of temperature during MRI of the human head," *J. Magn. Reson. Imaging*, vol. 28, no. 5, pp. 1303–1308, Nov. 2008, doi: 10.1002/jmri.21556.
- [102] M. Murbach *et al.*, "Thermal Tissue Damage Model Analyzed for Different Whole-Body SAR and Scan Durations for Standard MR Body Coils: Thermal Dose and Tissue Damage in MR RF Heating," *Magn. Reson. Med.*, vol. 71, no. 1, pp. 421–431, Jan. 2014, doi: 10.1002/mrm.24671.
- [103] F. F. J. Simonis, A. J. E. Raaijmakers, J. J. W. Lagendijk, and C. A. T. van den Berg, "Validating subject-specific RF and thermal simulations in the calf muscle using MR-based temperature measurements: Validating RF and Thermal Simulations with MRI Measurements," *Magn. Reson. Med.*, vol. 77, no. 4, pp. 1691–1700, Apr. 2017, doi: 10.1002/mrm.26244.
- [104] Y. Eryaman *et al.*, "Radiofrequency heating studies on anesthetized swine using fractionated dipole antennas at 10.5 T: RF Heating with Dipole Arrays at 10.5 T," *Magn. Reson. Med.*, vol. 79, no. 1, pp. 479–488, Jan. 2018, doi: 10.1002/mrm.26688.

- [105] I. Laakso and A. Hirata, "Dominant factors affecting temperature rise in simulations of human thermoregulation during RF exposure," *Phys. Med. Biol.*, vol. 56, no. 23, pp. 7449–7471, Dec. 2011, doi: 10.1088/0031-9155/56/23/008.
- [106] A. Kotte, G. van Leeuwen, J. de Bree, J. van der Koijk, H. Crezee, and J. Lagendijk, "A description of discrete vessel segments in thermal modelling of tissues," *Phys. Med. Biol.*, vol. 41, no. 5, pp. 865–884, May 1996, doi: 10.1088/0031-9155/41/5/004.
- [107] D. Shrivastava and J. T. Vaughan, "A Generic Bioheat Transfer Thermal Model for a Perfused Tissue," *Journal of Biomechanical Engineering*, vol. 131, no. 7, p. 074506, Jul. 2009, doi: 10.1115/1.3127260.
- [108] A. L. H. M. W. van Lier, A. N. T. J. Kotte, B. W. Raaymakers, J. J. W. Lagendijk, and C. A. T. van den Berg, "Radiofrequency heating induced by 7T head MRI: Thermal assessment using discrete vasculature or Pennes' bioheat equation," *J. Magn. Reson. Imaging*, vol. 35, no. 4, pp. 795–803, Apr. 2012, doi: 10.1002/jmri.22878.
- [109] Z. Wang, C. M. Collins, S. Zhao, and F. J. Robb, "The Effect of Human Model Resolution on Numerical Calculation of SAR and Temperature in MRI," in *Proceedings of the International Society for Magnetic Resonance in Medicine, 17th annual meeting*, Honolulu, HI, 2009, p. 4797.
- [110] D. Shrivastava, T. Hanson, J. Kulesa, J. Tian, G. Adriany, and J. T. Vaughan, "Radiofrequency heating in porcine models with a 'large' 32 cm internal diameter, 7 T (296 MHz) head coil: In Vivo RF Heating at 7 T," *Magn. Reson. Med.*, vol. 66, no. 1, pp. 255–263, Jul. 2011, doi: 10.1002/mrm.22790.
- [111] Q. Duan *et al.*, "Characterization of a dielectric phantom for high-field magnetic resonance imaging applications: Characterization of a dielectric phantom for high-field MRI," *Med. Phys.*, vol. 41, no. 10, p. 102303, Sep. 2014, doi: 10.1118/1.4895823.
- [112] C. Ianniello *et al.*, "Synthesized tissue-equivalent dielectric phantoms using salt and polyvinylpyrrolidone solutions," *Magnetic Resonance in Medicine*, vol. 80, no. 1, pp. 413–419, 2018, doi: 10.1002/mrm.27005.
- [113] M. N. Voelker *et al.*, "Quality Assurance Phantoms and Procedures for UHF MRI – The German Ultrahigh Field Imaging (GUF) Approach," in *Proceedings of the International Society for Magnetic Resonance in Medicine, 25th annual meeting*, Honolulu, HI, 2017, p. 3912.
- [114] S. Wood *et al.*, "Design and fabrication of a realistic anthropomorphic heterogeneous head phantom for MR purposes," *PLoS ONE*, vol. 12, no. 8, p. e0183168, Aug. 2017, doi: 10.1371/journal.pone.0183168.
- [115] A. Hellerbach, V. Schuster, A. Jansen, and J. Sommer, "MRI Phantoms – Are There Alternatives to Agar?," *PLOS ONE*, vol. 8, no. 8, p. e70343, Aug. 2013, doi: 10.1371/journal.pone.0070343.
- [116] M. Lazebnik, E. L. Madsen, G. R. Frank, and S. C. Hagness, "Tissue-mimicking phantom materials for narrowband and ultrawideband microwave applications," *Phys. Med. Biol.*, vol. 50, no. 18, pp. 4245–4258, Sep. 2005, doi: 10.1088/0031-9155/50/18/001.
- [117] Y. Yuan *et al.*, "A heterogeneous human tissue mimicking phantom for RF heating and MRI thermal monitoring verification," *Phys. Med. Biol.*, vol. 57, no. 7, pp. 2021–2037, Apr. 2012, doi: 10.1088/0031-9155/57/7/2021.
- [118] L. Winter *et al.*, "Magnetic resonance thermometry: Methodology, pitfalls and practical solutions," *International Journal of Hyperthermia*, vol. 32, no. 1, pp. 63–75, Jan. 2016, doi: 10.3109/02656736.2015.1108462.

- [119] J. R. James, Y. Gao, M. A. Miller, A. Babsky, and N. Bansal, "Absolute temperature MR imaging with thulium 1,4,7,10-tetraazacyclododecane-1,4,7,10-tetramethyl-1,4,7,10-tetraacetic acid (TmDOTMA⁻): Absolute Temperature Imaging with TmDOTMA⁻," *Magn. Reson. Med.*, vol. 62, no. 2, pp. 550–556, Aug. 2009, doi: 10.1002/mrm.22039.
- [120] N. N. Graedel, J. R. Polimeni, B. Guerin, B. Gagoski, and L. L. Wald, "An anatomically realistic temperature phantom for radiofrequency heating measurements: Realistic Temperature Phantom for Radiofrequency Heating Measurements," *Magn. Reson. Med.*, vol. 73, no. 1, pp. 442–450, Jan. 2015, doi: 10.1002/mrm.25123.
- [121] R. Pohmann and K. Scheffler, "A theoretical and experimental comparison of different techniques for B_1 mapping at very high fields: B_1 MAPPING TECHNIQUES," *NMR Biomed.*, vol. 26, no. 3, pp. 265–275, Mar. 2013, doi: 10.1002/nbm.2844.
- [122] U. Katscher, T. Voigt, C. Findekle, P. Vernickel, K. Nehrke, and O. Dossel, "Determination of Electric Conductivity and Local SAR Via B_1 Mapping," *IEEE Trans. Med. Imaging*, vol. 28, no. 9, pp. 1365–1374, Sep. 2009, doi: 10.1109/TMI.2009.2015757.
- [123] A. L. H. M. W. van Lier *et al.*, "B₁+ Phase mapping at 7 T and its application for in vivo electrical conductivity mapping," *Magn Reson Med*, vol. 67, no. 2, pp. 552–561, 2012, doi: 10.1002/mrm.22995.
- [124] V. L. Yarnykh, "Actual flip-angle imaging in the pulsed steady state: A method for rapid three-dimensional mapping of the transmitted radiofrequency field," *Magn. Reson. Med.*, vol. 57, no. 1, pp. 192–200, Jan. 2007, doi: 10.1002/mrm.21120.
- [125] L. I. Sacolick, F. Wiesinger, I. Hancu, and M. W. Vogel, "B₁ mapping by Bloch-Siegert shift," *Magn. Reson. Med.*, vol. 63, no. 5, pp. 1315–1322, May 2010, doi: 10.1002/mrm.22357.
- [126] A. K. Bitz *et al.*, "Assessment of RF Safety of Transmit Coils at 7 Tesla by Experimental & Numerical Procedures," in *Proceedings of the International Society for Magnetic Resonance in Medicine, 19th annual meeting*, Montreal, 2011, p. 490.
- [127] U. Katscher, C. Findekle, and T. Voigt, " B_1 -based specific energy absorption rate determination for nonquadrature radiofrequency excitation: B_1 -Based SAR Determination," *Magn Reson Med*, vol. 68, no. 6, pp. 1911–1918, Dec. 2012, doi: 10.1002/mrm.24215.
- [128] X. Zhang, P.-F. Van de Moortele, S. Schmitter, and B. He, "Complex B_1 mapping and electrical properties imaging of the human brain using a 16-channel transceiver coil at 7T," *Magn Reson Med*, vol. 69, no. 5, pp. 1285–1296, May 2013, doi: 10.1002/mrm.24358.
- [129] O. Kraff, A. K. Bitz, P. Dammann, S. C. Ladd, M. E. Ladd, and H. H. Quick, "An eight-channel transmit/receive multipurpose coil for musculoskeletal MR imaging at 7 T: Multipurpose coil for musculoskeletal MRI at 7 T," *Med. Phys.*, vol. 37, no. 12, pp. 6368–6376, Nov. 2010, doi: 10.1118/1.3517176.
- [130] C. Oezerdem *et al.*, "16-channel bow tie antenna transceiver array for cardiac MR at 7.0 tesla: 16-Channel Bow Tie Antenna Transceiver Coil Array for CMR," *Magn. Reson. Med.*, vol. 75, no. 6, pp. 2553–2565, Jun. 2016, doi: 10.1002/mrm.25840.
- [131] K. Nehrke and P. Börnert, "DREAM—a novel approach for robust, ultrafast, multislice B_1 mapping: DREAM B_1 Mapping," *Magn Reson Med*, vol. 68, no. 5, pp. 1517–1526, Nov. 2012, doi: 10.1002/mrm.24158.
- [132] B. R. Steensma *et al.*, "An 8-channel Tx/Rx dipole array combined with 16 Rx loops for high-resolution functional cardiac imaging at 7 T," *Magn Reson Mater Phy*, vol. 31, no. 1, pp. 7–18, Feb. 2018, doi: 10.1007/s10334-017-0665-5.

- [133] S. Brunheim *et al.*, “Fast and accurate multi-channel mapping based on the TIAMO technique for 7T UHF body MRI,” *Magn. Reson. Med.*, vol. 79, no. 5, pp. 2652–2664, May 2018, doi: 10.1002/mrm.26925.
- [134] P.-F. Van de Moortele *et al.*, “B1 destructive interferences and spatial phase patterns at 7 T with a head transceiver array coil,” *Magn. Reson. Med.*, vol. 54, no. 6, pp. 1503–1518, Dec. 2005, doi: 10.1002/mrm.20708.
- [135] F. Yetisir, B. Guerin, L. L. Wald, and E. Adalsteinsson, “SAR/B1+ calibration workflow for safe, high duty-cycle parallel transmission imaging at ultra-high field,” in *Proceedings of the International Society for Magnetic Resonance in Medicine, 24th annual meeting*, Singapore, 2016, p. 2211.
- [136] G. Tiberi, N. Fontana, A. Monorchio, R. Stara, A. Retico, and M. Tosetti, “Evaluation of 3D radio-frequency electromagnetic fields for any matching and coupling conditions by the use of basis functions,” *Journal of Magnetic Resonance*, vol. 261, pp. 38–42, Dec. 2015, doi: 10.1016/j.jmr.2015.09.015.
- [137] A. Beqiri, J. W. Hand, J. V. Hajnal, and S. J. Malik, “Comparison between simulated decoupling regimes for specific absorption rate prediction in parallel transmit MRI: Simulated Decoupling Regimes for SAR Prediction in Parallel Transmit MRI,” *Magn. Reson. Med.*, vol. 74, no. 5, pp. 1423–1434, Nov. 2015, doi: 10.1002/mrm.25504.
- [138] M. Restivo, A. Raaijmakers, C. van den Berg, P. Luijten, and H. Hoogduin, “Improving peak local SAR prediction in parallel transmit using in situ S-matrix measurements,” *Magn. Reson. Med.*, vol. 77, no. 5, pp. 2040–2047, May 2017, doi: 10.1002/mrm.26261.
- [139] P. Vernickel, C. Findeklee, J. Eichmann, and I. Graesslin, “Active Digital Decoupling for Multi-Channel Transmit MRI Systems,” in *Proceedings of the 15th Scientific Meeting, International Society for Magnetic Resonance in Medicine*, Berlin, 2007, p. 170.
- [140] G. Ferrand, M. Luong, A. Amadon, and N. Boulant, “Mathematical Tools to Define SAR Margins for Phased Array Coil In-Vivo Applications Given E-field Uncertainties,” in *Proceedings of the International Society for Magnetic Resonance in Medicine, 23rd annual meeting*, 2015, p. 1862.
- [141] C. M. Deniz, L. Alon, R. Brown, and Y. Zhu, “Subject- and resource-specific monitoring and proactive management of parallel radiofrequency transmission: Proactive Management of Parallel RF Transmission,” *Magn. Reson. Med.*, vol. 76, no. 1, pp. 20–31, Jul. 2016, doi: 10.1002/mrm.25828.
- [142] X. Li, J. W. Pan, N. I. Avdievich, H. P. Hetherington, and J. V. Rispoli, “Electromagnetic simulation of a 16-channel head transceiver at 7 T using circuit-spatial optimization,” *Magn Reson Med*, vol. 85, no. 6, pp. 3463–3478, Jun. 2021, doi: 10.1002/mrm.28672.
- [143] H. Han, R. Moritz, E. Oberacker, H. Waiczies, T. Niendorf, and L. Winter, “Open Source 3D Multipurpose Measurement System with Submillimetre Fidelity and First Application in Magnetic Resonance,” *Scientific Reports*, vol. 7, no. 1, Art. no. 1, Oct. 2017, doi: 10.1038/s41598-017-13824-z.
- [144] V. Rieke and K. Butts Pauly, “MR thermometry,” *J. Magn. Reson. Imaging*, vol. 27, no. 2, pp. 376–390, Feb. 2008, doi: 10.1002/jmri.21265.
- [145] J. C. Hindman, “Proton Resonance Shift of Water in the Gas and Liquid States,” *J. Chem. Phys.*, vol. 44, no. 12, pp. 4582–4592, Jun. 1966, doi: 10.1063/1.1726676.
- [146] M. R. Tarasek *et al.*, “Validation of MR thermometry: Method for temperature probe sensor registration accuracy in head and neck phantoms,” *International Journal of Hyperthermia*, vol. 30, no. 2, pp. 142–149, Mar. 2014, doi: 10.3109/02656736.2014.887794.

- [147] M. Pham *et al.*, “PRF thermometry accuracy at 7.0T for thermal MR applications with and without the presence of fat,” in *Proceedings of the International Society for Magnetic Resonance in Medicine, 25th annual meeting*, 2017, p. 5439.
- [148] J. De Poorter, C. De Wagter, Y. De Deene, C. Thomsen, F. Ståhlberg, and E. Achten, “Noninvasive MRI Thermometry with the Proton Resonance Frequency (PRF) Method: In Vivo Results in Human Muscle,” *Magn. Reson. Med.*, vol. 33, no. 1, pp. 74–81, Jan. 1995, doi: 10.1002/mrm.1910330111.
- [149] R. D. Peters and R. M. Henkelman, “Proton-resonance frequency shift MR thermometry is affected by changes in the electrical conductivity of tissue,” *Magn. Reson. Med.*, vol. 43, no. 1, pp. 62–71, Jan. 2000, doi: 10.1002/(SICI)1522-2594(200001)43:1<62::AID-MRM8>3.0.CO;2-1.
- [150] N. W. Lutz and M. Bernard, “Contactless Thermometry by MRI and MRS: Advanced Methods for Thermo-therapy and Biomaterials,” *iScience*, vol. 23, no. 10, p. 101561, Oct. 2020, doi: 10.1016/j.isci.2020.101561.
- [151] T. D. Greenberg *et al.*, “ACR guidance document on MR safe practices: Updates and critical information 2019,” *Journal of Magnetic Resonance Imaging*, vol. 51, no. 2, pp. 331–338, 2020, doi: 10.1002/jmri.26880.
- [152] David I. Hoult, “Sensitivity and Power Deposition in a High-Field Imaging Experiment,” *J Magn Reson Imag*, vol. 12, no. 1, pp. 46–67, 2000, doi: 10.1002/1522-2586(200007)12:1<46::AID-JMRI6>3.0.CO;2-D.
- [153] I. Graesslin *et al.*, “A specific absorption rate prediction concept for parallel transmission MR: A SAR Prediction Concept,” *Magn Reson Med*, vol. 68, no. 5, pp. 1664–1674, Nov. 2012, doi: 10.1002/mrm.24138.
- [154] Y. Zhu, L. Alon, C. M. Deniz, R. Brown, and D. K. Sodickson, “System and SAR characterization in parallel RF transmission: System and SAR Characterization in Parallel RF Transmission,” *Magn. Reson. Med.*, vol. 67, no. 5, pp. 1367–1378, May 2012, doi: 10.1002/mrm.23126.
- [155] C. M. Collins, Z. Wang, and M. B. Smith, “A Conservative Method for Ensuring Safety within Transmit Arrays,” in *Proceedings 15th Scientific Meeting, International Society for Magnetic Resonance in Medicine*, Berlin, 2007, p. 1092.
- [156] I. Graesslin *et al.*, “Comprehensive RF safety concept for parallel transmission MR,” *Magnetic Resonance in Medicine*, vol. 74, no. 2, pp. 589–598, 2015, doi: 10.1002/mrm.25425.
- [157] N. Boulant, M. Cloos, M. Luong, G. Ferrand, C. Wiggins, and A. Amadon, “Method for Monitoring Safety in Parallel Transmission Systems Based on Channel-Dependent Average Powers,” in *Proceedings of the International Society for Magnetic Resonance in Medicine, 19th annual meeting*, Montreal, 2011, p. 3850.
- [158] G. Eichfelder and M. Gebhardt, “Local specific absorption rate control for parallel transmission by virtual observation points: Local SAR Control for Parallel Transmission,” *Magn. Reson. Med.*, vol. 66, no. 5, pp. 1468–1476, Nov. 2011, doi: 10.1002/mrm.22927.
- [159] J. Lee, M. Gebhardt, L. L. Wald, and E. Adalsteinsson, “Local SAR in parallel transmission pulse design: Local-SAR Constrained pTx RF Design,” *Magnetic Resonance Medicine*, vol. 67, no. 6, pp. 1566–1578, Jun. 2012, doi: 10.1002/mrm.23140.
- [160] S. Orzada, T. M. Fiedler, H. H. Quick, and M. E. Ladd, “Local SAR compression algorithm with improved compression, speed, and flexibility,” *Magn. Reson. Med.*, vol. 86, no. 1, pp. 561–568, Jul. 2021, doi: 10.1002/mrm.28739.

- [161] R. Gumbrecht, “Development of customized pTx MR excitation methods and their safe application,” Doctoral Thesis, Friedrich-Alexander-Universität Erlangen-Nürnberg, 2013. [Online]. Available: <https://opus4.kobv.de/opus4-fau/files/3860/Doktorarbeit.pdf>
- [162] N. Boulant, V. Gras, A. Amadon, M. Luong, G. Ferrand, and A. Vignaud, “Workflow proposal for defining SAR safety margins in parallel transmission,” in *Proceedings of the International Society for Magnetic Resonance in Medicine, 26th annual meeting*, Paris, France, 2018, p. 295.
- [163] A. T. Hess, E. M. Tunnicliffe, C. T. Rodgers, and M. D. Robson, “Diaphragm position can be accurately estimated from the scattering of a parallel transmit RF coil at 7 T,” *Magnetic Resonance in Medicine*, vol. 79, no. 4, pp. 2164–2169, 2018, doi: 10.1002/mrm.26866.
- [164] S. Orzada, M. E. Ladd, and A. K. Bitz, “A method to approximate maximum local SAR in multichannel transmit MR systems without transmit phase information: Max Local SAR w/o Tx Phase Information,” *Magn. Reson. Med.*, vol. 78, no. 2, pp. 805–811, Aug. 2017, doi: 10.1002/mrm.26398.
- [165] N. Boulant, X. Wu, G. Adriany, S. Schmitter, K. Uğurbil, and P.-F. Van de Moortele, “Direct control of the temperature rise in parallel transmission by means of temperature virtual observation points: Simulations at 10.5 tesla: Control of Temperature Rise in Parallel Transmission,” *Magn. Reson. Med.*, vol. 75, no. 1, pp. 249–256, Jan. 2016, doi: 10.1002/mrm.25637.
- [166] B. R. Steensma, P. R. Luijten, D. W. J. Klomp, C. A. T. van den Berg, and A. J. E. Raaijmakers, “Tier based formalism for RF safety assessment of custom-built RF coils providing flexibility in the tradeoff between effort and overestimation,” in *Proceedings of the International Society for Magnetic Resonance in Medicine, 28th annual meeting*, 2020, p. 4193.
- [167] M. Murbach, E. Neufeld, W. Kainz, K. P. Pruessmann, and N. Kuster, “Whole-body and local RF absorption in human models as a function of anatomy and position within 1.5T MR body coil: MR RF Exposure as a Function of Large-Scale Anatomical Properties,” *Magn. Reson. Med.*, vol. 71, no. 2, pp. 839–845, Feb. 2014, doi: 10.1002/mrm.24690.
- [168] A. Sadeghi-Tarakameh *et al.*, “In vivo human head MRI at 10.5T: A radiofrequency safety study and preliminary imaging results,” *Magn Reson Med*, vol. 84, no. 1, pp. 484–496, Jul. 2020, doi: 10.1002/mrm.28093.
- [169] Ö. Ipek, A. J. Raaijmakers, J. J. Lagendijk, P. R. Luijten, and C. A. T. van den Berg, “Intersubject local SAR variation for 7T prostate MR imaging with an eight-channel single-side adapted dipole antenna array,” *Magn Reson Med*, vol. 71, no. 4, pp. 1559–1567, 2014, doi: 10.1002/mrm.24794.
- [170] F. Yetisir *et al.*, “SAR estimation error due to body model mismatch for fetal imaging at 3 Tesla,” in *Proceedings of the International Society for Magnetic Resonance in Medicine, 26th annual meeting*, Paris, 2018, p. 296.
- [171] Varian Associates, *User Guide: Whole-Body Imaging*, A0698 ed. Varian Associates Inc., 1998.
- [172] D. M. Pozar, *Microwave engineering*, 4. ed. Hoboken, NJ: Wiley, 2012.
- [173] D. I. Hoult, “The Principle of Reciprocity in Signal Strength Calculations - A Mathematical Guide,” *Concepts in Magnetic Resonance*, vol. 12, no. 4, pp. 173–187, 2000, doi: 10.1002/1099-0534(2000)12:4<173::AID-CMR1>3.0.CO;2-Q.
- [174] W. A. Edelstein, G. H. Glover, C. J. Hardy, and R. W. Redington, “The Intrinsic Signal-to-Noise Ratio in NMR Imaging,” *Magn Reson Med*, vol. 3, no. 4, pp. 604–618, 1986, doi: 10.1002/mrm.1910030413.
- [175] W. A. Edelstein, P. A. Bottomley, and L. M. Pfeifer, “A Signal-to-Noise Calibration Procedure for NMR Imaging Systems,” *Med Phys*, vol. 11, no. 2, pp. 180–185, 1984, doi: 10.1118/1.595484.

- [176] J. O. Bird, *Electrical circuit theory and technology*, Rev. 2. ed. Oxford: Newnes, 2003.
- [177] D. J. Schaefer, "Health Effects and Safety of Radiofrequency Power Deposition Associated with Magnetic Resonance Procedures," in *Magnetic Resonance Procedures: Health Effects and Safety*, 0 ed., F. G. Shellock, Ed. CRC Press, 2000. doi: 10.1201/9781420041569.

Appendices

A. Common Failure Modes for RF Coils

For MRI, most threats to human safety come from very high peak and longer term averaged powers from the transmit coils used during excitation. Most of the danger is in the RF heating of tissues induced by fields of the transmit coils. Under normal operation, this heating (SAR) is controlled by the RF monitoring and SAR supervision of the MRI console. However, because of the proximity of receive-only coils to the human body, other pathways for tissue heating can be established in the event of coil failure. These and some other common failure modes are listed below.

Localized RF Burns

- i. **Hazard:** Looping of the coil system cable inside the body coil
Effect: A large RF potential is induced on the shield of the cable from dB_1/dt
Mitigation: Reduce the cable length so that it cannot loop.
- ii. **Hazard:** The coil system cable runs close to the body coil
Effect: A large RF voltage is induced on the shield of the cable from the Tx E-field
Mitigation: Situate the cable away from the body coil, cable traps around the cable shield provide high impedances to shield potentials, the cable is insulated with non-conductive foam
- iii. **Hazard:** High E-fields in the vicinity of coil components
Effect: High current induced in tissue near the component
Mitigation: All coil components housed within an insulating plastic former, capacitors of the coil are distributed to reduce RF potentials

Overheating of Coil Parts, Fire

- i. **Hazard:** Coil not plugged in
Effect: Active control of blocking circuits in receive elements is disabled
Mitigation: System cannot scan if the coil cannot be identified, passive blocking circuits have been incorporated into receive-only elements, Operator warning to verify connection of coil
- ii. **Hazard:** Coil component failure in a receive element
Effect: Local heating of the failed circuit
Mitigation: Multiple blocking circuits incorporated to the element to minimize induced currents
- iii. **Hazard:** Coil component failure in a receive element
Effect: Local heating of the failed circuit causes sparks or expelled hot particles
Mitigation: All coil elements have been constructed within a coil housing, and the coil housing has been constructed with fire-rated materials ([UL 94-V0](#))

Electrical Shock

- i. **Hazard:** Large potentials (DC and AC) from control and other circuits within the coil
Effect: Leakage currents through former can cause shock

Mitigation: Coil former should meet the IEC 60601-1 (§8.9) requirements for “creepage” distances (see §II.B.1.1)

ii. **Hazard:** Contact with high potentials (DC and AC) within the coil

Effect: Shock from direct contact with a conductor

Mitigation: All conductors are housed within an insulating coil former, no exposed conductors

iii. **Hazard:** Broken coil housing exposes internal conductor(s)

Effect: Shock from direct contact with a conductor

Mitigation: Operator warning: no coil should be used if damaged, seek repair

Mechanical Hazards

i. **Hazard:** Broken coil housing involving a human contact surface

Effect: Sharp edges can cause injury

Mitigation: Operator warning: no coil should be used if damaged, seek repair

B. Example of Risk Analysis

Failure Modes and Effects Analysis								
Coil Identifier:								
Report by:								
Date:								
Part and Function	Potential Failure Mode	Cause	Local Effect	Likelihood (1 - 5)	Patient Effect	Severity (1 - 5)	Means of Control (Mitigation)	Detectable
Circuit Boards, Elements (Schematic: SK1001-01)								
Capacitors C1-C6	Components Opened or Shorted	Component failure, broken leads, improper mounting	Array Element detuned		Noisy Image		Active/Passive Blocking Circuits will prevent high current	Yes
Inductor L1	Inductor open	Component failure, improper mounting	Input blocking circuit failure		Noisy Image		QA Test on assembly, or secondary blocking circuit required for protection	Yes
Inductor L1	Inductor shorted	Component failure, improper mounting	Input blocking circuit failure, poor connection		Low image SNR		QA Test on assembly, or secondary blocking circuit required for protection	Yes
Inductors L2,L3	Inductor open	Component failure, improper mounting	Blocking circuit failure		Possible tissue heating, image acquired		QA Test on assembly, or secondary blocking circuit required for protection	No
Inductors L2,L3	Inductor shorted	Component failure, improper mounting	Blocking circuit failure		Coil detuned during transmit, possible high SAR		QA Test on assembly, or secondary blocking circuit required for protection	Yes

PIN Diodes, D1	Diode Shorted	Component failure, improper mounting	Array Element continuously detuned, input shorted		No signal, noisy Image		Blocking Circuit active continuously	Yes
PIN Diodes, D1	Diode Open	Component failure, broken leads, improper mounting	Active circuit failure, passive diodes activate		No effect, normal image acquired		Passive Blocking Circuit detunes element during transmit	No, unless current of control line is monitored
PIN Diodes, D2	Diode Shorted	Component failure, improper mounting	Array Element continuously detuned		No signal, noisy Image		Blocking Circuit active continuously	Yes
PIN Diodes, D2	Diode Open	Component failure, broken leads, improper mounting	Active circuit failure, no blocking impedance		Potential high SAR from element, local heating		Secondary blocking circuit with passive diodes active	No, unless current of control line is monitored
Diodes, D3,D4	Diodes Shorted	Component failure, improper mounting	Array Element continuously detuned, input shorted		No signal, noisy Image		Blocking Circuit active continuously	Yes
Diodes, D3,D4	Diodes Open	Component failure, broken leads, improper mounting	Failure of backup diodes, blocking circuit under active control		No effect, normal image acquired		Passive diode blocking circuit tested on assembly	No
Diodes, D5,D6	Diodes Shorted	Component failure, improper mounting	Array Element continuously detuned, input shorted		No signal, noisy Image		Blocking Circuit active continuously	Yes
Diodes, D5,D6	Diodes Open	Component failure, broken leads, improper mounting	Passive circuit failure, no blocking impedance		No effect, normal image acquired		Passive diode blocking circuit tested on assembly	No
Coil Former Assembly (Drawing: ME1001-01)								
Coil Mechanical Housing	Contact with accessible live parts	Exposed conductors, broken former	High voltage induced by body coil		Potential shock		No exposed conductors, Operator instructions to inspect coil for damage	Yes

C. Calculation of Sequence SAR and Supervision Thresholds

This appendix describes how to determine both the prospective local and average SAR for a given coil, load and sequence, as well as the power limits (trip levels) to be entered for real-time SAR supervision hardware to ensure that the SAR limits are not exceeded during actual scanning. Some calculations similar to these can be found in Varian's *User Guide: Whole-Body Imaging* [171], and in the NEMA MS 8 standard. Further calculations below refer to Pozar's *Microwave Engineering* [172].

Please note that this analysis applies exclusively to single-channel excitation (*not* array or pTx excitation).

C.1 Coil Sensitivity and Loading

C.1.1 Coil Sensitivity and Efficiency

We define coil sensitivity (in transmit mode) as the magnitude of rotating-frame B_1 (B_1^+) achieved by a unit of input power (1 W) entering the coil ports [173]

$$\psi = \frac{|B_1^+|}{\sqrt{P_{coil}}}. \quad (III.1)$$

A realistic RF coil has losses in its components (e.g., capacitors, conductors, etc.), and can also radiate power into free space, thus preventing all of the coil power from being dissipated in the exposed tissue (this is the power responsible for creating useful B_1 fields in the tissue). We define the coil's efficiency as

$$\eta = \frac{P_{tissue}}{P_{coil}}. \quad (III.2)$$

Efficiency is related to the coil's SNR in reception as well as to the loaded and unloaded quality factors (Q) which are readily measured on the RF workbench [174]

$$\eta = 1 - \frac{Q_{loaded}}{Q_{unloaded}} = \left(\frac{\psi}{\psi_0} \right)^2, \quad (III.3)$$

where ψ_0 is the intrinsic sensitivity or SNR, i.e., that achieved by that coil if all internal losses and radiation were eliminated.

C.1.2 Coil Loading

The sensitivity of a loaded coil is lower than that of the empty coil because of the effect of the additional losses. If we assume that the effect of the load on the B_1 pattern is negligible (i.e., minimal skin effect and interference patterns in the load), we can write this reduction in sensitivity in terms of the *loading factor* [175]

$$\left(\frac{\psi_{loaded}}{\psi_{unloaded}} \right)^2 = \frac{Q_{loaded}}{Q_{unloaded}} \leq 1, \quad (III.4)$$

and thus the change in Q can be used to estimate the change in sensitivity due to the load (including the sensitivity under different loads). In some scanners the $\psi_{unloaded}$ is a constant known from

measurements at the factory and the load factor of Eq. (III.4) is a variable determined at scan time to determine the actual power needed to achieve a given tip angle (c.f. Eq. (15)).

C.2 Reflections and Transmission Line Losses

The SAR supervision or monitoring system of an MR scanner typically samples the RF power output (see Figs. 2.1 and 2.2 of NEMA MS 8) at the power amplifier (RFPA), which can be separated from the coil by some times 10 m or more of transmission line (coaxial cable) plus other circuits such as power splitters and T/R switches. Over such lengths it is not uncommon to lose half the RF power to multiple losses, therefore it is important to account for them to determine the actual power delivered to the coil and subject. The following equations are for the simplest situation in which the RFPA is connected to the coil by a single section of transmission line. More complex situations that include multiple sections of transmission line separated by other circuits will require a more detailed network calculation, e.g., using network simulation tools.

C.2.1 Reflections

Power incident at the coil port, P_{port} , can be reflected, in part or totally, back to the RFPA. The amount of reflection is determined by how well the coil's input impedance, Z_{coil} , is matched to the transmission line's characteristic impedance, Z_0 . A mismatched coil is characterized by a reflection coefficient, $\Gamma = \frac{(Z_{coil} - Z_0)}{(Z_{coil} + Z_0)} = S_{11} \neq 0$. The power entering the coil is thus

$$P_{coil} = P_{port}(1 - |\Gamma|^2). \quad (III.5)$$

A *matched* coil ($Z_{coil} = Z_0$) accepts all incident power and therefore $P_{coil} = P_{port}$.

C.2.2 Transmission Line Losses

Attenuation along the transmission line is an important contribution to the losses that diminish the power incident at the coil port. In the case where the coil is matched, the line losses are expressed simply as the ratio of power entering the transmission line, P_{in} , and power entering the coil

$$\frac{P_{in}}{P_{coil}} = a, \quad (III.6)$$

where $a = e^{2\alpha l}$ is the matched-line loss, l is the physical length of the line, and $\alpha = \Re\{\gamma\}$ is the attenuation constant of the transmission line (γ is the complex propagation constant, not to be confused with gyromagnetic ratio below).

In the case where the load is *mismatched*, line losses are usually higher than matched-line losses because the resulting standing wave pattern creates current and voltage maxima that enhance power dissipation. A commonly-used approximation for mismatched-line losses is (see [172], Eqs. 2.92 and 2.93)

$$\frac{P_{in}}{P_{port}} = \frac{a - |\Gamma|^2/a}{1 - |\Gamma|^2}, \quad (III.7)$$

which is valid under the assumption that the line's characteristic impedance, Z_0 , is real (in general for a lossy line it is complex). Note that the corresponding formula (2.3-4) provided in the 2008 version of

NEMA MS 8 is *not* a reliable approximation. The exact formula for mismatched-line losses is (see AC6LA)

$$\frac{P_{in}}{P_{port}} = \frac{\Re\{Z_{in}\}}{\Re\{Z_{coil}\}} \left| \cosh \gamma l + \frac{Z_{coil}}{Z_L} \sinh \gamma l \right|^2, \quad (III.8)$$

where Z_{in} is the impedance seen by the RFPA at the input of the line (Eq. 2.91 in [172]).

Similarly to Eq. (III.5), the power entering the transmission line is

$$P_{in} = P_{RFPA} (1 - |\Gamma_{in}|^2), \quad (III.9)$$

where $\Gamma_{in} = \Gamma e^{-2\gamma l} = \frac{(Z_{in} - Z_0)}{(Z_{in} + Z_0)}$ is the reflection coefficient seen at the input of the transmission line and P_{RFPA} is the incident power from the RFPA (assumed to have an internal impedance = Z_0).

C.3 Pulse Sequence Power

The following expressions relate the parameters of the pulse sequence, including those of the RF pulses, to the time-averaged power delivered by the sequence (which is proportional to the time-averaged SAR limited by IEC 60601-2-33). Here, power is measured at the coil ports because it is the power that is directly related to SAR in the subject, irrespective of losses and reflections upstream.

C.3.1 RF Pulse Energy

The RF pulse energy delivered to a resonant coil with input resistance $Z_{coil} = R$ by a pulse of duration τ is

$$E_{pulse} = \frac{1}{R} \int_0^\tau V^2(t) dt, \quad (III.10)$$

where $V(t)$ is the voltage waveform of the pulse.

By substituting for $P_{coil} = V^2/R$ in Eq. (III.1) the pulse energy then becomes

$$E_{pulse} = \frac{1}{\psi^2} \int_0^\tau |B_1^+(t)|^2 dt, \quad (III.11)$$

which allows the RF pulse energy to be separated into a term defined by a coil parameter (ψ) and one by a pulse parameter (B_{1RMS}^+ below). This convenient mathematical separation is used in some system vendors' software to simplify prospective sequence SAR calculations.

The average⁸ power of the pulse is then

$$\overline{P_{pulse}} = \frac{E_{pulse}}{\tau} = \frac{1}{\tau \psi^2} \int_0^\tau |B_1^+|^2 dt = \left(\frac{B_{1RMS}^+}{\psi} \right)^2, \quad (III.12)$$

where we have applied the definition of RMS of the B_1 waveform over its duration.

⁸ overline is used to indicate quantities averaged over time

C.3.2 Tip Angle and Form Factor

If the excitation frequency is resonant with the Larmor frequency the tip angle θ is

$$\theta = \gamma \int_0^\tau |B_1^+(t)| dt = \gamma \overline{B_1^+} \tau, \quad (III.13)$$

where the second equality defines the average rotating frame B_1 and γ is the gyromagnetic ratio.

The tip angle is typically calibrated relative to a known value that we define the *reference* tip angle, θ_{ref} (e.g., 90°), and is associated with a reference average B_1^+ ,

$$\theta_{ref} = \gamma \overline{B_{1ref}^+} \tau. \quad (III.14)$$

The relative amplitude of the desired and reference tip angles defines the drive scale $\lambda = \theta/\theta_{ref}$. The reference pulse amplitude is associated with a reference power, $\overline{P_{ref}}$, which is related to that of the desired tip angle by

$$\overline{P_{pulse}} = \lambda^2 \overline{P_{ref}}. \quad (III.15)$$

Finally, the average and RMS of the B_1 waveform are related by the form factor [176]

$$\varphi = \frac{B_{1RMS}^+}{\overline{B_1^+}} \geq 1, \quad (III.16)$$

which is independent of any scaling applied to the waveform, and the equality holds for hard pulses. The form factor is thus a convenient pulse parameter (constant) used to relate the RMS field and thus pulse power (Eq. (III.12)) to the tip angle (Eq. (III.13)),

$$\psi \sqrt{\overline{P_{pulse}}} = B_{1RMS}^+ = \frac{\theta \varphi}{\gamma \tau}. \quad (III.17)$$

C.3.3 Average Sequence Power

For a sequence containing only one type (shape, magnitude and duration) of RF pulse repeated at every T_R (e.g., gradient echo) the average sequence power,

$$\overline{P_{scan}} = \delta \overline{P_{pulse}}, \quad (III.18)$$

is calculated by knowing the duty cycle of the RF pulse,

$$\delta = \frac{\tau}{T_R}. \quad (III.19)$$

For sequences without repetitions (i.e., single shot) the T_R is replaced with the total duration of the scan (sequence).

If the sequence contains $K > 1$ type and/or magnitude of RF pulse (e.g., spin echo) in each T_R , the average sequence power is obtained by adding the pulse energies of each pulse

$$\overline{P_{scan}} = \frac{1}{T_R} \sum_{k=1}^K E_{pulse,k}. \quad (III.20)$$

Finally, it is instructive to combine the equations above to express how sequence power changes as its parameters are changed. In the case of a sequence with only one type of RF pulse

$$\overline{P_{scan}} = \delta \left(\frac{\theta\varphi}{\gamma\tau\psi} \right)^2 = \frac{1}{\tau T_R} \left(\frac{\theta\varphi}{\gamma\psi} \right)^2, \quad (III.21)$$

which is a useful scaling relationship found in various forms throughout the literature (e.g., Schaefer's Eq. 3.10 [177]).

C.4 Prospective SAR Calculation

The objective of a prospective SAR calculation is to estimate the time-averaged SAR values in a specific experimental setup (sequence, coil and subject). Parameter combinations that are likely to exceed the SAR limits can therefore be excluded *before* the sequence is run.

C.4.1 Exposed Tissue Power and Average SAR

With the same assumptions of Appendix C.3 (no transmission line losses and reflections (Appendix C.2)) we can set $\overline{P_{coil}} = \overline{P_{scan}}$. For a sequence with only one type of pulse we then combine Equations (III.2), (III.3), (III.4), and (III.21) to give the exposed tissue power

$$\begin{aligned} \overline{P_{tissue}} = \eta \overline{P_{scan}} &= \frac{1}{\tau T_R} \left(1 - \frac{Q_{loaded}}{Q_{unloaded}} \right) \frac{Q_{unloaded}}{Q_{loaded}} \left(\frac{\theta\varphi}{\gamma\psi_{unloaded}} \right)^2 \\ &= \frac{1}{\tau T_R} \left(\frac{Q_{unloaded}}{Q_{loaded}} - 1 \right) \left(\frac{\theta\varphi}{\gamma\psi_{unloaded}} \right)^2. \end{aligned} \quad (III.22)$$

The exposed tissue power is used to define the average SAR over that tissue

$$SAR_{avg} = \frac{\overline{P_{tissue}}}{m_{exposed}}, \quad (III.23)$$

where $m_{exposed}$ is the mass of the subject that is exposed to at most 95% of the RF power dissipation. This mass may need to be estimated on a case-by-case basis depending on the coil and dimensions of the subject. The average SAR is then compared to the limits in [IEC 60601-2-33](#) and if needed the sequence parameters are adjusted.

C.4.2 Local SAR

Local, or hot spot SAR is the maximum of the spatial distribution of SAR (averaged over any 10 g of tissue in the case of IEC) which can lead to local tissue burns. Because the spatial distribution of the electric fields that give rise to SAR cannot be measured using MRI, a prospective calculation of local SAR typically requires input from simulations (see §II.C). The simulations must provide either a subject-specific or worst-case ratio of local to average SAR, x , so that local SAR can be obtained from the average SAR of Eq. (III.23) according to

$$SAR_{local} = \xi \cdot SAR_{avg}. \quad (III.24)$$

This value is then compared to the corresponding IEC limits and if needed the sequence parameters are adjusted.

C.4.3 Loading Factor Measurement

In the expression for exposed tissue power the combined effect of efficiency and loading factor (first term in parentheses in the 2nd line of Eq. (III.22)) is not strictly a sequence parameter because it depends on the coil and subject, as well as their mutual interaction. Moreover, that term does not achieve a maximum as a function of Q_{loaded} , and therefore an upper bound on $\overline{P_{tissue}}$ is not readily obtained (e.g., to estimate the maximum tissue power over all subjects in a study). However, the loading factor can be measured on the bench for a variety of subjects and the minimum obtained can be used to estimate a maximum value (including an appropriate safety factor) for the first term in parentheses in Eq. (III.22).

Alternatively, the loading factor can be measured at scan time relative to a reference value obtained using a reference phantom (corresponding to a sensitivity ψ_{ref}). This is achieved by adjusting the transmit power of a tip angle calibration sequence to obtain a reference tip angle (e.g., 90°). Eq. (III.4) can be written as

$$\frac{Q_{loaded}}{Q_{unloaded}} = \left(\frac{\psi_{loaded}}{\psi_{unloaded}} \right)^2 = \left(\frac{\psi_{loaded}}{\psi_{ref}} \right)^2 \left(\frac{\psi_{ref}}{\psi_{unloaded}} \right)^2, \quad (III.25)$$

where the 2nd term is a calibration constant determined either using the reference phantom on the bench or by the same tip angle calibration sequence (to measure $\psi_{unloaded}$ a small low-loss phantom is used). If only the amplitude of the RF pulse in the calibration sequence is varied, using Eq. (III.12) the first term of Eq. (III.25) can be written as

$$\left(\frac{\psi_{loaded}}{\psi_{ref}} \right)^2 = \left(\frac{B_{1RMS}^+}{B_{1RMS}^+} \right)^2 \frac{\overline{P_{ref}}}{P_{pulse}}, \quad (III.26)$$

because to achieve the same tip angle the B_1 must be the same for both phantoms. The ratio of transmit powers (2nd term of Eq. (III.26)) therefore allows a subject-specific measurement of the loading factor for use in Eq. (III.22).

C.5 Thresholds for SAR Supervision

The objective here is to determine the average power thresholds above which the SAR monitoring system will intervene to halt the scan. The equations below are provided for systems (typically experimental systems) where the thresholds can be entered directly by the operator. In other systems the parameters to manipulate must be determined by consulting the scanner manufacturer's software and hardware documentation. Typically, information such as coil parameters (sensitivity), body mass seen, etc. can be entered in specific files (e.g., the coil files), and the scanner's existing software will set the power limits accordingly.

C.5.1 Calculating Power Thresholds

The IEC SAR Limits depend on what body part is exposed and how much of it, on local and volume averages, and on the averaging time. The limits for short-term (10 s) and long-term (6 min) averaging are related simply by a constant factor and thus should not require separate entries.

Once the SAR limits for the specific experimental situation are determined from the standard, we need to calculate the corresponding powers *at the location along the transmit chain where they are sampled*. Conversely, most of the expressions above refer to power into the coil ports ($\overline{P_{coil}} = \overline{P_{scan}}$), therefore reflections and transmission line losses (Appendix C.2) must be included.

Consider as an example the common setups of Figs. 2.1a and 2.2 of NEMA MS 8, where the power is sampled at the RFPA's output. Assuming that the SAR monitoring system already includes calibrations for the coupling constants of the directional coupler, and using the approximate expression for mismatched line loss, Equations (III.2), (III.5), (III.7) and (III.9) can be rearranged to give

$$\overline{P_{RFPA}} = \overline{P_{tissue}} \frac{a - |\Gamma|^2/a}{\eta(1 - |\Gamma_{in}|^2)(1 - |\Gamma|^2)} \quad (III.27)$$

The RFPA power threshold for average SAR then becomes (Eq. (III.23))

$$\overline{P_{RFPA}} = \frac{m_{exposed}(a - |\Gamma|^2/a)}{\eta(1 - |\Gamma_{in}|^2)(1 - |\Gamma|^2)} SAR_{avg}, \quad (III.28)$$

and for local SAR (Eq. (III.24))

$$\overline{P_{RFPA}} = \frac{m_{exposed}(a - |\Gamma|^2/a)}{\xi\eta(1 - |\Gamma_{in}|^2)(1 - |\Gamma|^2)} SAR_{local}. \quad (III.29)$$

To satisfy both limits the smaller of the two powers must be chosen and entered into the SAR supervision system.

Note that, in principle, it is possible to measure the net power into the coil by monitoring the power it reflects (thereby avoiding the corrections for reflections and transmission line losses). However, reflected power may need to be monitored in multiple places (Fig. 2-1a of NEMA MS 8), and reflected power is also subject to attenuation which must be accounted for.

The terms for line attenuation and reflections are also challenging or time-consuming to measure for each experimental situation. Therefore it may be preferable to use a previously-measured line loss (a) and assume a worst-case reflection coefficient ($|\Gamma|$), which could be quite small if the coil is matched for each load. The reflected power measurement could then be used to halt the scan if a higher-than-expected reflection is detected.

D. Summary of Relevant Standards, Government and Industry Publications

Below is a list of active standards, as well as publications from governments and industry, that are relevant and cited in these recommendations. Applicable legislation varies depending on the jurisdiction, and those listed are provided only as examples. Versions are up-to-date as of time of writing.

Publication ID	Year	Title	Topic	Section
----------------	------	-------	-------	---------

AAPM (American Association of Physicists in Medicine)

<u>AAPM Report No. 100</u>	2010	Acceptance Testing and Quality Assurance Procedures for Magnetic Resonance Imaging Facilities	B ₀ magnetic field homogeneity measurement	II.A. <u>4.4.1</u> II.C. <u>4.1</u>
----------------------------	------	---	---	--

ACR (American College of Radiology)

<u>ACR MRI QC Manual</u>	2015	ACR Magnetic Resonance Imaging Quality Control Manual	B ₀ magnetic field homogeneity measurement	II.A. <u>4.4.1</u>
<u>ACR Large Phantom</u>	2018	Phantom Test Guidance for Use of the Large MRI Phantom	phantom design and use	II.C. <u>4.1</u>
<u>ACR MR Safety Manual</u>	2020	ACR Manual on MR Safety	general MRI safety practices	I. <u>2.1.2</u> II.A. <u>4.4.1</u>

ANSI (American National Standards Institute)

<u>ANSI Z136.1</u>	2014	Safe Use of Lasers	laser radiation safety	II.B. <u>3.1.2</u>
--------------------	------	--------------------	------------------------	--------------------

ASTM International (formerly American Society for Testing and Materials)

<u>ASTM D149</u>	2020	Standard Test Method for Dielectric Breakdown Voltage and Dielectric Strength of Solid Electrical Insulating Materials at Commercial Power Frequencies	dielectric insulating materials	II.A. <u>1.1</u>
------------------	------	--	---------------------------------	------------------

Publication ID	Year	Title	Topic	Section
<u>ASTM D648</u>	2018	Standard Test Method for Deflection Temperature of Plastics Under Flexural Load in the Edgewise Position	mechanical stability of plastics	II.A. <u>4.1</u>
<u>ASTM D1929</u>	2019	Standard Test Method for Determining Ignition Temperature of Plastics	flammability of plastics	II.A. <u>4.2</u>
<u>ASTM E595</u>	2015	Standard Test Method for Total Mass Loss and Collected Volatile Condensable Materials from Outgassing in a Vacuum Environment	out-gassing	II.A. <u>1.3.1</u>
<u>ASTM F2052</u>	2015	Standard Test Method for Measurement of Magnetically Induced Displacement Force on Medical Devices in the Magnetic Resonance Environment	ferromagnetic materials	II.A. <u>4.4.1</u>
<u>ASTM F2182</u>	2019	Standard Test Method for Measurement of Radio Frequency Induced Heating On or Near Passive Implants During Magnetic Resonance Imaging	SAR measurement	II.C. <u>2.2.2</u>
<u>ASTM F2213</u>	2017	Standard Test Method for Measurement of Magnetically Induced Torque on Medical Devices in the Magnetic Resonance Environment	ferromagnetic materials	II.A. <u>4.4.1</u>

Publication ID	Year	Title	Topic	Section
<u>ASTM D4565</u>	2015	Standard Test Methods for Physical and Environmental Performance Properties of Insulations and Jackets for Telecommunications Wire and Cable	cable bending test	II.A. <u>2.5</u>

EIA (Electronic Industries Alliance, now Electronic Components Industry Association)

<u>EIA-364 series</u>	various	Electrical Connector Performance Test Standards	connector reliability (TP-09), ferromagnetism (TP-54A and 88), etc.	II.A. <u>2.5</u> II.A. <u>4.4.1</u>
-----------------------	---------	---	---	--

EU (European Union)

<u>EU Directive 2013/35</u>	2013	Minimum health and safety requirements regarding the exposure of workers to the risks arising from physical agents (electromagnetic fields)	Electromagnetic Field (RF) safety	II.C. <u>1</u>
<u>EU Medical Device Regulation 2017/745</u>	2017	Medical Devices Directive	safety requirements for medical devices	II.A. <u>1.3</u> II.A. <u>2.2</u> II.A. <u>5</u>

FDA (Food and Drug Administration, USA)

<u>FDA Guidance 340</u>	2016	Submission of Premarket Notifications for Magnetic Resonance Diagnostic Devices	General MRI and RF coil safety	I. <u>2.1.2</u> I. <u>2.5</u> II.C. <u>1</u>
<u>FDA Guidance 793</u>	2014	Criteria for Significant Risk Investigations of Magnetic Resonance Diagnostic Devices - Guidance for Industry and Food and Drug Administration Staff	MRI safety	II.C. <u>1</u>

Publication ID	Year	Title	Topic	Section
<u>FDA Guidance 1807</u>	2016	Reporting of Computational Modeling Studies in Medical Device Submissions - Guidance for Industry and Food and Drug Administration Staff	Computational EM (simulations)	II.C.7
<u>FDA Guidance 19011</u>	2020	Magnetic Resonance (MR) Receive-only Coil – Performance Criteria for Safety and Performance Based Pathway	RF coil safety	I.2.1.2 II.B.1.3

ICNIRP (International Commission on Non-Ionizing Radiation Protection)

<u>ICNIRP EMF Guidelines</u>	2020	Guidelines for Limiting Exposure to Electromagnetic Fields (100 kHz to 300 GHz)	RF safety	II.C.1.3
------------------------------	------	---	-----------	----------

IEC (International Electrotechnical Commission)

<u>IEC 60050-192</u>	2015	International electrotechnical vocabulary – Part 192: Dependability	definitions	I.1
<u>IEC 60060 series</u>	2010	High-voltage test techniques	dielectric insulating materials	II.A.1.1
<u>IEC 60243 series</u>	2013	Electric strength of insulating materials - Test methods	dielectric insulating materials	II.A.1.1
<u>IEC 60417</u>	2002	Graphical symbols for use on equipment	labelling	II.A.5
<u>IEC 60512-24</u>	2010	Connectors for electronic equipment - Tests and measurements - Part 24-1: Magnetic interference tests	connector magnetism	II.A.4.4.1

Publication ID	Year	Title	Topic	Section
<u>IEC 60529</u>	2013	Degrees of protection provided by enclosures (IP Code)	ingress protection	II.A. <u>1.2</u>
<u>IEC 60601-1</u>	Ed. 3.2: 2020	Medical electrical equipment – Part 1: General requirements for basic safety and essential performance	safety requirements for medical devices	throughout
<u>IEC 60601-1-2</u>	2014	Medical electrical equipment - Part 1-2: General requirements for basic safety and essential performance - Collateral Standard: Electromagnetic disturbances - Requirements and tests	electromagnetic compatibility for medical devices	II.B. <u>1.3</u>
<u>IEC 60601-2-33</u>	2010/ AMD2: 2015	Medical electrical equipment – Part 2-33: Particular requirements for the basic safety and essential performance of magnetic resonance equipment for medical diagnosis	requirements specific to MRI scanners; some sections supersede those in 60601-1	throughout
<u>IEC 60695-2-13</u>	2014	Fire hazard testing - Part 2-13: Glowing/hot-wire based test methods	flammability of materials	II.A. <u>4.2</u>
<u>IEC 60695-11-10</u>	2013	Fire hazard testing - Part 11-10: Test flames - 50 W horizontal and vertical flame test methods	flammability of materials	II.A. <u>4.2</u>
<u>IEC 60812</u>	2018	Failure modes and effects analysis (FMEA and FMECA)	risk management	I. <u>2.1.3</u>

Publication ID	Year	Title	Topic	Section
<u>IEC 60878</u>	2015	Graphical symbols for electrical equipment in medical practice	labelling	II.A.5
<u>IEC 61000-4-2</u>	2008	Electromagnetic compatibility (EMC) - Part 4-2: Testing and measurement techniques - Electrostatic discharge immunity test	ESD immunity	II.B.1.3
<u>IEC 61025</u>	2006	Fault tree analysis (FTA)	risk management	I.2.1.4
<u>IEC 62366-1</u>	2015	Medical devices - Part 1: Application of usability engineering to medical devices	usability	II.A.5
<u>IEC 62366-2</u>	2016	Medical devices - Part 2: Guidance on the application of usability engineering to medical devices	usability	II.A.5
<u>IEC/IEEE 62209-1528</u>	2020	Measurement procedure for the assessment of specific absorption rate of human exposure to radio frequency fields from hand-held and body-mounted wireless communication devices – Part 1528: Human models, instrumentation, and procedures (Frequency range of 4 MHz to 10 GHz).	SAR measurements	II.C.4.1 II.C.4.5

Publication ID	Year	Title	Topic	Section
<u>IEC/IEEE 62704-1</u>	2017	Determining the peak spatial-average specific absorption rate (SAR) in the human body from wireless communications devices, 30 MHz to 6 GHz - Part 1: General requirements for using the finite difference time-domain (FDTD) method for SAR calculations	RF/SAR simulations	II.C. <u>3.2</u>

IEEE (Institute of Electrical and Electronics Engineers)

<u>IEEE C95.1</u>	2019	IEEE Standard for Safety Levels with Respect to Human Exposure to Electric, Magnetic, and Electromagnetic Fields, 0 Hz to 300 GHz	RF safety	II.C. <u>3.2</u>
<u>IEEE C95.3</u>	2021	IEEE Recommended Practice for Measurements and Computations of Electric, Magnetic, and Electromagnetic Fields with Respect to Human Exposure to Such Fields, 0 Hz to 300 GHz	RF/SAR simulations	II.C. <u>2.2</u> II.C. <u>3.1</u>
<u>IEEE 1597.2</u>	2011	IEEE Recommended Practice for Validation of Computational Electromagnetics Computer Modeling and Simulations	RF/SAR simulations	II.C. <u>2</u> II.C. <u>3.1</u> II.C. <u>4</u>

Publication ID	Year	Title	Topic	Section
----------------	------	-------	-------	---------

IPC International (formerly Institute of Printed Circuits)

<u>IPC-2221B</u>	2012	Generic Standard on Printed Board Design	PCB design guidelines	II.B. <u>1.1.1</u>
------------------	------	--	-----------------------	--------------------

ISO (International Organization for Standardization)

<u>ISO 75</u>	2013	Plastics – Determination of temperature of deflection under load	mechanical stability of plastics	II.A. <u>4.1</u>
<u>ISO 871</u>	2006	Plastics – Determination of ignition temperature using a hot-air furnace	flammability of materials	II.A. <u>4.2</u>
<u>ISO 7010</u>	2019	Graphical symbols – Safety colours and safety signs – Registered safety signs	labelling	II.A. <u>5</u>
<u>ISO 9772</u>	2012	Cellular plastics – Determination of horizontal burning characteristics of small specimens subjected to a small flame	flammability of materials	II.A. <u>4.2</u>
<u>ISO 9773</u>	1998	Plastics – Determination of burning behaviour of thin flexible vertical specimens in contact with a small-flame ignition source	flammability of materials	II.A. <u>4.2</u>
<u>ISO/TS 10974</u>	2018	Assessment of the safety of magnetic resonance imaging for patients with an active implantable medical device	AIMD test procedures (e.g., effects induced by gradient switching)	II.B. <u>1.2</u>
<u>ISO 10993-1</u>	2018	Biological evaluation of medical devices – Part 1: Evaluation and	biocompatibility	II.A. <u>1.3</u>

Publication ID	Year	Title	Topic	Section
		testing within a risk management process		
<u>ISO 10993-10</u>	2010	Biological evaluation of medical devices – Part 10: Tests for irritation and skin sensitization	biocompatibility	II.A.1.3
<u>ISO 14971</u>	2019	Medical devices – Application of risk management to medical devices	risk management; see also ISO/TR 24971:2020	I.1 I.2.1 I.2.2.1
<u>ISO 15223-1</u>	2016	Medical devices – Symbols to be used with medical device labels, labelling and information to be supplied – Part 1: General requirements	labelling	II.A.5
<u>ISO 31000</u>	2018	Risk management — Guidelines	risk management	I

NASA (National Aeronautics and Space Administration)

<u>NASA – GSFC S-311-P-10</u>	1992	Connectors, Electrical, Rectangular, Miniature, Polarized Shell, Rack and Panel, for Space Flight Use	connector magnetism	II.A.4.4.1
-------------------------------	------	---	---------------------	------------

NEMA (National Electrical Manufacturers Association)

<u>NEMA MS 2</u>	2008 R2014	Determination of Two-Dimensional Geometric Distortion in Diagnostic Magnetic Resonance Images	B ₀ magnetic field homogeneity measurement	II.A.4.4
<u>NEMA MS 4</u>	2010	Acoustic Noise Measurement Procedure for Diagnostic Magnetic Resonance Imaging (MRI) Devices	sound pressure	II.B.3.1.4
<u>NEMA MS 8</u>	2016	Characterization of the Specific Absorption	SAR measurement	III.C

Publication ID	Year	Title	Topic	Section
		Rate (SAR) for Magnetic Resonance Imaging Systems		
<u>NEMA MS 10</u>	2010	Determination of Local Specific Absorption Rate (SAR) in Diagnostic Magnetic Resonance Imaging (MRI)	phantoms SAR measurement	II.B. <u>5.1</u> II.C. <u>4.1</u> II.C. <u>4.6</u>
<u>NEMA MS 14</u>	2019	Characterization of Radiofrequency (RF) Coil Heating in Magnetic Resonance Imaging Systems	RF coil heating	II.B. <u>5.2.1.2</u> II.B. <u>5.4</u>

UL (Underwriters Laboratories)

<u>UL 94</u>	2013	Standard for Tests for Flammability of Plastic Materials for Parts in Devices and Appliances	flammability of materials	II.A. <u>4.2</u>
--------------	------	--	---------------------------	------------------